Solar-Terrestrial Centre of Excellence

Annual Report 2011

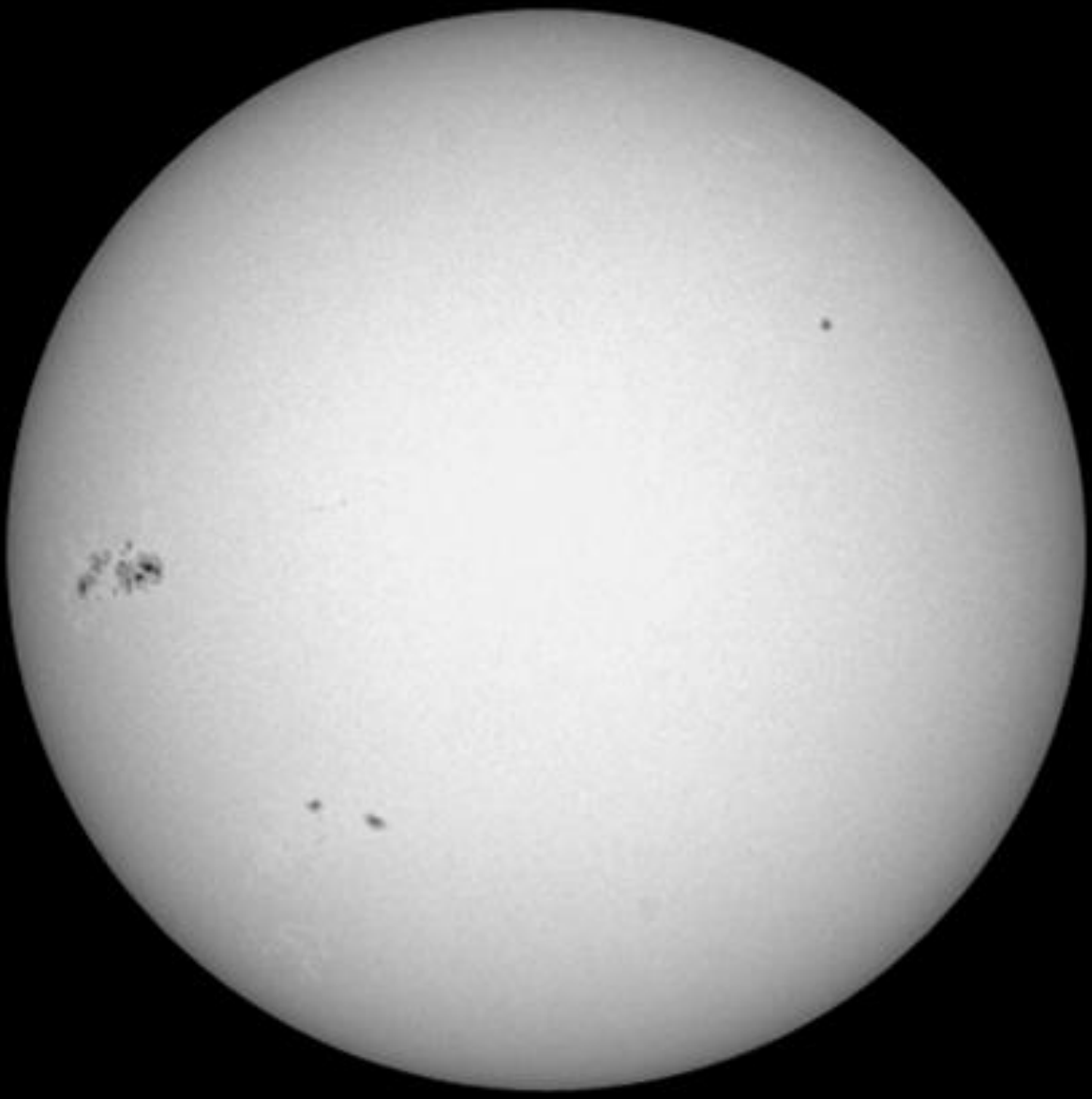

Belgian Science Policy Office belspo

Royal Observatory of Belgium

RMI

aeronomie.be

.be

STCE

Solar-**T**errestrial **C**entre of **E**xcellence

http://stce.be/

Ringlaan 3

B-1180 Brussels

Tel.: +32 2 373 0211

Fax: + 32 2 374 9822

Front-page: The Sun on 4 November 2011 as photographed through the USET White Light Telescope. The big sunspot group is NOAA11339, one of the largest groups so far this solar cycle.

Table of Contents

Preface

Dear Reader,

In front of you lies the Annual Report of the Solar-Terrestrial Centre of Excellence for its activities in 2011. You will immediately notice that it takes a completely new format and approach as in previous years. Indeed, rather than making it into a long and heavy-to-digest exhaustive description of all that's happened in our team during the year, we've decided to henceforth write an annual report that is lighter to produce and read and that focuses really on the highlights of the year.

To put the report in perspective, particularly concerning the operational activities related to Space Weather and Space Climate, a first section is added that describes the state of the Sun during the year, using images produced by various instruments that for most of them have an STCE involvement.

The year 2011 has shown further growth of the STCE towards the target of a dense collaboration between the different scientific groups involved, and building on that, a focus on international excellence. This has given us the solid ground to strengthen our expertise, making us evident partners in many projects proposed under different programmes. STCE is involved in several currently running EU-FP7 and ESA-SSA projects. STCE supports developments co-funded through ESA-PRODEX and ESA-GSTP. Scientists involved in the STCE are frequently asked to fill leading or coordinating positions in advisory or decisions making bodies in the fields that we cover. Thus, STCE has members in the Steering Board of Space Weather Working Team (ESA), in the SSA Users Representatives Group (ESA), in the UN-COPUOS working group on long-term sustainability of space travel (UN), in the Inter-programme Coordination Team on Space Weather (WMO), just to name a few.

We hope that you enjoy reading this new style report. Please do not hesitate to contact us if you want to make some suggestion for improvement or if you would like to get more information about any of the particular topics or about any of the STCE activities. Or, if you really want to learn more about the STCE, why not come and visit us?

Ronald Van der Linden
General Coordinator of the Solar-Terrestrial Centre of Excellence
Director General of the Royal Observatory of Belgium

Structure of the STCE

The Solar-Terrestrial Centre of Excellence is a project of scientific collaboration that focuses on the Sun, through interplanetary space, up to the Earth and its atmosphere and includes a Space Weather application and service center.

The solid base of the STCE is the expertise that exists in the 3 Federal Scientific Institutes of the Brussels Space Pole: the Royal Observatory of Belgium, the Royal Meteorological Institute and the Belgian Institute for Space Aeronomy. The STCE supports fundamental solar, terrestrial and atmospheric physics research, is involved in earth-based observations and space missions, offers a broad variety of services (mainly linked to space weather and space climate) and operates a fully established space weather application center. The scientists act at different levels within the frame of local, national and international collaborations of scientific and industrial partners. The STCE benefits also from the platforms of interaction offered through the (SWWT, SWENET, SSA), EU (COST, FP7) and others (e.g. ISES).

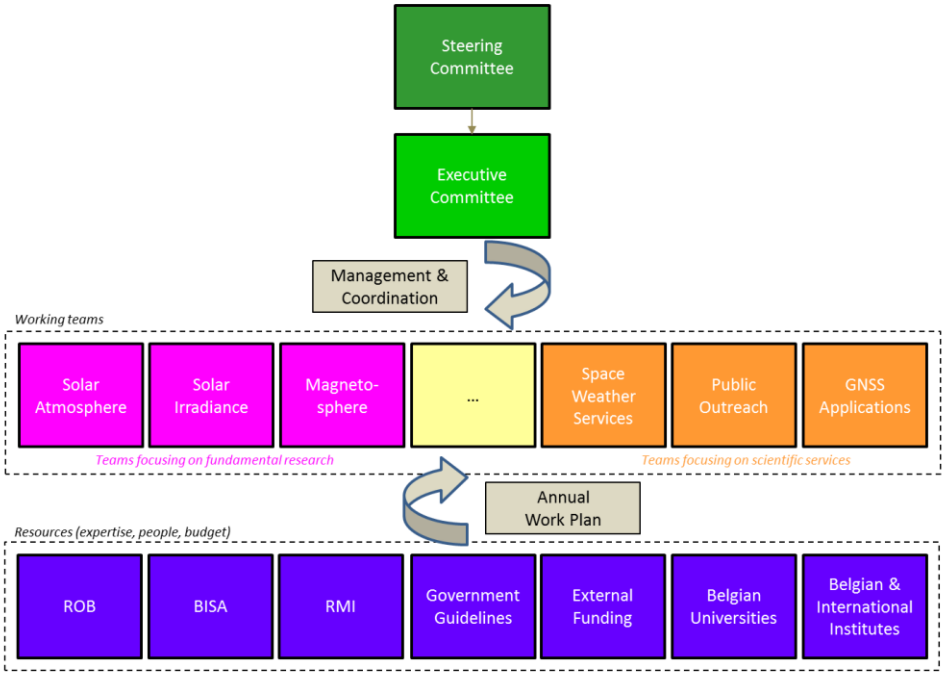

Figure 1: The STCE management structure

The STCE's strengths are based on know-how, sharing knowledge, manpower, infrastructure and a reliable network in the Sun-Space-Earth interconnection.

In order to optimize the coordination between the various working groups and institutions, as well as the available resources such as ICT, personnel and budget, a management structure for the STCE was put into place, consisting of a steering committee and an executive committee.

The ***steering committee*** takes all the final decisions on critical matters with regard to the STCE. It assures the integration of the STCE into the 3 institutions and the execution of the strategic plans. It is composed of:

- Director General "Research Programs and Applications"

  Dr. Dominique Fonteyn (BELSPO)

- Director General of the 3 institutions at the Space Pole

  Dr. Ronald Van der Linden (ROB)
  Dr. Daniel Gellens (RMI)
  Dr. Martine De Mazière (BISA)

The ***executive committee***, amongst many other tasks, assures the global coordination between the working groups and the correct use of the budgetary means for the various projects. It also identifies new opportunities and is advisory body to the Steering Committee. It is composed of:

- Global Coordinator

  Dr. Ronald Van der Linden (ROB)

- Leaders of the research teams

  Dr. David Berghmans (ROB)
  Dr. Carine Bruyninx (ROB)
  Dr. Johan De Keyser (BISA)
  Dr. Michel Kruglanski (BISA)
  Dr. Stanimir Stankov (RMI)
  Dr. Steven Dewitte (RMI)

- Assistant of the Global Coordinator

  Dr. Petra Vanlommel (ROB)

Figure 2: An international team of solar-terrestrial researchers is taking the lunch together. Aside their expertise in the various space weather domains, they also share other commonalities like speaking English, taking their sandwich from the same bakery, or coming to the Space Pole by bike.

Monitoring Space Weather: Solar-Terrestrial Highlights in 2011

After the long minimum and a slow increase over the last 2 years, solar activity finally picked up in 2011. The official yearly sunspot number (SSN), as determined by the SIDC (Solar Influences Data analysis Center), rose from 16.5 to 55.7, which is the highest since 2003. The second half of the year was a lot more active than the first half, with a highest monthly SSN of 96.7 in November.

This rise in solar activity is not a surprise. Indeed, the prediction of the SSN is done by a panel of experts. Such a panel was also formed for the prediction of the current Solar Cycle 24 (SC24). It was chaired by NOAA and composed of several international experts, among them Ronald Van der Linden, general manager of the STCE. In May 2009, this Solar Cycle 24 Prediction Panel came to a consensus opinion that the maximum of SC24 would take place in 2013, with a maximum *smoothed* monthly SSN of around 90 (between 70-110). So far, solar activity seems indeed to be on this track.

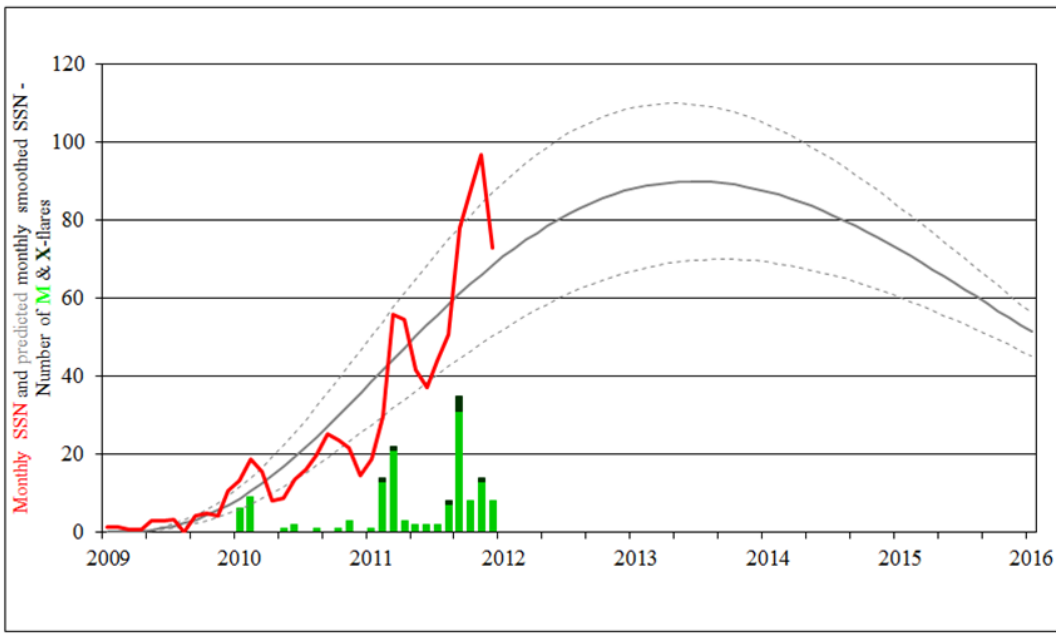

Figure 3: This figure shows the monthly SSN and the predicted smoothed monthly SSN, as well as the number of Medium and eXtreme flares. Observed data are till December 2011, predicted SSN are till December 2015.

There were only 2 days without sunspots in 2011 (14 January and 14 August), which is a lot less than in the previous years (e.g. 262 spotless days in 2009!). The southern hemisphere was still considerably inactive, with 86 spotless days, compared to only 18 on the northern half.

The appearance of big groups was also unequally distributed over the solar hemispheres (see Figure 4). Indeed, of the 20 biggest groups that appeared in 2011, 14 were on the northern hemisphere. These include the 2 super groups NOAA 1302 and NOAA 1339, which were visible in resp. September and November. These groups had sunspot areas 8-9 times the total surface area of the Earth, and were easily visible with the naked eye.

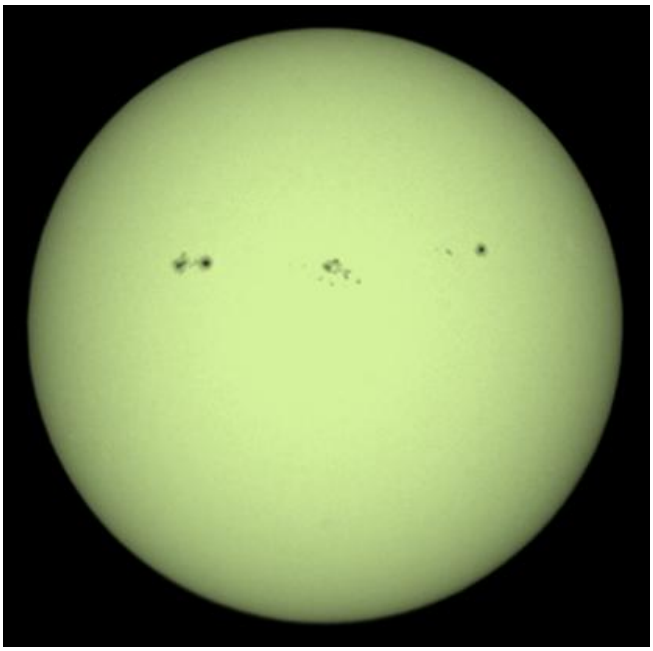

Figure 4: The Sun on August 1, 2011, as seen through the White-Light (WL) telescopes of the ROB, showing (from left to right) NOAA 1263, 1261 and 1260. NOAA 1263 would produce the largest solar flare so far in SC24 (X6.9 on 9 August). NOAA 1261 would produce the flares and CMEs that would lead to a severe geomagnetic storm on 5 August. Notice also the lack of sunspots on the southern solar hemisphere.

The appearance of bigger and more complex sunspot groups resulted in more and increasingly powerful solar explosions. The first X-class solar flare of SC24 was produced by NOAA 1158 on 15 February. It ended a 1524-days lull in these eXtreme flares, the last such event dating back already from 14 December 2006! In total, the Sun produced 8 X-flares as well as 111 M-flares (medium class) in 2011. That is a remarkable increase compared to 2010, which registered no X-flares and only 23 M-flares. Nonetheless, these numbers need to be put in perspective: Over the same period, SC24 registered -so far- only 20-50% of the number of M- and X-flares produced by previous solar cycles. Meager indeed!

Up to now, the strongest flare in SC24 occurred on 9 August 2011 in NOAA 1263. Peaking at X6.9, it is currently ranked 36th since systematic GOES X-ray measurements began in 1976. Only on 7 occasions the 2011 flares were clearly accompanied by solar energetic particles (SEP; high speed protons). All of these belonged to the weakest class of proton events, and had little terrestrial influence.

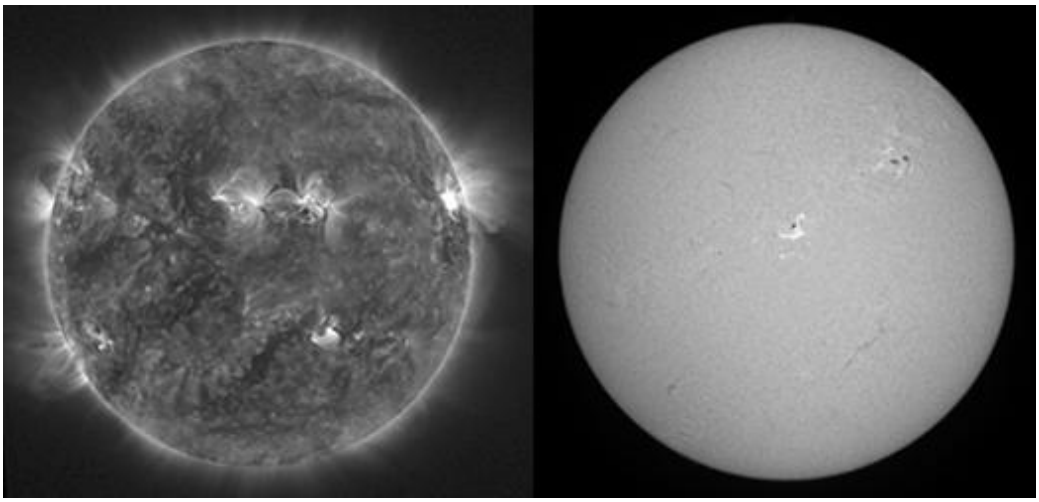

Figure 5: On the left the X6.9 flare as seen by PROBA2/SWAP on 9 August. Right: One of the numerous M-flares (M1 in NOAA 1305 on 1 October) as observed by the ROB's H-alpha telescope. Just like the WL-telescopes, this instrument is also mounted on the Uccle Solar Equatorial Table (USET).

However, the -visually- most impressive solar explosion was not produced by one of these X-class solar flares, but by a medium M2-flare on June 7, 2011. In a relatively small sunspot group near the Sun's southwestern limb, magnetic instabilities suddenly ejected a huge amount of matter into space. This is commonly called a coronal mass ejection (CME). In this case however, a significant part of the relatively cold material fell back on the solar surface in a gigantic fountain-like pattern, often brightening on those places where it touched down. The whole event was imaged in detail by several ground and space observatories, including PROBA2, and got quite some media attention.

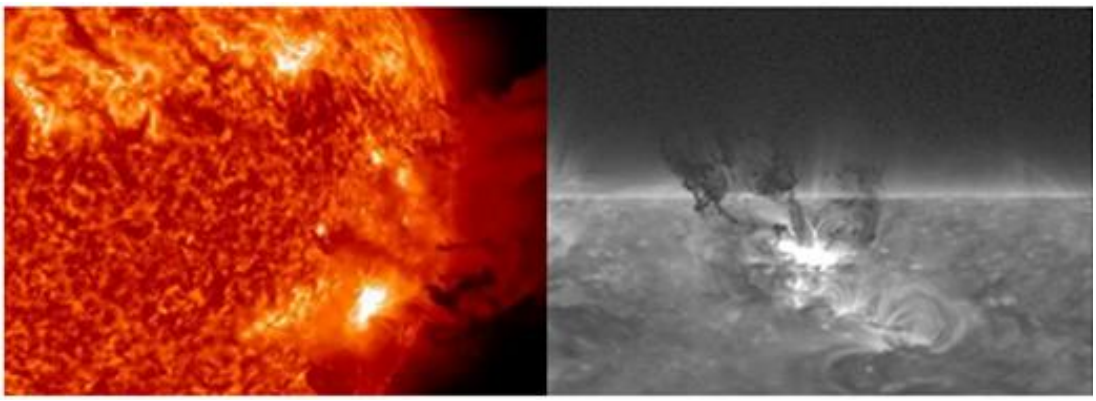

Figure 6: The visually spectacular CME of 7 June as seen by NASA's SDO/AIA 304 instrument and by PROBA2/SWAP. The material is dark because it is relatively cool (still 80.000 degrees hot!) compared to the rest of the solar corona (1 million degrees). Where this material crashes back into the lower and denser solar atmosphere, a brightening can be seen.

Just like the X6-flare, the 7 June eruption took place near the solar limb. Being directed away from the Earth, the accompanying CME had very little impact on the geomagnetic environment. However, other solar explosions were much better positioned to influence Earth. In 2011, several periods with severe geomagnetic storming stand out.

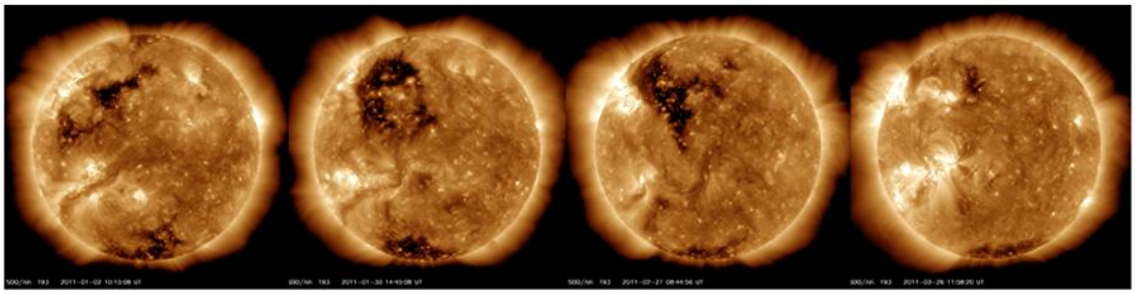

Figure 7: Geomagnetic disturbances are not only caused by CMEs, but also by coronal holes (CH). These SDO/AIA 193 images show the rise and fall of a recurrent CH and were taken on 2 January, 30 January, 27 February and 26 March (interval of about 1 solar rotation). In each case, the high-speed, low-density solar wind resulted in brief periods of minor geomagnetic storming a few days later.

On 3 and 4 August, NOAA 1261 unleashed respectively an M6- and an M9-flare. The explosions were accompanied by the ejection of 2 plasma clouds, which were not squarely directed at Earth. As the first cloud had to make its way through the much slower solar wind, the second one – although having the same initial speed of about 800 km/s, and having left the Sun 15 hours later – was able to catch up ("cannibalize") with the first CME. Earth did only receive a glancing blow of the resulting monster-CME.

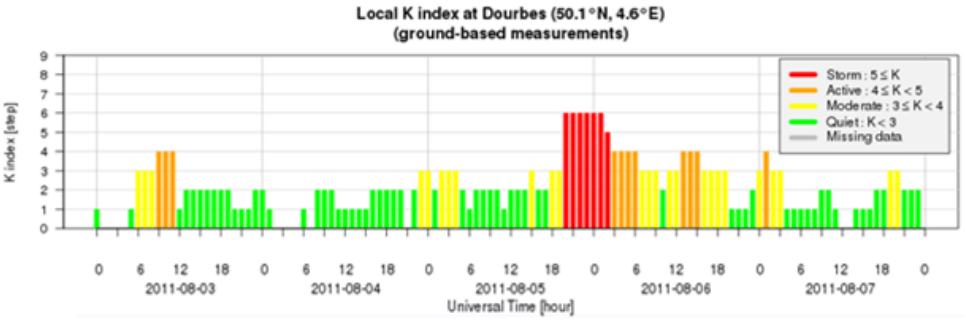

Figure 8: Magnetometers at Dourbes recorded the geomagnetic storm in the night of 5-6 August. Major storming was locally observed for over 6 hours.

Nonetheless, even then the speed and density of the cloud compressed the protective geomagnetic field enough to directly expose the geostationary satellites to the harsh environment of the solar wind's energetic particles. As the direction of the CMEs magnetic field was strongly southward, it also allowed an easy connection with the Earth's magnetic field triggering a severe geomagnetic storm. Hence, in the night of 5-6 August, aurorae were visible at geographical latitudes comparable to Belgium, albeit low above the horizon.

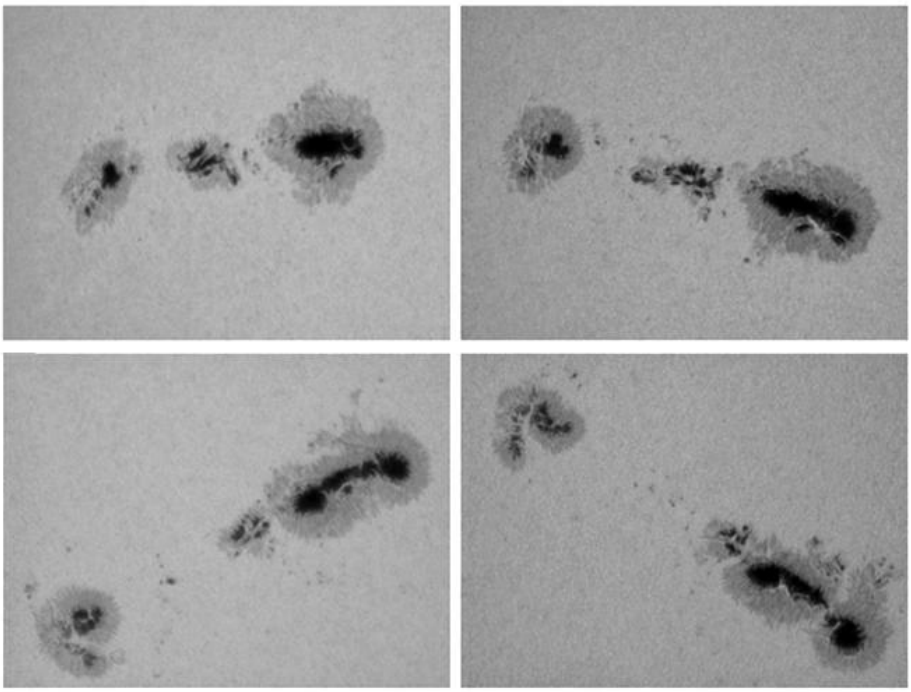

Figure 9: Ominously looking sunspot group NOAA 1302 as it appeared from 25 to 28 September. These exquisite images were taken by Bruno Nolf, member of the Belgian Solar Section of the Vereniging Voor Sterrenkunde. The contribution of amateur solar observers in various domains of solar research (SSN, H-alpha, radio,…) is highly valued by the STCE.

On 6 September, NOAA 1283 produced an M5- and an X1-flare hurling a couple of CMEs directly at Earth. These hit Earth on 9 September. The ensuing 18-hour lasting geomagnetic storm "only" reached severe storm levels, with no aurorae visible in Belgium.

Late in September, the very active region NOAA 1302 appeared. During its 13-day-transit over the solar disk, it produced 17 M- and 2 X-flares, which is comparable to what the Sun produced in 2010, *for the entire year*! Just like earlier in the month, these M- and X-flares had noticeable influences on the radio-communication on the Earth's sunlit side.

The flares released on 24 September resulted in very severe geomagnetic storming on 26 September, with similar results as early August.

The CME from a filament eruption that occurred on 22 October caused a severe geomagnetic storming 2 days later. Geostationary satellites were briefly exposed to the energetic solar wind. However, this storm will especially be remembered for its magnificent display of blood red aurorae, visible as far south as Texas and California. The event provides additional info for this rare and not-fully-understood type of aurora.

In conclusion, it can be stated that solar activity is now really on the rise to a maximum most probably in 2013. As the number and complexity of the sunspot groups increase, so will also the number of solar eruptions and CMEs. Hence, it is fairly obvious to conclude that Earth and its technology will suffer more and more heavily from these events in the years to come.

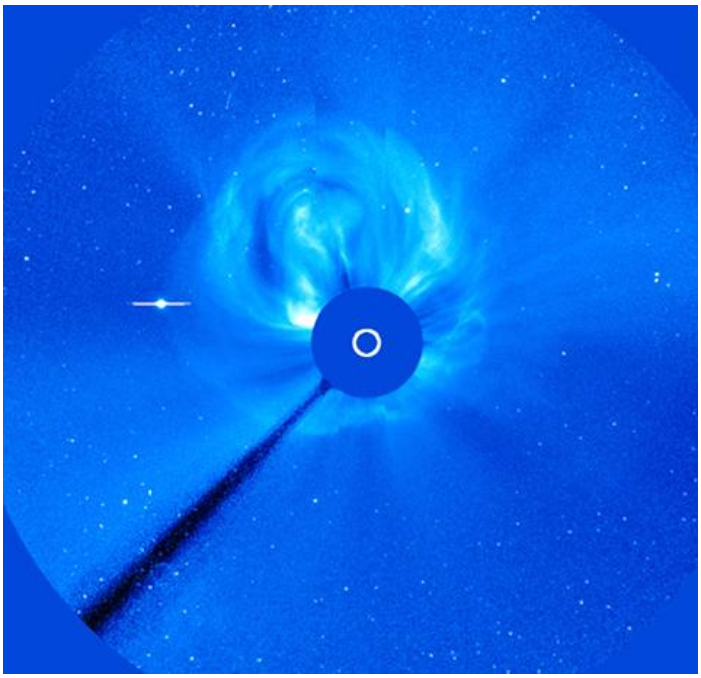

Figure 10: Halo CME as observed through one of the coronagraphs onboard the SOHO spacecraft on 4 October. Fortunately, the CME was caused by an eruption on the backside of the Sun. This was confirmed by the STEREO-satellites observing the Sun currently at near 90°-angles with the Earth. Hence, this CME is directed away from the Earth. However, tiny Mercury (bright dot on the left) was in the direct line of fire. These observations give enough advanced warning to the ground controllers to take the necessary protective measures for the Messenger spacecraft, which is orbiting this scorching hot planet since March 2011.

The 8th European Space Weather Week

The STCE as the host for the European and Worldwide Space Weather Community

The STCE organized the 8th edition of the annual European Space Weather Week, THE European event that is compulsory in the agenda of all people involved in space weather, be it scientists, students, users, product developers commercial entities, funding agencies, national delegates etc.

The ESWW is unique because it involves all aspects of space weather: from science to operations to applications, from scientists to users.

This year's edition welcomed around 330 participants worldwide, some coming from as far afield as South Korea, China and Brasil. The ESWW gives huge international visibility to the Solar-Terrestrial Centre of Excellence and to all Belgian Space Weather-related activities in general. We pride ourselves also in contributing to a positive image of our country by including a taste of its cultural wealth.

Figure 11: The poster announcing the eighth edition of the ESWW. The ESWW logo in the top left corner expresses that we can't neglect space weather: Earth in the grip of the Sun, THE space weather source.

Space weather is a very dynamic field that is continuously progressing. Especially in Europe, the space weather community is growing in professionalism and maturity. Space weather got a boost in recent years thanks to the significant investments by e.g. the EU 7th Framework Programme (FP7) and by the Space Situational Awareness (SSA) Programme from the European Space Agency (ESA). The growing number of space weather programmes highlights the raised awareness and the increased importance of space weather. Indeed, our vulnerability to it is increasing as we rely more and more on space technology.

The European Space Weather Week offers the platform for different groups with an interest in space weather to meet in a formal and informal environment, during the plenary sessions, the numerous splinters and several side events like the tutorial, the space weather fair, the debate-evening.

The ESWW started off in the ESTEC site of ESA in the Netherlands in 2004. From 2006 onwards, STCE took over the organization of the event and organized it in different parts of Belgium. Brussels, Bruges and – this year – Namur hosted the ESWW.

The content line up has always been tidily cross linked with what was and is living within the space weather community. Science, applications, innovations within the field, modeling,… were discussed

during the plenary and poster sessions. But it was clear that the participant's initiatives and input needed space. Starting with the fourth edition, the participants got the opportunity to fill contents blocks themselves in parallel sessions. These splinter meetings provide the chance to meet in smaller groups and address key issues in a style that complements the predefined plenary sessions. For ESWW4, we had 10 splinters, ESWW5: 10, ESWW6: 13, ESWW7: 16, and ESWW8: 29!

Since the fifth edition, scientific side-events have become a new important key aspect. These non-regular events are one of the attraction poles that make the ESWW different from regular science conferences. The Space Weather Tutorial and Quiz opens the week since the fifth edition. We shifted from the classical lectures to a supersonic introduction to the definition of space weather, a series of small workshops and a 'Question & Answer' session during ESWW8. To conclude the 2011 edition, we fired 'true or false' questions with lightning speed during the 'Rocket quiz'. The tutorial is successful: It is evolving to an interactive format and the number of participants grows steadily. In 2011, we had around 120 people and a commercial company in the class room.

Figure 12: The ESWW is an excellent opportunity to meet other people involved in space weather. At the ESWW, you get to know the people, projects and agencies.

Figure 13: An impression of the debate in 2011 with Stuart Clark as moderator and 5 panel members.

The Space Weather Fair is what it says: A market with stands advertising for a space weather product and application. If your stuff doesn't get the attention it deserves, the Fair offers an alternative. The success of the fair has grown throughout the years with 6 stands in 2008, 7 in 2009, 12 in 2010, and 16 in 2011.

The contest 'The Best of' introduced a friendly competition between young scientists to win the title for the best oral or poster presentation.

The First Attendees Meeting, FAM was held during the fifth edition of the ESWW. It was a meeting for people new in space weather and for those coming for the first time to the Space Weather Week. It took the form of a press conference with 'Question & Answers', through a panel consisting of the members of the scientific organizing committee on one side and the audience on the other side. The resulting one hour scientific panel debate is since 2009 part of the program. This year, around 150 people in the audience listened to and questioned a panel of experts about space weather risks to navigation.

Another innovative event is the End users' lunch, added since ESWW7. This year's edition was particularly well-received. The recipe is now clear: mix a well described subject – Geomagnetically

Induced Currents in this case – with a selection of participants that have a profile matching the subject, add a good moderator and some good food, and you get a successful cocktail.

Mrs. Laruelle, Minister of Science, visited the ESWW8 on the welcome evening and expressed the need of space weather research. Belgium is one of the European countries that make considerable efforts in funding and supporting this relative new science. Also present were Mr. Denis Mathen – Governor of Namur and Mr. Jean-Marc Van Espen – Deputy of Namur.

Figure 14: Mrs. Laruelle, Minister of Science, visited ESWW8.

Besides the science and business, the ESWW offers a variety of social activities: a keynote lecture, a 'science café' with beer tasting, the conference dinner, an excursion to the underworld of Brussels, mini-Europe, a quiz, a musical intermezzo, a welcome reception - one year with dinosaurs watching you, the other year with the art of Salvador Dali in your back, with historic music instruments in the background, ...

What has the Solar-Terrestrial Centre of Excellence to do with the European Space Weather Week? Everything: a scientific partner, the key organizer, from the smallest issues to the big stuff, the host institute with Belgium as the host country. The STCE is within the ESWW community a VIP: a Very Important Partner.

It's only thanks to the organizational talent of Anne Vander Syppe and Petra Vanlommel, the IT support of Sarah Willems, Elke D'Huys, Bram Bourgoignie, the support of Olivier Boulvin, Olivier Lemaître, Sophie Raynal, the graphical skills of Wim Van der Putte, the aid of the technical service of the Royal Observatory of Belgium, … that the ESWW could grow into the event it is now.

Public Outreach

Spreading the news

Already since its foundation, the STCE recognizes the need and urge to communicate about its developments, science, and services. This effort is not restricted to the persons and groups within the scientific community, but goes well beyond that. In particular, we also target the general public and the press, children, companies and political agencies. We want to open up the concept 'space weather' and make it accessible for all that could have a potential interest and learn to understand the information that is offered and how to use our services.

- Hot News

In 2011, we sent out several press releases to the (Belgian) press. Of course, we have to say those things that are relevant for the general public. It is nice to know that the Sun produces radiation storms and ejects plasma clouds at speeds between 300 and 2000 km/s. It's nice to know that navigation is affected by space weather. But we must not forget to tell how these solar events impact them. We have to repeat our message such that the general public and the press become aware of space weather. We cannot forget that the general public covers 99.99% of the population and represents the public opinion.

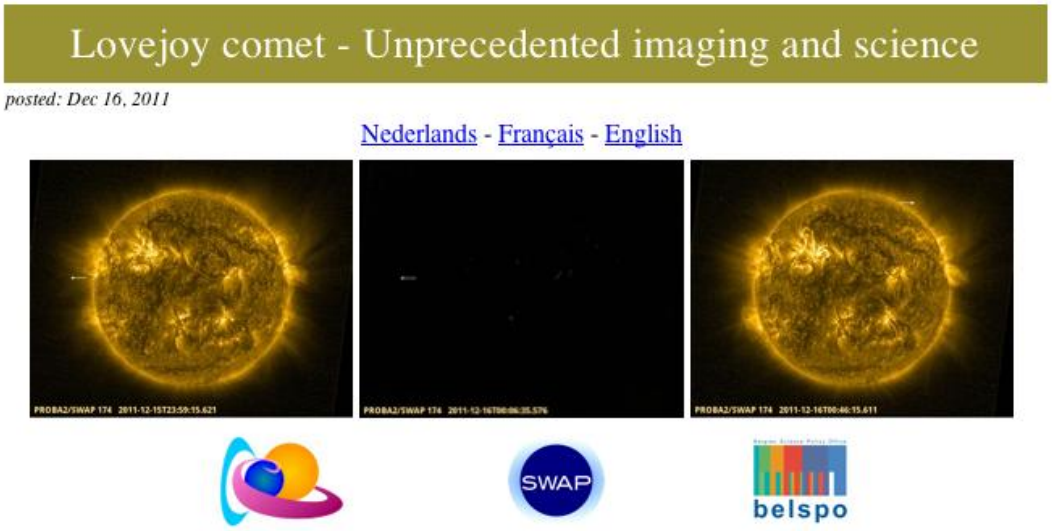

Figure 15: The comet Lovejoy came into the field of view of PROBA2 on December 16. It was only the second time ever that a comet was observed in an extreme-ultraviolet (EUV) solar telescope.

A large group, of course not as large as the general public, consists of people with a strong interest in space and space weather. We reach them through the website on which we publish on a regular base 'News Items' (Check out http://www.stce.be/news/index.php). These items provide information on important projects, solar events and its repercussions on the Earth, our science, satellite observations,... In 2011 we reported about special events like a solar eclipse seen by PROBA2, the comet Lovejoy, and solar activity.

- PROBA2@school

Since 2010, we do a special effort to promote “our” satellite PROBA2 in high schools. The project was baptized PROBA2@school. It started as a collaboration with the Vliebergh-Senciecentrum (VSC), which is part of the ‘Academisch Vormingscentrum voor Leraren’ of the KU Leuven, Belgium. The center offers teachers and representatives of educational studies the opportunity to follow extra courses to keep up with new developments in the field of education and scientific research. The goal of the project was to capture the attention of teachers in Dutch high schools in Belgium and give them information about Space Weather and the PROBA2 satellite.

The information booklet ‘Ruimteweer waarnemen met een Belgische satelliet’ (D’Huys and Vanlommel 2010) was presented during a Wednesday afternoon: Key issues of space weather, space weather forecasting and PROBA2 passed the scene. It can be used by the teachers to prepare lectures on this theme.

Figure 16: On the left, the booklet that presents space weather, space weather forecasting and PROBA2. On the right, an image showing students practicing image processing using SWAP EUV images.

The schools involved could visit the PROBA2 Science Center at the Space Pole. It's a day filled with information about space weather and PROBA2, a tour in the solar dome, a chat with the PROBA2 operators and a visit of the PROBA2 operation room, practical workshops about image processing, as well as a 'space weather and PROBA2 quiz'. The students get a sniff of how it works here and who does the work. They get a bite of space weather, the Sun and PROBA2 through workshops. There, they learn to use, interpret and handle satellite images, get to know the secrets of a satellite and how it is built.

Schools that were unable to come, got a visit from us and our scale model of PROBA2. The scale model is a 1:1 model made by the technical service at ROB. Our PROBA2 has travelled in the meanwhile already through many cities in Belgium.

The PROBA2@school project has been successful and continues to be so. The response from teachers and students has been very positive.

- STCE stand at Le Bourget

The STCE was an exhibitor at the 49th International Paris Air Show – Le Bourget, which took place on June 20 – 26. The STCE stand illustrated the involvement of Belgium in space and space weather, highlighting several projects like the RWC, BRAMS (Belgian RAdio Meteor Stations), the Demelab activities (Detectors, UV filters, Virtex-5 FPGA for onboard image processing), PROBA2, SIMBA (Sun-earth IMBAlance radiometer) and Picard. Information about space weather and the different STCE projects was provided to the visiting public and professionals.

Figure 17: STCE stand at Le Bourget, with screens, instruments and posters.

A large public was attracted by the still "new concept" of space weather. The STCE scientists were questioned about the influence of the Sun on our planet and about the Sun's life and cycles. The STCE stand at Le Bourget was a real success. The team hopes to participate in the next edition of this airshow.

The STCE Newsletter

The STCE Newsletter was released on December 15, 2011. It is an online, English space weather bulletin, issued on a weekly basis. The newsletter gives an update of the solar activity, the geomagnetic activity and the geomagnetic measurements done in Dourbes. The letter informs about the PROBA2 satellite measurements and performances. It presents solar and space weather highlights and background information about the STCE science or STCE activities in general. It lists the national and international meetings and conferences in the field of Space Weather. Interested people, scientists, students, users and STCE members are invited by e-mail to check the latest news.

The Solar-Terrestrial Centre of Excellence is not a virtual institute. It is an institute of people, scientists, engineers, IT-people,… that work around a common theme: "the Sun, Space and the Earth". This common ground needs to be put explicitly on the foreground. One way is by simply communicating about the work we do. Several STCE projects provide information through their own website: the European Space Weather Portal, the SIDC website, the PROBA2 website,… All are very nice, but the result is that all this information is given in a fragmented form.

We wanted to strengthen the communication within the STCE and to the community interested in space weather. We wanted to bring the fragmented STCE news together such that it is visible at a glance. The efforts that were done within the STCE deserve more attention. More people should be able to find their way to all this information. And so the idea of the STCE Newsletter was born.

The STCE Newsletter has a simple and straightforward identity: a weekly digital journal, archived online, with short informative texts pimped up with images. At the same time, it is an extra channel to reach people outside the solar-terrestrial community. Interested people, be it scientists, laymen, students or users, people belonging to the solar-terrestrial science community, professionals and non-professionals alike are invited by email to check the latest news.

Figure 18: The STCE newsletter communicates to the STCE members and others interested. The bulletin makes sure that people keep track of the most important issues and events within the STCE.

The content is provided by STCE members. It offers a common platform to communicate on their work, what's happening on the Sun, in space, on Earth, and on newly developed applications and products.

Figure 19: A snapshot from the STCE website of one of the STCE Newsletters. The Sun released a big solar light flash on July 12. Through the newsletter, figures, links to movies and background information on this solar event find their way to an extended public, even beyond the STCE community. The bulletin about the solar and geomagnetic activity of the last week is a fixed item, together with the geomagnetic observations done in Dourbes. The STCE Newsletter items reflect on what happened the previous week in the solar and geo-scenery, on progress in projects, on hot news about instruments,... as long as there is a solar-terrestrial connection.

Good to know you!

- Annual STCE meeting

With the sentence 'Good to know you' in mind, we organize every year a meeting for all STCE members and people interested in the STCE. This annual meeting grew from a regular 1 day meeting filled with a non-stop series of presentations to an event spread over several days with room for discussion, collaboration and - of course – also simply providing information.

The 2011 edition focused on the past highlights and future opportunities and challenges. STCE members proposed a workshop during the month of May. All people within and beyond the STCE with an interest in the subject could join and contribute. In this way, common interests and overlaps became visible and could immediately be discussed. We had 6 workshops, each emphasizing another subject:

- Retrieval of Aerosol Properties from Satellite and Ground-based measurements,
- Radio Science Workshop,
- Water vapor, meteorology and climate,
- Accessing and Exploitation of SDO data,
- Ionospheric research and services: present status and future development,
- Alfvén Waves in Solar & Space Plasmas.

The actual annual meeting took place on 07 June 2011. The appetizer session started with the 'hot' news from Picard, a micro-satellite to study the relationship between the Earth's climate and the Sun's variability. Picard had already 1 candle on its birthday cake: It was launched on June 15, 2010. Steven Dewitte is the Principal Investigator (PI) of the instrument SOVAP, SOlar VAriability Picard, which was made in Belgium and is measuring the variability of the solar energy output - very relevant for climate change.

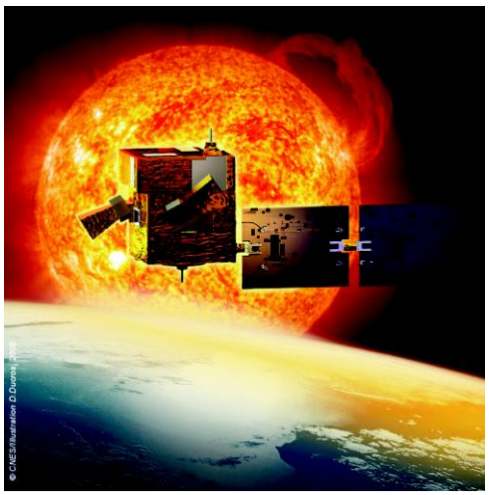

Figure 20: The PICARD satellite was launched in June 2010 with onboard the SOVAP instrument of which Steven Dewitte is the principal investigator.

The next item on the agenda was the ESA program 'Space Situational Awareness'. The STCE can play an important role in the space weather part of the program. An overview of the STCE highlights, opportunities and challenges concluded the opening session. Then the workshop conveners presented a wrap up with a focus on the collaborations within and outside the STCE. Participants of the aerosol workshop concluded that a comparison between the dust aerosols measured over the desert could be compared with those over the ocean, the different aerosol groups could converge their aerosol models and the software tests. The radio group focused on 3 questions: Which are all the radio science projects carried out on the plateau, which techniques and methods are used, can the groups share the software or even the hardware? It turns out that the different radio groups -BRAMS, Humain Radio-astronomy Station, SAFIR, GNSS- found different links. Three institutes from outside the STCE (KULeuven, VITO, IAS) participated in the workshop on 'Water vapor, Meteorology and Climate'. The discussions led to a constructive return on each other's work and to an inter-comparison study of the different topics. The

Alfvén waves workshop convened the people busy with fundamental physics of space plasmas. They will investigate possible cross links between terrestrial auroras and solar flares and adopt the theory of turbulence to the solar wind. The discussions within the SDO workshop could be possibly translated into actions to improve the technical performance of the SDO data center. On the other hand, SDO could offer valuable data for several FP7 and space weather related projects. The ionosphere group coupled the ionosphere research and developments performed at the RMI with the GNSS-based ionospheric research at ROB, and with the plasmaspheric research at BIRA-IASB. These ionospheric monitoring services are of direct use for the space weather forecast services.

The annual meeting turned out to be a success by providing a trigger to break out of people's confined science team. The meeting's overview is at http://www.stce.be/annualmeeting/annualmeeting2011.php

- Science & Coffee

Within our STCE community, we pay special attention to sharing information and science. The annual meetings are a school example for this. The STCE however recognizes the importance of communication with the whole science community. In this frame, the STCE developed a 'visitors program'. STCE collaborators can propose visitors to the STCE in order to enhance collaboration. Preference is hereby given to visitors who can work with different teams at the Space Pole. Each is requested to give a seminar or a series of lectures such that everybody can benefit from the work visit. These seminars are freely accessible for all. The series of seminars is of course not limited to visitors only: Space Pole staff are also invited to share their know-how. Information about our activities, seminars and abstracts are provided on a google calendar

http://www.stce.be/seminars/agenda.php

Fundamental Research

Science underlies understanding and predicting the space environment.

The long-term goal of this project is to perform first-class science in various domains related to solar-terrestrial science (solar interior and surface, solar atmosphere, solar wind, auroral physics, solar-terrestrial relationships …) in close collaboration with the science staff of the Institutes and other Belgian and international scientific teams. The main objective is to achieve a better understanding and modeling of fundamental plasma physics processes in the solar-terrestrial connection from the Sun to the Earth. Among other components, this includes theoretical investigation of plasma waves, instabilities, and wave-particle interactions, and their applications in the solar atmosphere, solar wind, and terrestrial magnetosphere.

A small-sunspot deficit in solar cycle 23

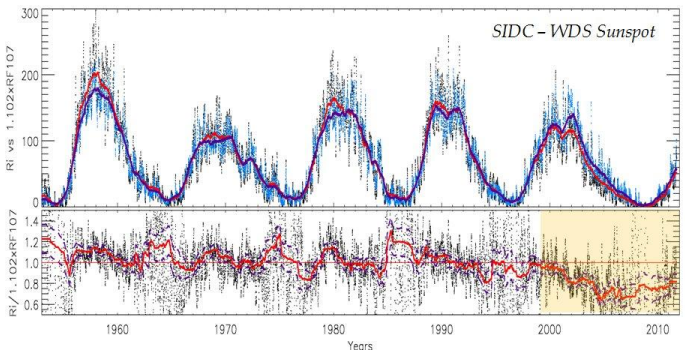

Figure 21: Comparison (top) and ratio (bottom) of the sunspot index Ri and the F10.7cm radio flux, showing the deviation after about year 2000.

Since the last maximum of solar activity in 2000, a systematic discrepancy has appeared between the international sunspot index R_i, produced at ROB, and several other solar indices and fluxes (Figure 21). This anomaly could be due to a flaw in the R_i index calculation but it could also correspond to other unusual properties of the past solar cycle: internal rotation, surface flow speeds and longest minimum of activity since one century (Figure 22).

In order to diagnose the source of this discrepancy, we exploited the much more detailed information contained in several sunspot catalogs. For this purpose, in the context of the SoTerIA project (FP7), we worked with the two richest catalogs currently available: the Debrecen Photographic Data (DPD) and the NSO/USAF catalog available from NOAA. As those catalogs contain different but complementary information, we merged them into what must be the richest sunspot catalog currently available. In order to guarantee the completeness and accuracy of the output, this merging involved the identification of defects, inconsistencies and mismatches in both catalogs. As a complement, this validation process made partly use of the Uccle sunspot catalog based on the 70-year-long ROB collection of sunspot drawings (Figure 23), which is still in construction (completion foreseen in 2012).

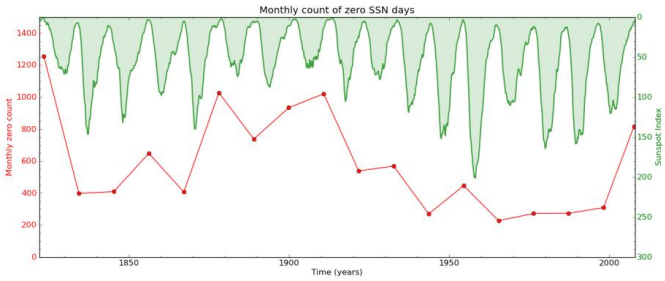

Figure 22: Total number of spotless days during the last 18 minima of the solar cycle. It shows the strong anti-correlation with the cycle amplitude (green, reversed scale). The last minimum exceeds all minima since the early 20th century.

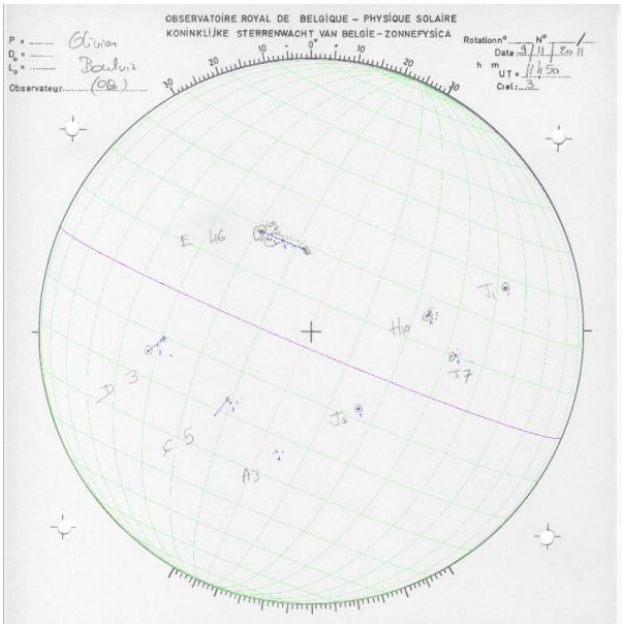

Figure 24: Sunspot drawing for November 9, 2011 (USET, ROB) showing the Sun at its most recent peak of activity. Screenshot with overlays from the DigiSun on-screen measuring software developed at the ROB.

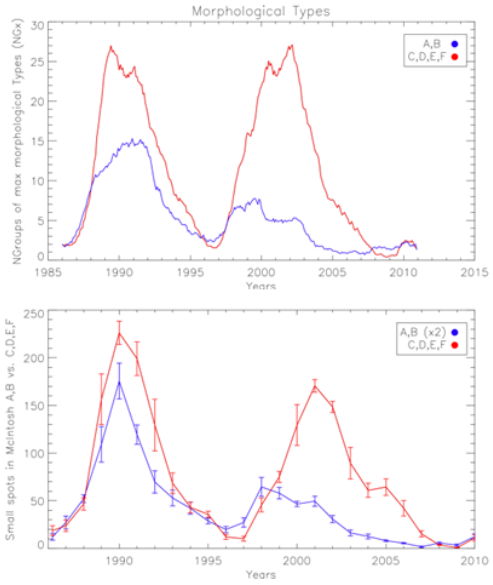

Figure 23: Count of small sunspot groups (A,B, in blue) and large sunspot groups (C,D,E,F, in red) during cycles 22 and 23 (left plot). Count of small spots inside groups on the same period (right plot). Both show a strong deficit affecting only the small spots.

Our investigations first showed that there was no intrinsic flaw in the sunspot index itself, which hinted at a true physical change in the Sun. We thus conducted extensive statistics of the populations of sunspots according to their sizes and lifetimes, considering both entire sunspot groups and also the individual sunspots forming each group. Our results show that, while the count of large groups was not different in cycle 23 compared to earlier cycles, small groups showed a strong deficit by a factor of 2 to 3 in cycle 23 (Figure 24). This deficit also appears in the groups themselves where the relative number of small spots with the shortest lifetimes (< 2 days) has dropped in all active regions, even the large ones, in cycle 23. This transition took place around 2000, i.e. at the time when the relation between the sunspot index R_i and other solar indices started to deviate.

Based on this detailed and independent evidence, the index deviation can then be naturally interpreted by the higher contribution of small spots in the sunspot index value compared to most other solar indices, which are heavily weighted in favor of the largest spots and magnetic fields. This strongly scale-dependent change in the distribution of sunspot magnetic fields calls for an interpretation. It matches rather well another independent observation: the steady decline of the average magnetic field strength in the core of sunspots reported by Penn & Livingston (2009, 2011). Both effects are not reproduced by the current flux transport dynamo models of the solar cycle. They may involve a distributed dynamo effect, not only confined deep inside the Sun, but with an additional component closer to the surface and acting on small-scale magnetic fields. Further investigations of such long-term changes in the regime of solar activity will rely on past and present synoptic observations, such as the white-light and Hα photographic and CCD images routinely produced by USET.

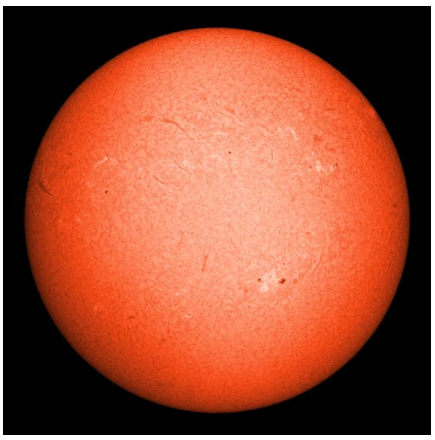

Figure 25: Synoptic image of the chromosphere at a fairly high level of activity on December 6, 2011 (Hα, USET, ROB)

Observation of quasi-periodic pulsations during solar flares

Solar flares are powerful energy release events in the solar atmosphere that are characterized by the sudden increase of electromagnetic radiation in a wide spectral range. Quasi-periodic pulsations (QPP) are frequently observed during such flares, most of the time in radio and hard X-ray wavebands. They consist in fluctuations of the irradiance occurring on various time-scales (from milliseconds to several minutes).

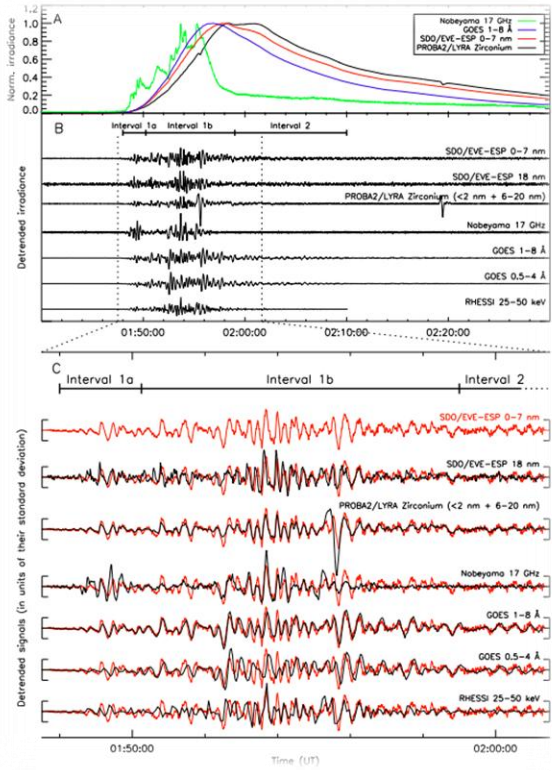

Figure 26: Simultaneous observations of a flare in several wavebands

Several instruments observed an X- flare on February 15, 2011 and the associated QPP during its rising phase, in many wavebands:

- ***Hard X-rays (RHESSI)***
- ***Soft X-rays (SDO/EVE, PROBA2/LYRA, GOES)***
- ***Extreme UV (SDO/EVE, PROBA2/LYRA)***
- ***Radio (Nobeyama Radiopolarimeters)***

Panel A: variation of irradiance in radio (green), soft X-rays (blue, red) and Soft X-rays/Extreme Ultra-Violet (black).

Panel B: QPP are revealed by removing the global trend of the irradiance. As the QPP emission represents only a few percent of the increase of irradiance in most wavebands, it is necessary to filter the signal to reveal them.

Panel C: a zoom over the time interval during which QPP occurred. The same fluctuations are present in many wavebands, but with different time delays (the red curve, in soft X-rays, is repeatedly overlaid for comparison).

The first X-flare of the new 11-year solar cycle occurred on February 15, 2011. X-flares are the most powerful kind of flares; they represent a small fraction of the total number of flares within a solar cycle. We took this opportunity to study a QPP event simultaneously in as many wavebands as possible, taking advantage of the unprecedented wavelength coverage offered by recent launches of solar observation satellites, including the satellite PRoject for On-Board Autonomy (PROBA2) operated by ROB (http://proba2.oma.be/).

Oscillations in the range of periods that we observed (11 s) are thought to be associated with Magneto-Hydro-Dynamic (MHD) waves, a kind of waves that appears in magnetized plasmas (the solar corona is almost completely ionized and pervaded by the Sun's magnetic field). By interpreting the QPP in terms of a stationary wave mode in the flaring magnetic loop, it is possible to derive information on various physical phenomenon and quantities involved in the eruption. The period of oscillation depends on the plasma density, magnetic field strength and length of the flaring loop (van Doorsselaere et al. 2011, ApJ 740, 90). The time lags of the fluctuations between different wavelengths are influenced by the effect of energetic charged particles being trapped in the magnetic loop, as well as by cooling effects in the plasma that is strongly heated during the flare (Dolla et al. 2012, ApJ 749, L16). Researchers are only

starting to exploit the possibilities of QPP in order to shed light on the mechanisms that drive solar eruptions.

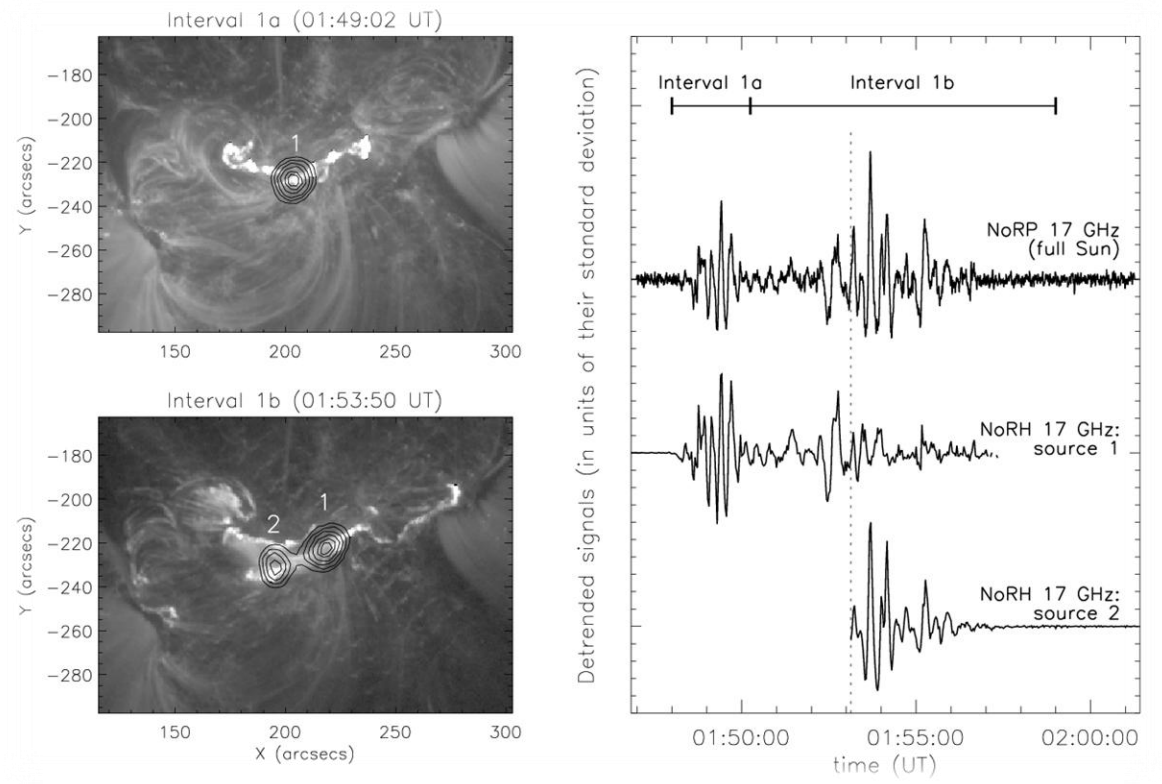

Figure 27: Localization of the QPP emission - During the particular event of February 15, the QPP appeared grouped into two main "packets" (which we isolate in time intervals called "1a" and "1b"). No solar imagers provided fast enough observations to identify the regions that emitted the QPP, except the Nobeyama Radio Heliographs (Japan). Strong radio sources were present during the rising phase of the flare (left panel: radio intensity contours overlaid on an EUV image from SDO/AIA). They proved to be the location of the QPP in radio wavebands (right panel). The first QPP packet was associated with source "1", which started to move when this packet event ended. A second QPP packet started and was associated with source "2" that had just appeared. The radio sources are close to the bright "ribbons" seen in EUV; these ribbons correspond to locations where highly energetic particles produced during the flare in the corona precipitate toward the solar surface.

A remarkable radio-event: a stationary shock

The Humain station near Marche-en-Famenne is a radio astronomy facility that is run by ROB since the mid-1950s. Since 2008, some of the radio telescopes on site are refurbished to host a new set of receivers dedicated to space weather monitoring and science studies linked to solar eruptive events (flares and CMEs).

A Callisto spectrograph observes the Sun since June 2008 and is following the rise of the solar activity cycle by recording an increasing number of solar radio bursts. If most of them are type III bursts linked to small reconnection events, Callisto has witnessed a series of remarkable events in the course of 2011, especially during the summer and the fall of that year.

Apart from the above mentioned type III bursts, solar radio astronomers are also very keen on observing type II bursts, which are signatures of coronal shock waves triggered by solar flares and coronal mass ejections. The drift in frequency is an indication of the velocity of the driver of the shock, which might not be easily determined by other means.

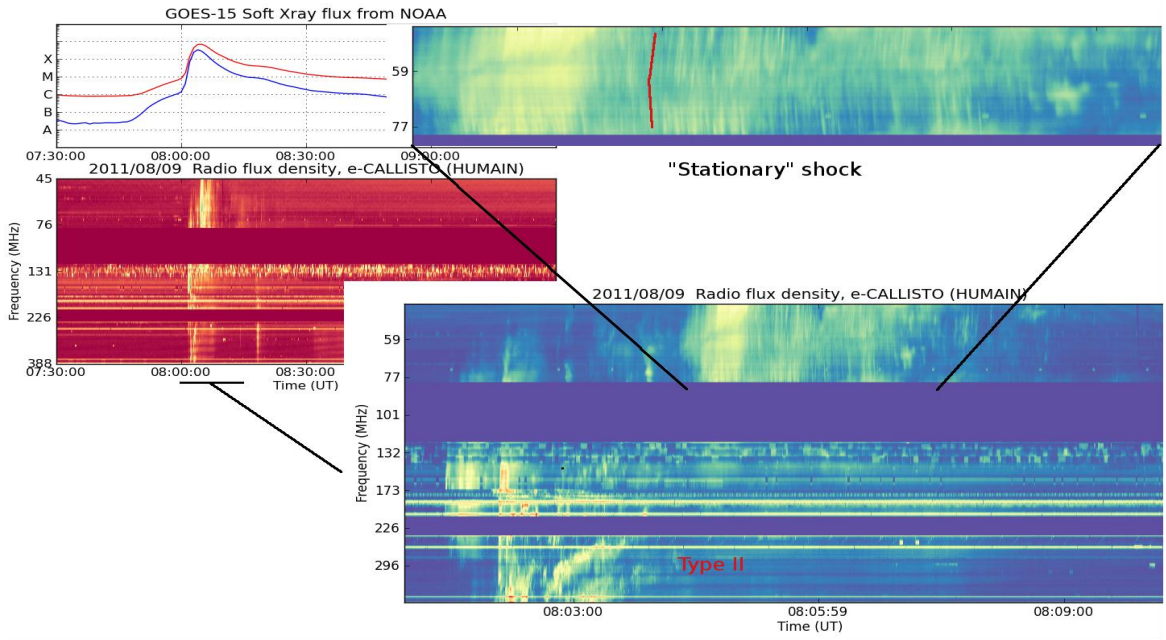

Figure 28: Flare event of August 9, 2011. The « classical » type II burst is indicated in red (bottom figure). On the top right figure, sunward and anti-sunward directions are shown in red to guide the eye.

On August 9, 2011, an X6.9-flare occurred around 08:00 UT in NOAA AR 1263, close to the west solar limb. The flare was accompanied by a fast halo CME and a type II burst indicating that a coronal shock wave propagated in the wake of the CME or of a blast wave produced by the flare. We clearly see the type II burst around 08:03 UT (see Figure 28).

However, a minute and half later, higher up in the corona, a usual shock signature can be observed (top right panel of Figure 28). We suppose it's a shock signature since we do see fine structures often detected in classical type IIs, which are called "herringbones". They are "type III-like" signatures of electron beams accelerated at the shock both in sunward and anti-sunward directions, which results in

oppositely drifting individual bursts. These are clearly seen in this event (two red lines are drawn to guide the eyes).

Very few events of this kind have been observed so far, and the exact nature of the associated shock is still not understood, especially so high in the corona. At higher frequencies, the concept of a "termination shock" occurring in a specific reconnection geometry has been invoked, but it's not clear yet if this can be transposed to the frequency range of this event.

Data from the Callisto instrument in Humain are available on the website http://sidc.be/humain within 15 minutes. Quicklook files, combined with GOES light curves are automatically produced.

Plasma waves and their solar-terrestrial applications

Results were obtained in the following domains:

1. Suprathermal tails and beams (i.e. protons that have velocities significantly larger than the average thermal velocity of the studied plasma of the solar wind) are prominent but still unexplained features of the proton velocity distributions measured in the solar wind. Since the turbulence of kinetic Alfvén waves (KAWs, i.e. Alfvén waves modified by temperature) is observed in the same velocity range, we tried to find out if this turbulence can generate proton beams and tails. Our analytical and numerical solutions demonstrated that the KAW turbulence can be responsible for the suprathermal proton tails observed in the solar wind (see Figure 29).

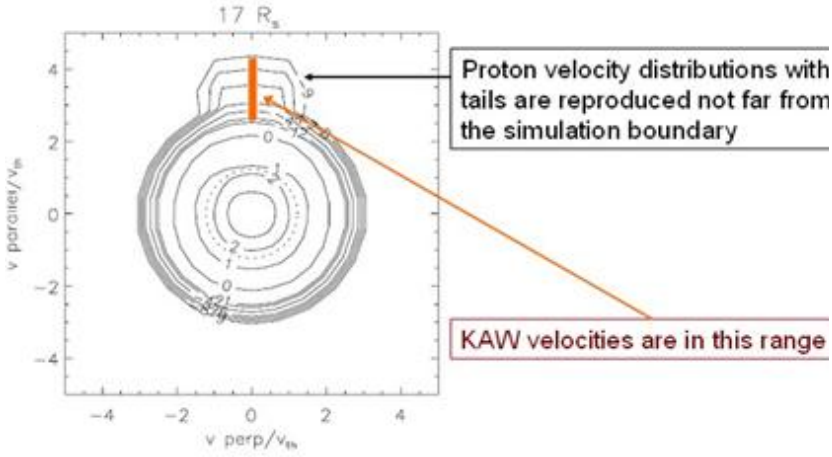

Figure 29: Proton velocity distribution obtained numerically at 17 solar radii (Rs) assuming a displaced Maxwellian as boundary condition at 14 Rs (Pierrard and Voitenko, 2012, submitted). A pronounced suprathermal tail is generated by the KAW turbulence.

Earthward-propagating inertial Alfvén waves (IAWs, i.e. Alfvén waves modified by electron inertia effects) are efficient in accelerating auroral electrons that are responsible for the polar lights. Our goal is to find the source of these IAWs and explain their observed spectral properties. By developing a second-order nonlinear theory for IAWs and studying their power-law turbulent spectra, the initial results suggest that auroral IAWs are powered by large-scale MHD waves via turbulent cascade.

2. A non-dissipative transition from MHD to kinetic Alfvén turbulence has been intensively studied during the last few years. Our goal is to consider dissipative effects in the MHD/kinetic turbulence transition, which are important for particles energization in space plasmas, and also for the transition itself. We found that the nonlinear Landau damping of high-amplitude KAW pulses accelerates protons from well sub-Alfvénic to well super-Alfvénic velocities. This process increases significantly the energy release in plasmas driven by turbulence.

3. A 3D dynamic model of the plasmasphere that was already developed by Pierrard and Stegen in 2008 has now been coupled to the international reference ionosphere model to determine the number density and temperatures of the different particles at lower altitudes from 60 to 2000 km (Pierrard and Voiculescu, 2011). An example of the coupled model is illustrated on Figure 30. In addition to the electron number density, the plasmaspheric model was also developed to include temperature profiles and ion composition (Pierrard and Borremans, 2012b). Moreover, a density-energy description of the radiation belts was obtained by using the kinetic approach (Pierrard and Borremans, 2012a).

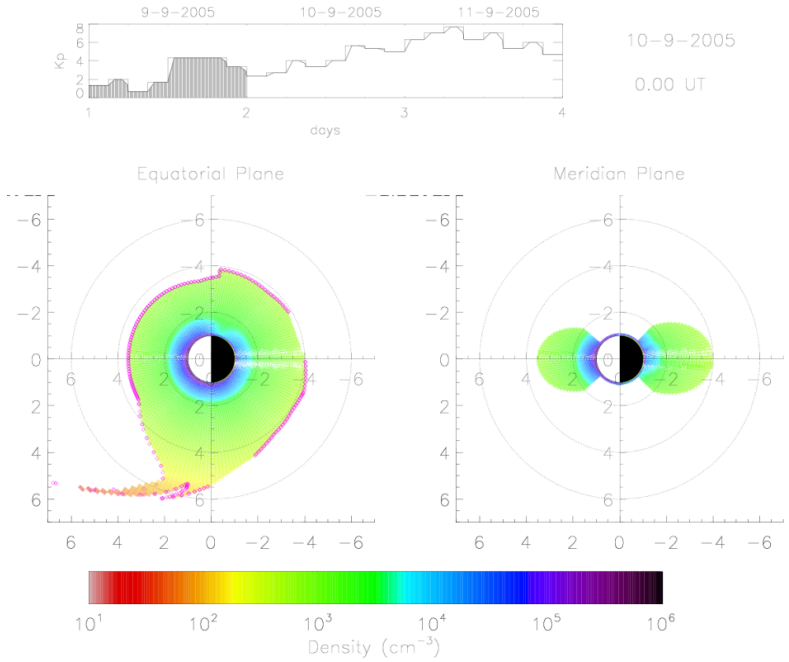

Figure 30: Density of the electrons obtained with the ionosphere-plasmasphere coupled model in the geomagnetic equatorial plane (left panel) and in the meridian plane corresponding to 12:00 to 24:00 MLT (right panel) on 10 September 2005 at 0:00 UT. The geomagnetic activity level index Kp observed from 9 to 11 September 2005 is illustrated on the upper panel (Pierrard and Borremans, 2012b).

4. Solar wind models were developed using the kinetic approach (Pierrard, 2012a). The solar wind heat conduction in particular was studied with collisionless exospheric models (Pierrard, 2011a). Effects of suprathermal particles (i.e. particles that have velocities significantly larger than the average thermal velocity of the plasma cloud) in space plasmas (Pierrard, 2012b) in general and in the solar wind in particular (Lazar et al., 2012) were emphasized, as such distributions with an enhanced population of suprathermal particles are often observed.

Atmospheric effects on GNSS applications

The objective of this research is to assess and mitigate the influence of the Earth's atmosphere on high-precision GNSS applications taking advantage of new GNSS satellite signals. When travelling from GNSS (Global Navigation Satellite System) satellites to receiving antennas located on the Earth, the radio-frequency signals emitted by GNSS (such as GPS, GLONASS and Galileo) interact with the Earth's atmosphere. The two atmospheric layers that influence the most the propagation of these GNSS signals are the troposphere and the ionosphere.

The troposphere is the lowermost atmospheric shell while the ionosphere is stretching from a height of about 50 km to more than 1000 km. The delay induced by the troposphere on the GNSS signal propagation is due (1) to the presence of the "dry"/hydrostatic atmospheric gases and (2) to the presence of water vapor in the atmosphere. The hydrostatic component of the tropospheric delay can easily be modeled from surface pressure measurements while the second part, the "wet" or non-hydrostatic tropospheric delay, is proportional to the atmospheric Integrated Water Vapor (IWV) and is therefore highly variable in both space and time.

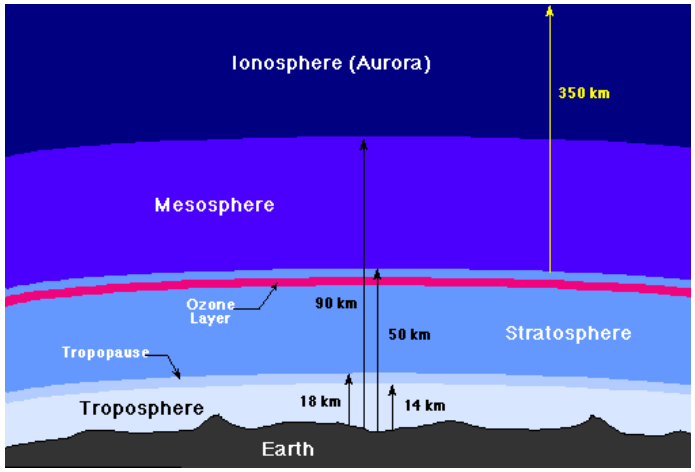

Figure 31: Subdivision of the Earth's atmosphere in different layers

The ionosphere is the upper part of the atmosphere. It received this name because it is ionized by the Sun's ultra-violet light; it is a shell of free electrons, electrically charged atoms and molecules that surrounds the Earth. As most of the space weather starts at the Sun, also the Earth's ionosphere is undergoing the effects of space weather. Moreover, the number of free charged particles in this atmospheric layer is the main parameter which disturbs the radio wave propagation and is of first importance for many applications (e.g. radio communication). In particular the ionospheric refraction implies GNSS signal delays. As the ionosphere is a dispersive medium, the ionospheric delays depend on the GNSS signal frequency, so that by using the difference between the delays observed in the signals of different frequencies, it is possible to determine the Slant Total Electron Content (STEC) between a GNSS ground receiver and a satellite. Then, the STEC is projected in Vertical Total Electron Content (VTEC) expressed in TEC units (1 TECU = 10^{16} $e^{-}.m^{-2}$) and which is independent of the satellite elevation.

Both the ionosphere and the troposphere refract the GNSS satellite signals. On one hand, they are error sources for GNSS applications. Tropospheric refraction causes errors of about 2-50 m on GNSS signals, while the errors caused by the ionospheric refraction can reach up to 50-150 m. On the other hand, GNSS observations from a ground network of permanently observing GNSS stations with known position allow to extract information on both the troposphere and the ionosphere.

GNSS allows computing positions on the Earth with precisions ranging from several meters down to a few mm, depending on the sophistication of the hardware and software used. When high-precision GNSS applications are targeted, the Earth's atmosphere becomes a predominant error source. The

effect of the tropospheric refraction on the propagation of GNSS signals can be corrected using several a priori models which satisfy the less demanding GNSS applications, like dm-m level GNSS positioning and navigation. For high-precision applications where mm accuracy is desired, the tropospheric error is precisely parameterized and estimated with the final position solution. As the ionosphere is a dispersive medium, GNSS applications can be corrected for first-order ionospheric effects by combining two GNSS signals having different frequencies. However, this first-order correction does not remove the full effect of the ionosphere.

- *Quantification of second-order ionospheric delays on GNSS signals*

The October 2003 geomagnetic storm (often called the Halloween storm) was one of the largest ionospheric storms yet recorded. Using GNSS data obtained by stations in the United States during this Halloween storm, we showed that the second order ionospheric effects on GNSS signals can be due to either the delays in the signals or (in combination with) errors in the satellite clocks computed by the International GNSS Service (IGS) without correction of the 2nd order ionospheric delays. In Figure 32 (left), we clearly see the deviating IGS satellite clock synchronization errors as soon as the ionospheric storm starts. In the same Figure 32 on the right, the associated TEC (Total Electron Content) in the ionosphere along the satellite signal path is plotted. As we know that for some stations this Slant TEC (STEC) can reach 600 TECU, the effect observed for the station ALGO (Canada) could be amplified by a factor 4 for other stations.

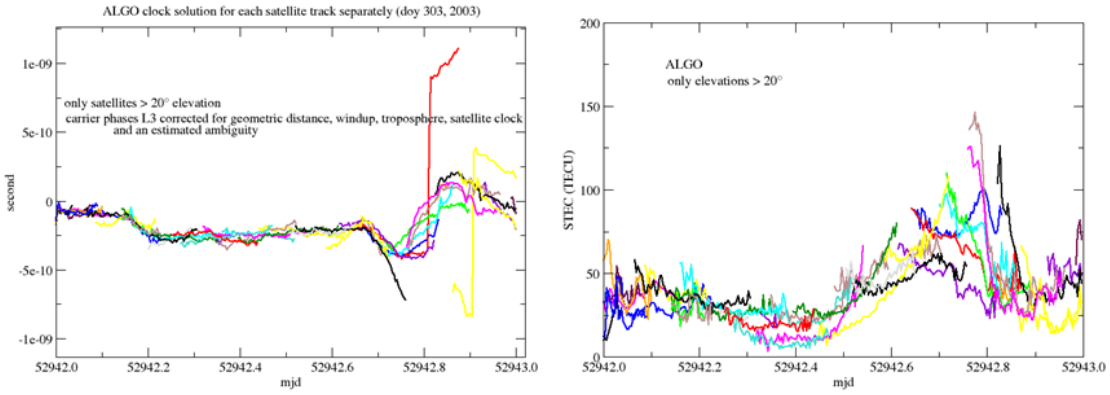

Figure 32: Improvement of modeling the 2nd order ionospheric delays for high precision applications. Left: Clock solutions obtained with the different satellite tracks separately during the day of the Halloween storm in 2003. Right: STEC corresponding to the satellite tracks depicted in the clock solutions (same color codes as in left figure).

STCE scientists also studied the optimal strategy for the mitigation of the higher-order ionospheric effect in scientific GNSS products (satellite clocks, satellite orbits, geocenter, Earth rotation parameters). Different models used to mitigate higher-order ionospheric effects have been evaluated and compared; they concern three parameters that enter in the modeling: STEC, the magnetic field, and the electron density. The impact of these parameters on the high-applications is still under evaluation. Furthermore, second-order ionospheric effects can also be removed from the combination of three-frequency signal measurements. Different combinations of three frequency signals measurements (carriers or codes) can be built with triplets of Galileo carriers and codes as well as modernized GPS. However, we have demonstrated that the proximity of the GNSS frequencies in the L band produces a huge increase in the measurement noise when the three-carriers are combined. We also showed that the combination of 2

GNSS signals from the L band with a possible future K_u band frequency signal could remove the 2nd order delays without any noise amplification with respect to the dual-frequency combination.

- *Ionospheric Climatological Modeling*

One of the future challenges of the space weather community is to predict the Earth's ionospheric state in response to variations of the solar activity. For that purpose it is important to understand the relation between the Sun's activity and the ionosphere. The beginning of the 23rd solar cycle (May 1996) coincided with the start of a catalog of global ionospheric monitoring based on GNSS data. In addition, many parameters of the solar activity are historically measured. This means that the relation between solar activity parameters and GNSS-derived VTEC can now be studied on a global scale for the entire 23rd solar cycle. The ultimate goal is to better understand the physical processes in the ionosphere during quiet activity as well as during stormy events and to improve the prediction of the ionospheric VTEC which is still a challenge for the space weather community.

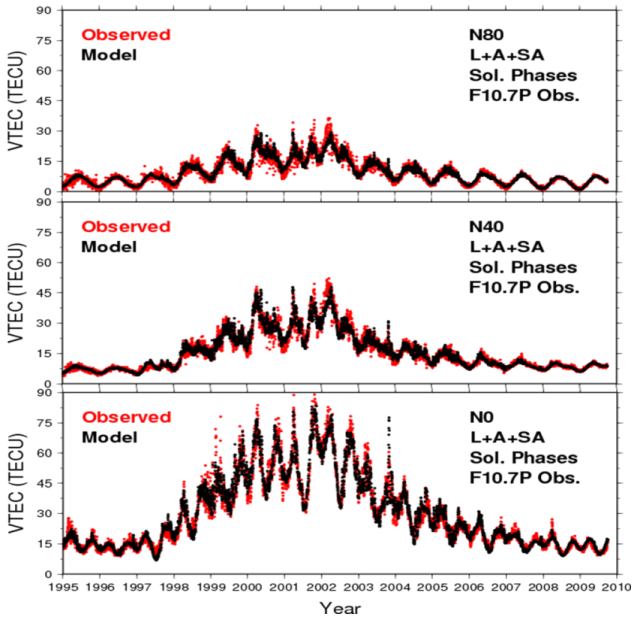

Figure 33: Estimated daily mean VTEC (=model in black) and observed (in red) for different geomagnetic latitudes. Bottom: geomagnetic equator. Middle: mid-latitude region. Top: polar region.

The study of the link between solar parameters such as the Sunspot Number (SSN) or solar Extreme Ultraviolet (EUV) emission and the GPS-based ionospheric Total Electron Content has been done for the first time for the previous solar cycle (1995-2008). We studied the linear correlations between the Daily Mean Vertical Total Electron Content (DMVTEC) in the ionosphere and the Sunspot Number on one hand and the F10.7P (a proxy used to derive the EUV which is not directly measured on the Earth's surface since it is almost entirely absorbed in the upper atmosphere) on the other hand. The best linear correlation (R=0.94) is obtained between F10.7P and DMVTEC. Moreover, when considering different seasons and solar activity phases (minimum, transition and maximum), this linear correlation is larger during the winter period in the southern hemisphere (R=0.97) and during transition phases in the solar activity (R=0.77±0.10).

Considering the results on the linear correlation between DMVTEC and F10.7P, we investigated the best way to model DMVTEC at a given latitude and a given time from only the F10.7P parameter as input. Using least squares, we estimated the coefficients of a model consisting of 1) a combination of annual, semi-annual and linear terms, and 2) a discretization with respect to the solar cycle phases (see Figure 33), in order to minimize the residuals between the modeled and observed DMVTEC. With the obtained model and for the period 1995-2009.7, the residuals between the modeled and the observed DMVTEC are below 3 TECU for 87% of the days at high latitudes, 85% at middle latitudes, and 77% at equatorial latitudes. The outliers (differences > 15 TECU between the model and the observations) are due to intense ionospheric storm events.

Instrumentation and experiments

Validation and first scientific results of the SOVAP instrument

The Solar Variability – Picard (SOVAP) instrument is one of the two instruments measuring the Essential Climate Variable (ECV) Total Solar Irradiance (TSI) onboard of Picard. SOVAP is a dual channel cavity radiometer with a left and a right channel. SOVAP is the sixth Differential Absolute Radiometer (DIARAD) developed by the Royal Meteorological Institute of Belgium (RMIB) in space, and it provides continuity for DIARAD/VIRGO on SOHO which has been monitoring the TSI since 1996. SOVAP also includes a Bolometric Oscillation Sensor (BOS) developed by the Royal Observatory of Belgium (ROB) which consists of a black and a white flat plate with full hemispherical view receiving both solar and terrestrial radiation. The BOS is particularly useful for Earth Radiation Budget (ERB) studies as it can cross-calibrate the terrestrial and the solar radiation.

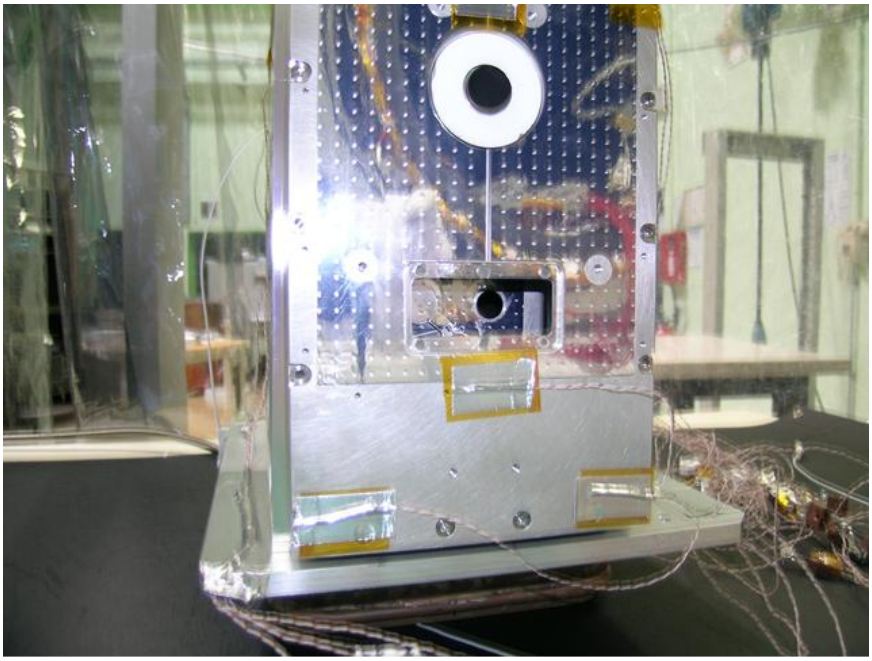

Figure 34: SOVAP-instrument prior to thermal vacuum testing, with one channel opened, and one channel closed in the bottom, and with the BOS black and white sensor plates on the top.

SOVAP-DIARAD has a double differential design, allowing differential left-right and differential open-closed measurements. The left and right channels of SOVAP-DIARAD are opened or closed to solar radiation by the opening or closing of a shutter in front of each channel. Already prior to the launch in June 2010 the operation of the right channel shutter appeared to be less reliable than the left one. By its use after the launch, the right shutter friction diminished and therefore the right shutter bounces back to closed position when it is commanded to be opened. During the first occultation season in November 2010, the right shutter was opened permanently. Depending on the Left and Right channel shutter operations, the following operation modes have been used:

- Nominal Right channel measurements. During the so-called 'Auto 3' mode, the left shutter is closed, and the right shutter sequentially opens and closes. The mode corresponds to the double differential operation. It has a sampling period of 3 minutes and an instrument noise level of 0.1 W/m². This mode has been used to measure the absolute level of the TSI and to verify the short-term stability of the right channel. The mode has been used intermittently from

22 July 2010 until 28 August 2010. It had to be abandoned due to problems opening the right shutter.

- Nominal Left channel measurements. During the so-called 'Auto 2' mode, the right shutter is closed, and the left shutter sequentially opens and closes. The mode corresponds to the double differential operation. It has a sampling period of 3 minutes and an instrument noise level of 0.1 W/m². This mode has been used to measure the absolute level of the TSI and to measure the variation of the TSI from 28 August 2010 to 27 October 2010. The exposure time has deliberately been kept low at about 1 hour per month, in order to guarantee that the left channel was not ageing due to solar UV exposure.
- Continuously opened Right channel measurements. During the so-called 'Rad 10' mode, the right shutter is opened, and the left shutter is closed. This mode has been used since the permanent opening of the right shutter during the first occultation period on 18 November 2010. Compared to the nominal modes, this mode has the advantage of increased time resolution, but the disadvantage of decreased accuracy and stability as it only has the single differential left-right operation. The SOVAP measurements are organized in packets of 90 seconds, consisting of nine 10-seconds measurements. In the routine Rad 10 measurements, the TSI is measured at seconds 20, 40, 70, 80 and 90 within the 90-seconds packet. In a dedicated Rad 10 high rate measurement mode, TSI measurements are obtained every 10 seconds. The increased time resolution of the Rad10 measurements is particularly useful for measuring p mode irradiance variations without aliasing.
- Left channel measurements with opened right shutter. During the so-called 'Auto 15' mode, the right shutter is open, and the left shutter sequentially opens and closes. The mode corresponds to the double differential operation. It has a sampling period of 3 minutes and an instrument noise level of 0.1 W/m². As a continuity of the nominal Left channel measurements up to 27 October 2010, this mode has been used from 10 August 2011 onwards. Again the exposure time has deliberately been kept low at about 1 hour per month, in order to guarantee that the left channel was not ageing due to solar UV exposure.

Figure 35 illustrates the first SOVAP measurements compared to the existing long-term TSI measurements. 'Sova-P left' are the measurements with the nominal Left channel, in the so-called 'Auto 2' mode. 'Sova-P right' are the measurements with the nominal Right channel, in the so-called 'Auto 3' mode. 'Sova-P new' are the SOVAP measurements from the combined new 'Rad10' and 'Auto15' modes, the absolute level of these measurements has been adjusted to the mean of the 'Auto 2' and 'Auto 3'

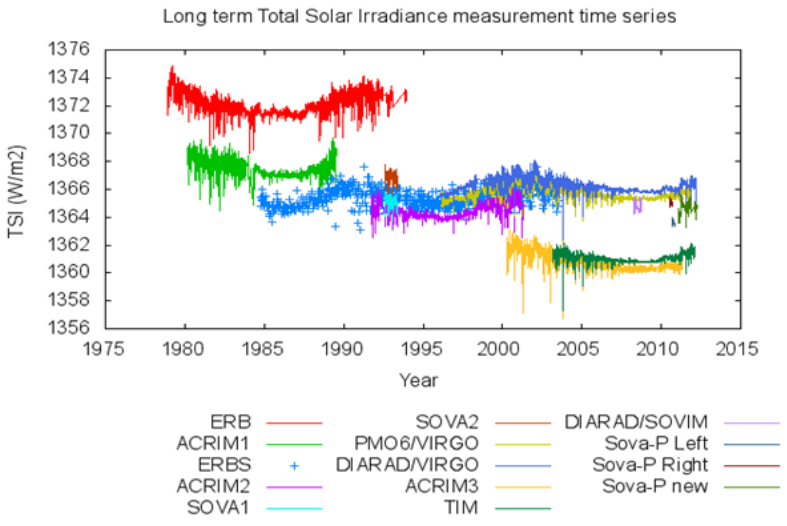

Figure 35: Existing long-term Total Solar Irradiance measurements with addition of the first SOVAP measurements.

levels. Since the launch of TIM/SORCE in 2003, the absolute level of the TSI, also known as the 'solar constant', is an open question. Our first SOVAP absolute levels are therefore preliminary and will be further investigated in the future.

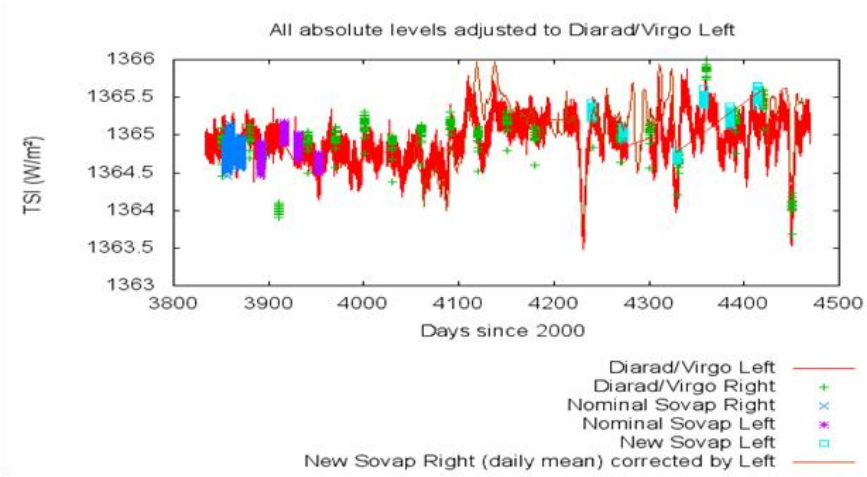

Figure 36: Validation of SOVAP measurements by comparison with the older DIARAD/VIRGO measurements

Figure 36 shows the comparison of the TSI variations measured by SOVAP compared to those measured by our older reference instrument DIARAD/VIRGO. The TSI variations measured by SOVAP in its nominal modes – 'Left = Auto2' in purple and 'Right = Auto3' in blue – as well as those in the new 'Auto15' mode in light blue, agree very well with the DIARAD/VIRGO variations in red. Also the daily mean 'Rad10' measurements in brown show a reasonable agreement with DIARAD/VIRGO.

Figure 37 shows a zoom on the TSI measurements at the end of solar cycle 23 and the beginning of solar cycle 24. As the TSI measurements that were active prior to the launch of PICARD – VIRGO, ACRIM3 and TIM/SORCE – are ageing, the Picard TSI measurements of SOVAP and PREMOS will become the primary instruments for the continuation of the important TSI ECV record.

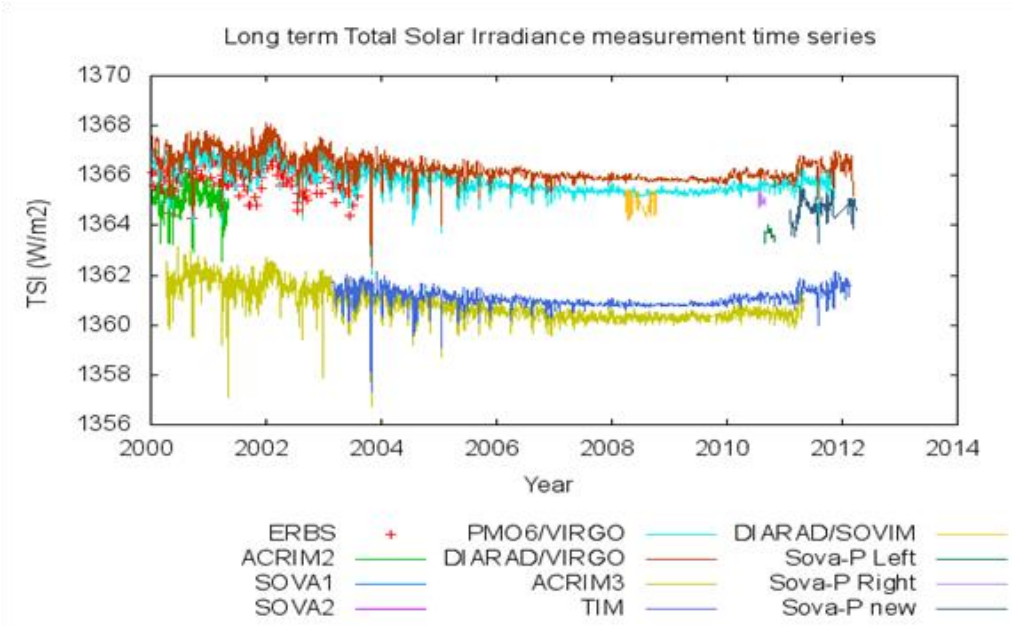

Figure 37: TSI measurements during the end of solar cycle 23 and the beginning of solar cycle 24. SOVAP provides continuity for the ageing VIRGO, TIM/SORCE and ACRIM3 instruments.

Solar radiation measurements

The activities performed in 2011 are covering 3 different work packages: the preparation and the use of a NIR spectroradiometer for a SOLSPEC validation campaign, the VUV spectrometry (Vacuum UV, i.e. typically any measurement below 200 nm), and the characterization of space qualification models or ground-based instruments.

1. SOLSPEC

The space experiment SOLAR SOLSPEC (SOLar SPECtrum, launched on February 7, 2008) is dedicated to the measurement of the extraterrestrial solar spectral irradiance from 166 to 3088 nm onboard the COLUMBUS module of ISS.

SOLSPEC is a space qualified spectroradiometer equipped with three separated channels (UV-VIS-IR). An internal lamp unit (tungsten, deuterium and hollow cathode lamps) provides onboard relative calibration capabilities for monitoring the stability of the wavelength scale and the trends in the channels response due to ageing in space environment. SOLSPEC is integrated on the CPD solar tracker (Coarse Pointing Device) of COLUMBUS.

SOLSPEC was fully operational during the year 2011 for solar or internal lamp spectral measurements. The mission was organized in 'Sun Windows' (periods of approximately 10 days of solar observations per month). The strategy was a compromise between the need to accumulate a large amount of data and the need to reduce the exposure of the optical components to the hard space environment.

The validation of the solar irradiance measured by SOLSPEC (in collaboration with LATMOS, France) is in progress. The data processing was first focalized on the NIR where the radiometric performances are improved in comparison to SOLSPEC ATLAS (first generation of the SOLSPEC instrument). The NIR spectral range is now extended to 2.9 µm (2.4 µm for SOLSPEC ATLAS). The actual results were compared up to 2.4 µm to the IR spectrum provided by the SIM instrument (on the SORCE platform) and the reference ATLAS 3 spectrum.

A composite solar spectrum has been compiled for the quiet sun conditions (corresponding to May – June 2008) starting from the UV, VIS and NIR irradiance provided by SOLSPEC.

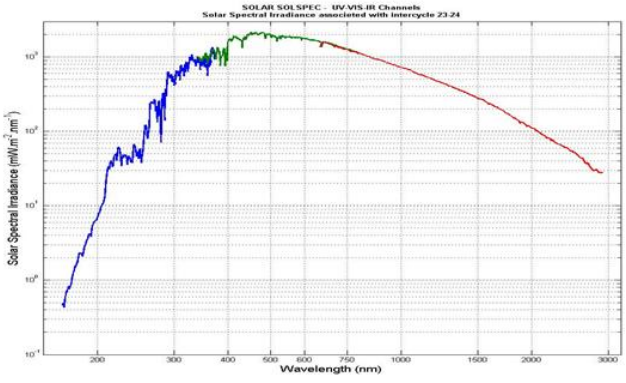

Figure 38: Solar spectrum corresponding to the quiet sun period (beginning of cycle 24)

2. Laboratory calibration facility

- Ground-based high accuracy absolute measurements of the NIR direct solar spectral irradiance

Accurate UV-VIS measurements of the solar spectral irradiance above the atmosphere are performed since the end of the seventies. The NIR measurements (between 1 and 2.4 µm) are more recent. The solar irradiance in this range is related

to the continuum emitted by the photosphere. The first NIR spectrum was obtained from space by the SOLSPEC instrument (missions ATLAS) in the nineties. More recently, new NIR spectra were obtained from the SIM instrument on SORCE and from SCIAMACHY (ENVISAT). The new version of SOLSPEC, on board of ISS (as part of the SOLAR payload) is also measuring the NIR solar spectrum since 2008 over an extended spectral range (up to 3.1 µm) and an improved spectral resolution (around 7 nm).

Actually, some discrepancies are observed between all the available NIR spectra from space instruments, mainly for a broadband spectral range centered on ~1.6 µm. The amplitude of the discrepancies (up to 10 %) is not in accordance with the standard uncertainties of each instrument or any solar variability (< 0.05 % at these wavelengths). Thus, it is necessarily due to instrumental problems.

For SOLAR SOLSPEC, any source of error presenting the right amplitude and spectral dependence could be identified to explain the discrepancy. SOLSPEC was absolute calibrated before the launch in front of the black body (primary standard of spectral irradiance) at the PTB (Germany). Then, it was decided to perform in 2011 a ground-based validation campaign in the NIR for SOLAR SOLSPEC. The objectives were to use a commercial double spectrometer (from Bentham Company, UK) designed for the NIR and similar to SOLSPEC (PbS detector, phase sensitive detection, ~10 nm of spectral resolution…) and to retrieve the TOA (top of atmosphere) spectral irradiance through atmospheric windows using the Bouguer-Langley technique.

- The operating mode

The atmospheric windows for ground-based operations were identified as wavelengths for which molecular absorptions are below 0.5 %. The extinction of the direct Sun is then only due to the Rayleigh scattering and the aerosols. Only a few windows can be used between 600 and 2500 nm, around 700-900 nm, 1050 nm, 1250 nm, 1600 nm and 2100-2200 nm. The window around 1600 nm is of great importance. It corresponds to the minimum opacity of the photosphere (due to the minimum absorption coefficient of H^-) and the maximum discrepancy between the measurements.

For this challenging campaign, high quality results can only be obtained when three requirements are satisfied: a very stable instrument, an accurate absolute calibration in spectral irradiance and a good site of measurements so one can apply the Bouguer-Langley technique. Thus, the following actions were taken:

- ✓ The radiometric characterization of the Bentham instrument (wavelength scale, thermal behavior …) was performed at the laboratories of IASB. Its optical robustness was confirmed. The entrance optics is a telescope designed for direct measurements of the Sun and connected to the instrument by a fiber optic.
- ✓ The absolute calibration was performed at the PTB, in front of the same standard of spectral irradiance (the black body) used for SOLSPEC.
- ✓ The site of the Izaña Observatory (2390 m, Tenerife Island), providing very low and stable levels of aerosols was chosen for the campaign.

A set of four secondary standards of spectral irradiance (1000 W tungsten halogen lamps) was selected for monitoring the absolute calibration after the transportation from the PTB and Izaña, and also after the campaign. The Sun was directly observed using a solar tracker (from EKO, Japan) during the campaign (duration: three months).

- Results

The PTB radiometric scale has been transferred to the double monochromator with a standard uncertainty better than 2 % above 800 nm. At Izaña, this calibration curve has been verified using the set of four 1000 W lamps. Small changes had already been detected and corrected prior to the campaign, with an uncertainty of about 1 %.

The small trends observed for the calibration during the whole campaign were also characterized using the lamps and the Sun. The data processing is in progress. The results presented below are for the first weeks of the campaign during which perfect days of observations were often encountered.

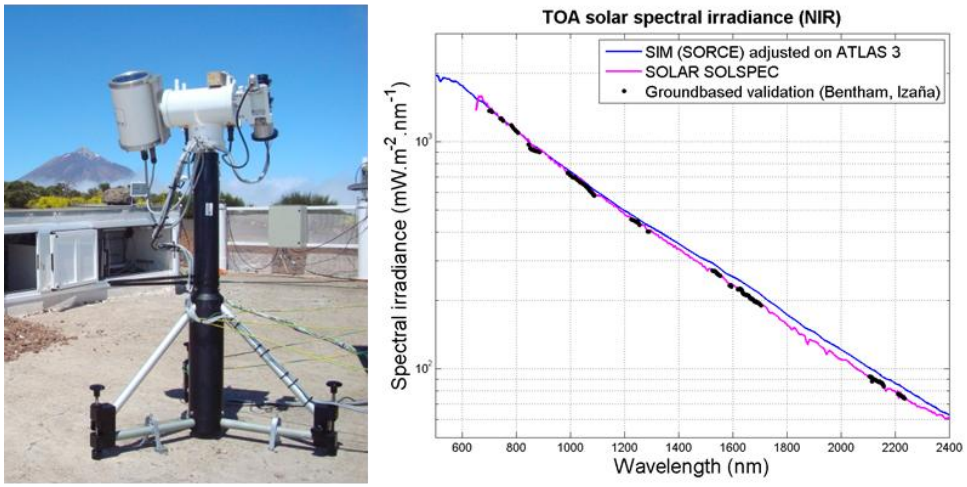

Figure 39: Left: the solar tracker and entrance optics during the solar measurements at Izaña. Right: comparison between SOLAR SOLSPEC, SIM (adjusted on ATLAS 3) and the ground-based validation.

The results show that the TOA spectral irradiance deduced from ground-based measurements are in accordance with the SOLAR SOLSPEC measurements (for which the standard uncertainties are below 2 %). The Bentham and SOLSPEC are fully independent instrumentations but calibrated in front of the same black body. The principle of measurements from the ground and space is also completely different. These two sets of data are also compared to the SIM corrected data. It means that the SIM NIR irradiance has been adjusted on the reference ATLAS 3 before publication. On this figure, SIM is then a representation of the ATLAS 3 spectrum but with a lower spectral resolution (~30 nm). SIM is not in agreement with the SOLAR SOLSPEC irradiance and its ground-based validation.

- Conclusions

The fine analysis of the entire campaign data series and the determination of uncertainties using the concept of metrology are still in progress. Actual results are of great importance due to the role of the NIR Sun irradiance for the Earth thermal balances (interactions with the atmosphere and the oceans). This was one of the principal motivations for this campaign.

3. VUV spectrometry and characterization of instruments

The development of laboratory facilities for working below 200 nm (Vacuum UV) is in progress. This facility is dedicated to the characterization of various components (detector, filters …) for EUV and space projects. It will be complementary to the DeMelab facility, but for spectral ranges extended to shorter wavelengths. The equipment (PMT detector designed for the vacuum) is in progress. The other part of

the equipment (the future pre-disperser of the complete system) is under testing with its detector and its motorization (stepper motor), and is also wavelength calibrated using spectral arc lamp (mercury lamp). This small spectrometer is intended to be used as a pre-disperser to the B225 McPherson spectrometer (1 meter of focal length). It will help us to reach the high quality of internal stray light rejection obtained usually with a double monochromator.

During 2011, the angular response of the Brewer double monochromator of the RMI has been measured in our laboratory with a dedicated calibration facility. New equipment (monochromatic light beam, absolute calibration,…) has been delivered and tested in 2011. They will be used for the characterization of subsystems of the space projects ALTIUS and NOMAD.

Solar Orbiter selection and APSOLUTE tests

On October 4, 2011, Solar Orbiter was selected by the European Space Agency (ESA) as a future space mission in the Cosmic Vision program. The Solar Orbiter mission will be the next major space observatory for heliophysics. Its launch is currently foreseen in 2017 and it will take the spacecraft about 3 years to cruise to its orbit around the Sun. Once the satellite arrives near the Sun, it will take 168 days to orbit it. Solar Orbiter will be the first satellite to provide close-up views of the Sun and its polar regions thanks to an orbit perihelion at 0.28 AU and latitudes higher than 25 degrees.

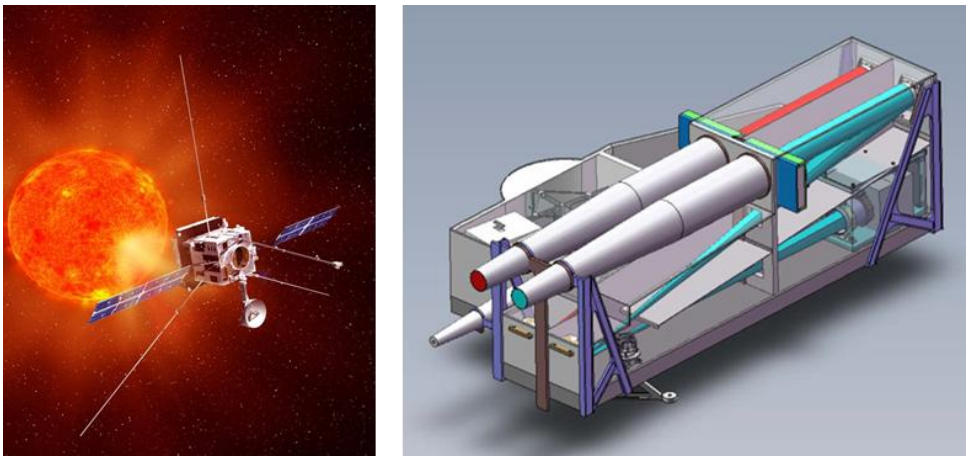

Figure 40: Schematic representation of the Solar Orbiter satellite (left) and of the EUI optical bench system with 2 High Resolution Imagers and 1 Full Sun Imager (right).

Together with our Belgian, British, French, German and Swiss partners, the STCE team "Advanced technology for Solar Observations" meets the challenge of building a new generation solar Extreme Ultraviolet Imager (EUI). EUI onboard Solar Orbiter consists of a suite of two high-resolution imagers (HRI) and one dual-band full Sun imager (FSI) that will provide EUV (17.4 and 30.4 nm) and Lyman-α (121.6 nm) images of the solar atmospheric layers. More info about the mission and the partners can be found on http://eui.oma.be .

For the EUI instrument, an UV CMOS Active Pixel Sensors (APS) prototype called APSOLUTE (APS Optimized for Low-noise and Ultraviolet Tests and Experiments) was developed in collaboration with CMOSIS (Belgium) and the Centre Spatial de Liège (CSL).

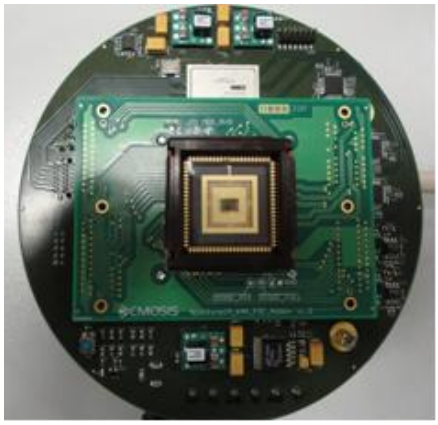

Figure 41: APSOLUTE prototype (256x256) contains 16 pixel variants organized in blocks of 64x64 pixels

APSOLUTE is a back-side illuminated (BSI) CMOS image sensor made in 0.18 µm CMOS process with 10 µm pixels pitch. The EUV sensitivity is achieved with back-side illumination on a Silicon-on-Insulator material based solution. The epitaxial silicon (Si) layer is thinned down to less than 3 µm.

The use of this uncommon technology had several reasons. Indeed, the traditional imagers (for visible applications) are illuminated from the front side. Here for the EUV applications, we used another technology to allow the imager to be illuminated from the back-side. This is also mandatory if one wants that the imager is sensitive to the EUV light where photons do not penetrate a lot inside the Si material.

The term ‘epitaxial’ means that a film is grown on top of the crystalline substrate in an ordered fashion such that the atomic arrangement of the film accepts crystallographic structure of the substrate. Grown atomic layer by atomic layer (= epitaxial), this epitaxial Si layer has a better quality than the Si substrate one, which is mandatory for science grade detector fabrication.

Two types of prototype image sensors have been built: a 256x256 pixel sensor containing 16 design variants, organized in blocks of 64x64 pixels (see Figure 41), and a 1024x1024 pixel sensor that implements the ‘best guess design’ out of the 16 variants.

The sensor applied a so-called “dual-transfer” design to achieve high dynamic range (DR) and to minimize the noise contribution from the analog chain: it consists of two gain paths (low and high) for all pixels in each row. The final image is reconstructed off-chip by the selection of the Low or High gain signal for each pixel independently as shown in Figure 42.

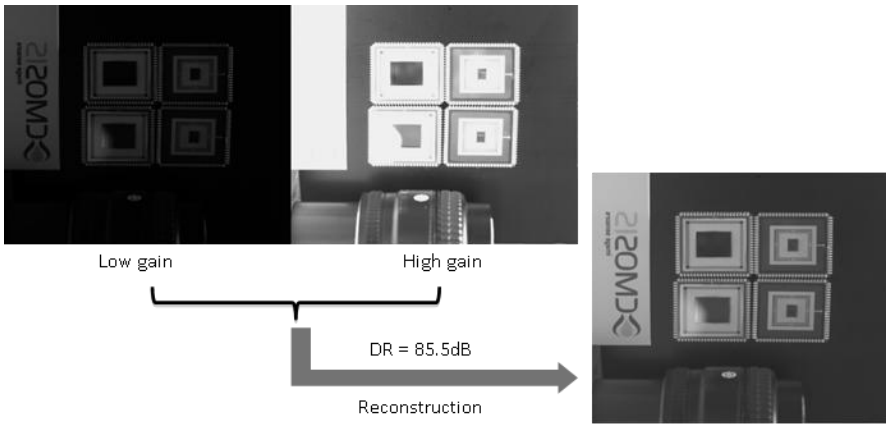

Figure 42: Images of the APSOLUTE prototypes (1024x1024) showing the dual gain operation (Low and High gain) and the final image after reconstruction.

In 2011, a set of measurement calibration campaigns and radiation tests have been carried out to characterize and compare the design variants, and reach a technology readiness level (TRL 5) to assess the maturity of evolving technologies compatible with the overall EUI project development schedule.

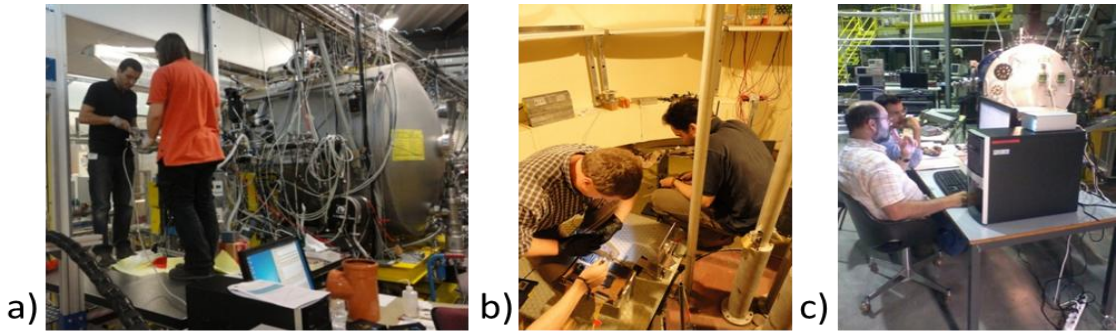

Figure 43: Photographs of the different facilities used to test APSOLUTE (a) at PTB synchrotron, Germany, (b) at Gamma ray ionization facility, Belgium and (c) at Heavy ions facilities, Belgium.

The first results of the XUV-to-VIS sensitivity calibration, including the noise level measurement and the radiation hardness, were performed in 2011. BSI imagers were characterized before, during and after the following radiation tests:

- Total Ionization Dose, using Co60 gamma-ray sources up to 150 kRad (Si),

- Single Event Effect tests with ions cocktails up to a LET of 67.7 MeV.cm^2/mg,
- Displacement Damages performed with proton and a cumulated fluence of 4E11 #/cm^2.

Two EUV calibration campaigns were also performed at the PTB/BESSY II synchrotron in Berlin (Germany) in July and November 2011.

The characterization tests of the back-side illuminated APSOLUTE prototype(s) were mainly performed at DeMeLab (Detector Measurement Laboratory) in the visible range for the design selection. All measurements have been repeated several times to check the stability and the reproducibility of the prototypes. Sequential acquisition software and data processing tools have been developed to estimate the detector parameters.

As an example, the Photon Transfer Curve (PTC) shown in Figure 44 is computed using the processing tools to determine the read noise (in dark condition), the conversion gain (under visible light) for each gain settings (High and Low) and the Full Well Capacity (FWC).

The results of all calibration campaigns indicated that APSOLUTE reached the TRL5.

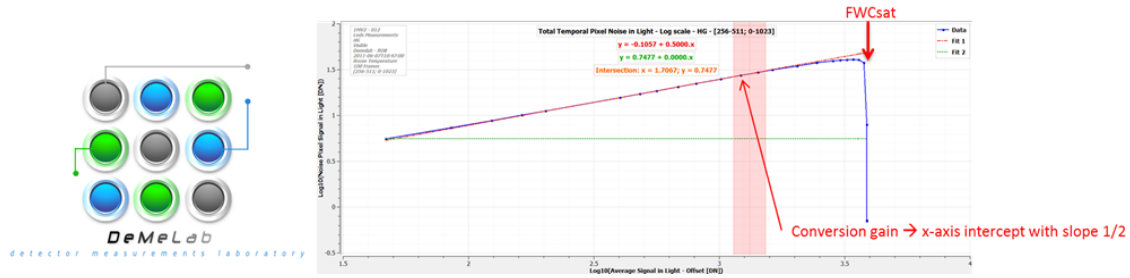

Figure 44: Example of Photon transfer curve (PTC) of APSOLUTE measured at DeMeLab (STCE/ROB). These data are then used to reconstruct the image in Figure 42.

Applications and Modeling

Solar Physics: detection and tracking of active regions and coronal holes

Accurate determination of active regions and coronal holes properties on coronal images is important for a wide range of applications. Active regions appear as bright regions on X-rays and EUV images. As regions of locally increased magnetic flux, they are the main source of solar eruptions. A catalog describing their key parameters such as location, shape, area, mean and integrated intensity allows for example to relate those parameters to the occurrence of solar eruptions.

Coronal holes on the other hand appear as relatively dark regions in X-rays and EUV images and therefore are typically defined as regions of low emission in the solar corona. There is a strong association between coronal holes and high-speed solar wind streams which has been known since the 1970s. Coronal holes are usually identified as the sources of the fast wind from where the wind flows out in the corona and is accelerated in open expanding magnetic funnels. Solar eruptions and fast solar wind can cause several problems for technologies on Earth and in space, and can endanger astronauts. In this way, the Sun causes what we call "space weather". Almost all space weather originates either from an active region or a coronal hole.

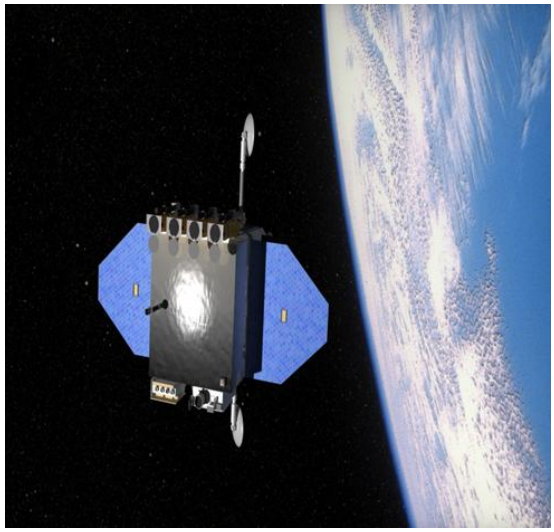

Figure 45: Artist's concept image of the SDO satellite orbiting Earth. Credit: NASA

In the 1960s, NASA launched the Pioneer 6, 7, 8, and 9 spacecraft, that were tasked with observing the solar wind and interplanetary magnetic fields, forming the first space-based space weather network and recording 512 bits per second. By comparison, the recently launched Solar Dynamics Observatory (SDO) is currently relaying solar data back to Earth at a rate of 150 000 000 bits per second. With SDO returning the equivalent of an image with 4096 by 4096 pixels every second, human analysis of every image would require a large team of people working 24 hours a day!

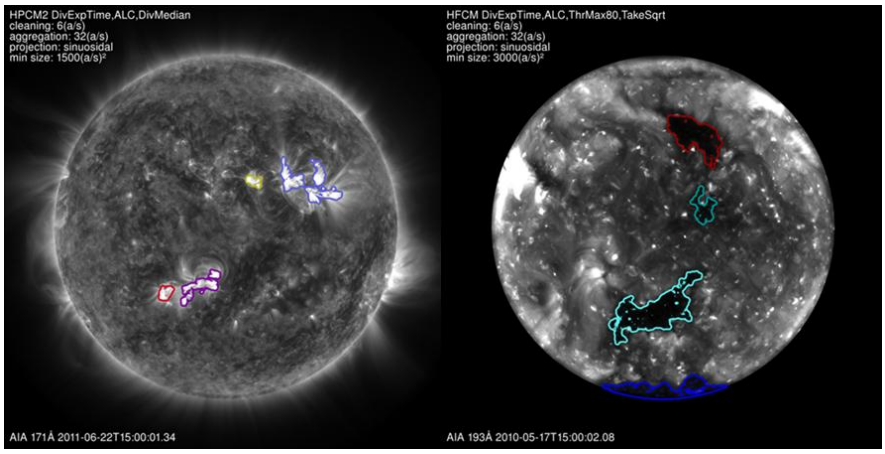

Figure 46: Left: overlay of Active Regions as detected by the SPOCA module on an AIA 171Å image from 22 June 2011. Right: extraction of Coronal Holes on an AIA 193Å image from 17 May 2010.

Technological advances such as improving communication bandwidths and onboard processing power allow us to record data with a much greater cadence and spatial resolution than ever before. However, there are problems with the storage, transfer, and analysis of such a large flow of data. SDO generates around 1 TB of data per day which is unprecedented in solar physics. Getting this volume of data to researchers around the world, as well as storing it in convenient places for analysis, is essential to make good use of it. An effective solution to the problem is to use automated feature-detection methods, which allow users to selectively acquire interesting portions of the full data set.

In the fall of 2008, NASA selected a large international consortium, the Feature Finding Team (FFT) to produce a comprehensive automated feature-recognition system for SDO. One of the goals of the consortium is to analyze images from SDO and to produce software modules that can keep up with the SDO data stream, and detect, trace, and analyze numerous solar phenomena. The Royal Observatory of Belgium was part of the FFT consortium and was responsible for SPOCA (Spatial Possibilistic Clustering Algorithm), the module for Active Region and Coronal Hole detection.

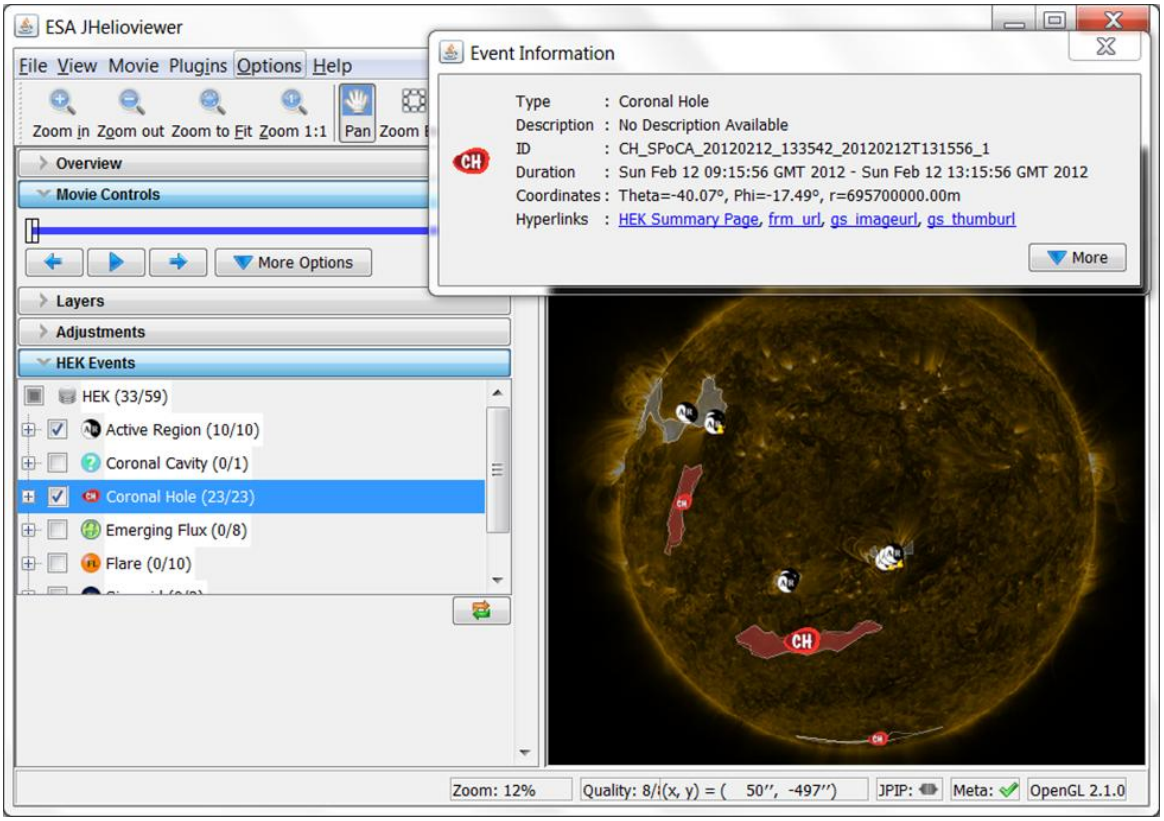

Figure 47: Screenshot from the ESA JHelioviewer tool. The picture on the right displays the AIA 171Å image taken on 12 February 2012 at 9:02:12, together with Active Region and Coronal Hole location and chain-code information that are recorded in the HEK. An 'Event Information' window pops up when clicking on an event or feature (here the large coronal hole located in the southern hemisphere)

In January 2011, the Active Region module of SPOCA was ready to run in near real-time on SDO images at LMSAL (Lockheed Martin Solar and Astrophysical Laboratory). One year later, the coronal hole detection module was also made operational. Both modules now produce entries to the Heliophysics Event Knowledgebase (HEK), a database of solar features and events maintained by LMSAL. This database can be accessed through the widespread solarsoft library of IDL and hence permits users to

locate data about individual events as well as carry out statistical studies on large numbers of events. The HEK website is at http://www.lmsal.com/hek/

Since the data are analyzed in near real-time as soon as they arrive at the SDO Joint Science Operations Center and have undergone basic processing, the system is able to produce timely space weather alerts and to guide the selection and production of quicklook images and movies. For example, the ESA JHelioviewer visualization tool includes the products coming from the HEK database.

3D stereo work & linking in-situ with remote sensing

The majority of images and data of our Sun and the interposing interplanetary space are taken from the Earth, satellites orbiting the Earth and near Earth satellites. However, in October 2006 NASA launched the STEREO (Solar-TErrestrial RElations Observatory) satellites to observe the Sun from different viewpoints. STEREO consists of two satellites, with one positioned ahead of Earth in its orbit and the other trailing behind. The position of the satellites provides two new viewpoints of the Sun and its related activity, allowing solar scientists to see the structure and evolution of the Sun in greater detail and create 3D reconstructions of its features.

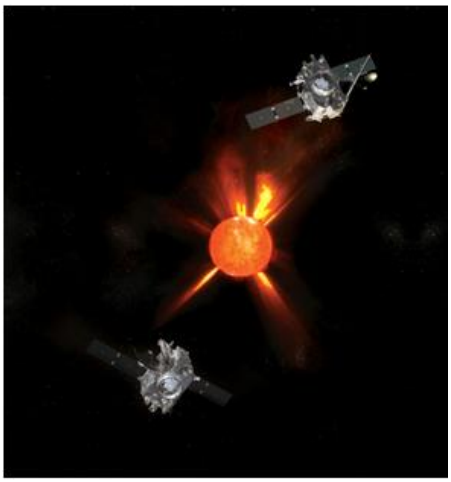

Figure 48: Artist's view of the STEREO satellites observing the Sun. (credits: NASA)

Each STEREO satellite is equipped with several imaging instruments, including EUV imagers for observing the solar disk in the extreme ultraviolet wavelengths, coronagraph imagers which essentially block the Sun to allow observations of the faint interplanetary space surrounding the Sun, and Heliospheric imagers which observe the space between the Sun and the Earth.

In recent years, an important area of research in the field of solar and space physics has been the study of space weather, which looks at how hot material (plasma) produced by the Sun moves out through the solar system (interplanetary space). There is a continual flow of material from the Sun known as the solar wind, which is punctuated by fast and slow streams and occasionally more energetic phenomena. There has been particular interest in how space weather affects the Earth, the Earth's weather and our satellites orbiting the Earth. One of the most energetic forms of space weather is known as Coronal Mass Ejections or CMEs, which is the sudden eruption of material from the solar surface into interplanetary space. CMEs can manifest themselves as geomagnetic storms when they interact with the Earth, which in turn can affect electrical systems and create auroras seen near the polar regions. Therefore, it is important to determine if and when a CME might hit the Earth or orbiting satellites.

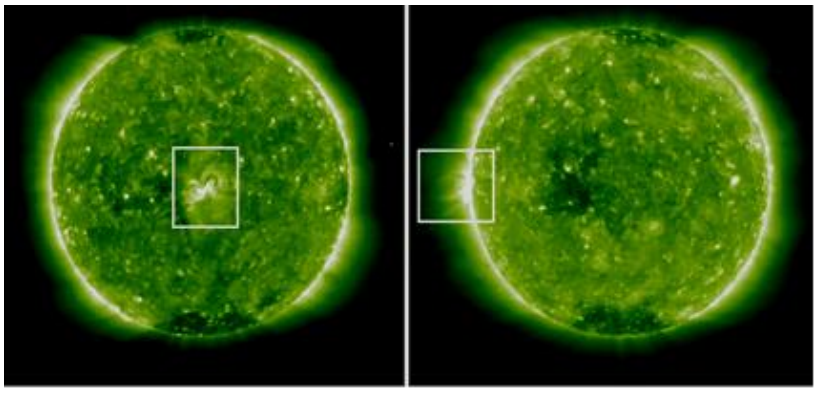

Figure 49: Two false color images of the Sun, taken at the same time from the different STEREO spacecraft perspectives. The source region of a CME is highlighted by a white box; this region can be seen towards the center of the solar disc from one perspective and on the limb (edge) from the other. The images are taken with a EUV filter allowing images of the Sun to be taken at ~1.5 million degrees.

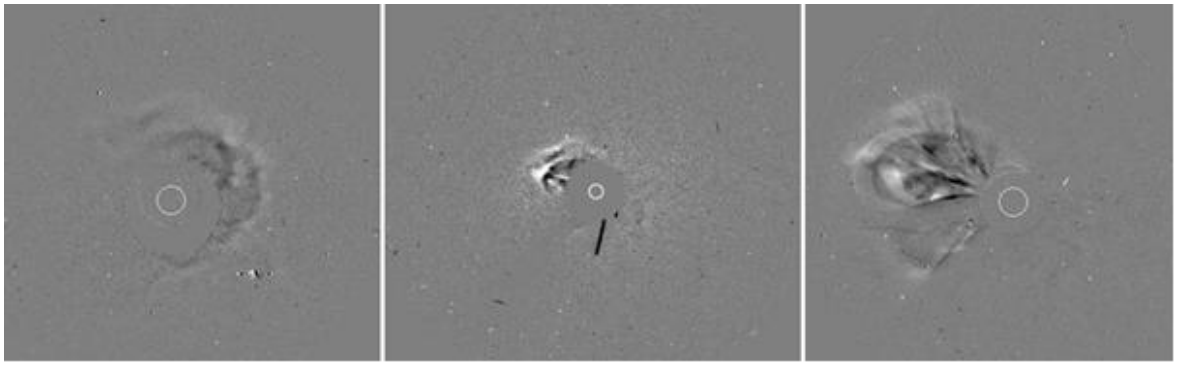

Figure 50: Three images of the same Coronal Mass Ejection (CME) taken from different perspectives. Each image is taken with a coronagraph, where the bright Sun is blocked to reveal the faint surrounding interplanetary space. The images on the left and right are taken by the STEREO spacecraft which are positioned ahead and behind the Earth in its orbit. The central image is from the Solar and Heliospheric Observatory near the Earth. The images highlight the complex structure of a CME.

In-situ observations of space weather are made from satellites, which measure ambient conditions at the position of the satellite. Such observations are made with various instruments including magnetometers, which measure the local magnetic field; and particle detectors which measure the solar wind speed, density and temperature of the ambient interplanetary conditions. CME signatures can be identified by abrupt changes in the magnetic field and particle velocities.

We have linked STEREO observations to in-situ data to show that observations of CMEs made in coronagraph images close to the Sun can be used to make accurate and reliable predictions of CME transit times and directions, and more importantly if these solar storms will be Earth directed. This work will be used with space weather predictions, such as those produced in the space weather forecasts produced at ROB.

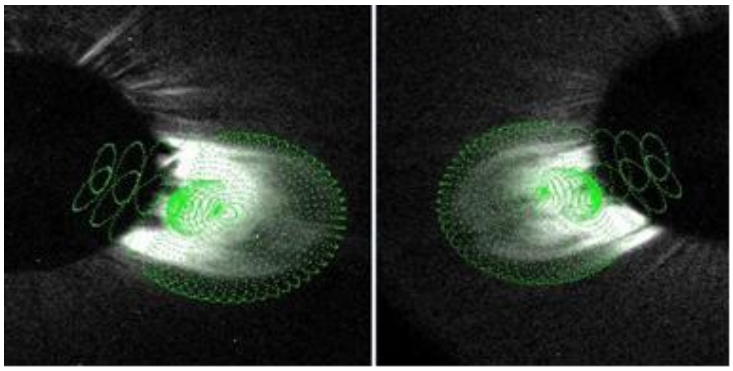

Figure 51: Two images of the model fitting technique used to numerically model a (CME). The background black and white images show a CME viewed in coronagraph images from the STEREO satellites. The green lines outline the model fitted to the observations.

To predict the propagation of an individual CME, a model is fitted to observations of the eruption close to the Sun. The model provides information pertaining to the CME such as the direction of propagation and the CME's 3D geometrical configuration. This information can be used to calculate the angular width, direction and speed of the CME, which in turn can be used to see if the CME will be Earth directed. In-situ observations made from satellites orbiting the Earth and by both STEREO spacecraft are then used to verify if the predicted arrival time and direction of a CME were correct.

The model was used to estimate the propagation of 26 CMEs. Of these, it was found to predict 88% of the CMEs successfully, and a further 9% were found to lie within predicted error margins, and only one event (3%) can be considered as not successfully described by the model. Therefore, the model used to predict the arrival of CMEs can be used with a high degree of certainty when making space weather forecasts. Further information can be obtained from Rodriguez et al. 2011.

GNSS-based monitoring, modeling and forecasting of the ionospheric activity

The electron concentration (Ne) is the main parameter which describes the state of the ionosphere, the latter depending strongly on the level of solar activity. Indeed, extreme UV and X-rays emitted by the Sun are the main source of ionization in the ionosphere. For this reason, space weather is the main driver of ionospheric disturbances. In particular, geomagnetic storms are often the cause of strong variability in the ionospheric electron concentration. The ionospheric Total Electron Content (TEC) is another parameter of interest. The influence of the ionosphere on GNSS measurements depends on GNSS wave frequency and on TEC. Hence, we can use GNSS signals to monitor the ionosphere.

- Exploit the new GNSS signals for ionosphere monitoring

We have developed an innovative methodology for reconstructing the Total Electron Content (TEC) by using triple frequency Global Navigation Satellite System (GNSS) measurements.

The availability of triple frequency GNSS measurements increases the number of linear combinations which are useful for ambiguity resolution in the aim of TEC reconstruction. Especially, the combinations which are used make the resolution of original integer ambiguities feasible.

Instead of being estimated by the carrier-to-code or carrier-to-GIM (Global Ionospheric Map) leveling process, or computed by a least-square adjustment in the unlevelled carrier phase process, the Geometric-Free (GF) ambiguity is thus reconstructed from the original ambiguities without the need for TEC modeling. The TEC values are then reconstructed from the usual GF phase combination. Since the model errors were limiting the accuracy of the TEC to several TEC units, this innovative ambiguity resolution procedure allows an improvement of the TEC accuracy with regard to dual frequency techniques.

This triple frequency TEC reconstruction methodology has been validated on GPS and Galileo simulated data, as well as on real data from the GIOVE-A and GIOVE-B satellites.

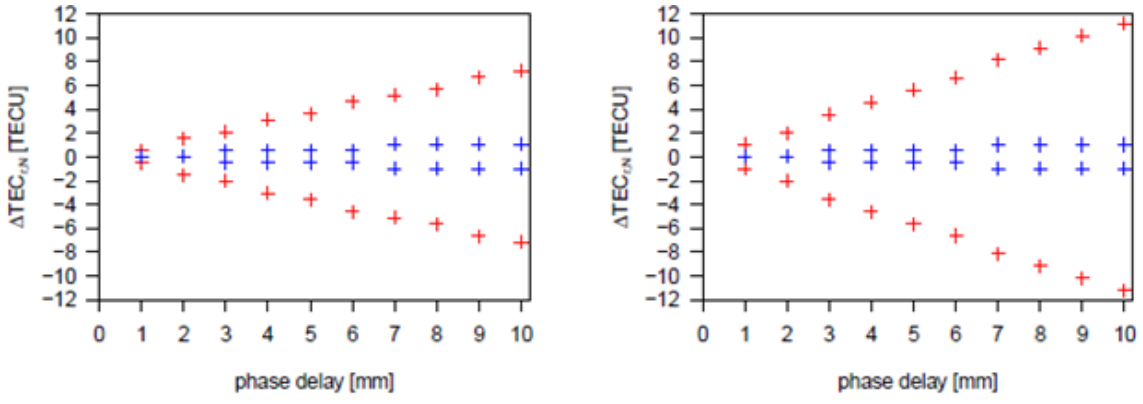

Figure 52: Influence of multipath delays and measurement noise on GPS (left) and Galileo (right) reconstructed TEC values with L2/L5 (red) and L1/L5 (blue) GF phase combination. The figure shows the error caused by phase hardware delays on the GPS and Galileo reconstructed TEC values (ΔTECr,N) in these two cases as a function of the magnitude of the phase hardware delays.

In order to test the triple frequency TEC reconstruction methodology on simulated GNSS measurements, we have developed simulation software providing realistic triple frequency GPS and Galileo code and

phasing measurements. We concluded that the precision of the reconstructed TEC values from simulated data is about 0.1 TECU for GPS and Galileo, and that -even though phase hardware delays might be larger than 1 mm- their influence on the resolution of the original ambiguities, and therefore on the reconstructed TEC values, might be smaller than 1-2 TECU for GPS and Galileo. In these conditions, the accuracy of the reconstructed TEC is improved with regard to existing dual frequency techniques.

In order to test the triple frequency TEC reconstruction methodology on real GNSS measurements, we used a dataset consisting of GIOVE-A/-B data for a few days in 2008 in four GESS stations. As a prerequisite, we performed the preprocessing of the observation and navigation data. Furthermore, we performed several statistical tests aimed at validating the assumptions about the distribution and magnitude of code and phase multipath delays and measurement noise.

Using the results of the ambiguity resolution procedure, we computed the final reconstructed TEC values for the whole dataset. These values confirm the low solar activity period and the fact that the best way to reconstruct TEC is to use frequencies that are as far apart from each other as possible, i.e. L1/L2 or L1/L5. It has to be stressed that, as mentioned earlier, these TEC values might be biased by a non-negligible error (5 TECU) caused by the satellite phase center offset (PCO) and by the receiver antenna (PCO) and variations (PCV).

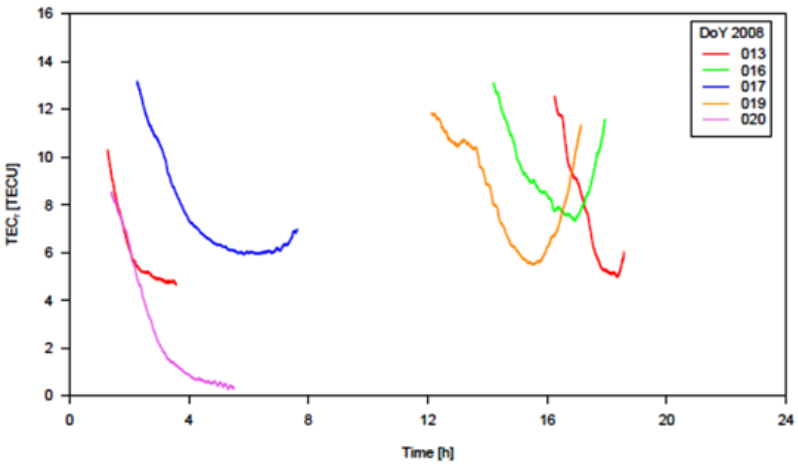

Figure 53: Reconstructed TEC values for the GNOR station for several days in the year 2008.

Figure 53 shows the reconstructed TEC values for the GNOR station. We obtain relatively low TEC values, which can be explained by the low solar activity. The day-to-day variations can be explained by the differences of local time and the changes in the satellite position which determines the position of the ionospheric piercing point.

- Explore the new RMI digital ionosonde capabilities

For more than half a century, RMI has been conducting ionospheric scientific research with the help of vertical incidence sounders; one of the most reliable instruments available to the scientific community. In April 2011, a new digital ionosonde, Lowell Digisonde-4D (Figure 54), was installed at the Geophysical Centre in Dourbes (http://dourbes.meteo.be). Digisonde-4D is state-of-the-art equipment using radar principles of remote sensing to evaluate with high-accuracy and precision the conditions of the ionospheric plasma above the station. It boasts multiple functionalities supported by a fully automated operational and database management system. Thus, high quality measurements are obtained and immediately distributed to the international digital ionosonde network database (DIDBase). The digisonde was also equipped with new transmit-and-receive antennas which substantially improved the quality of measurements. Both the installation and the initial calibration went smoothly and since then

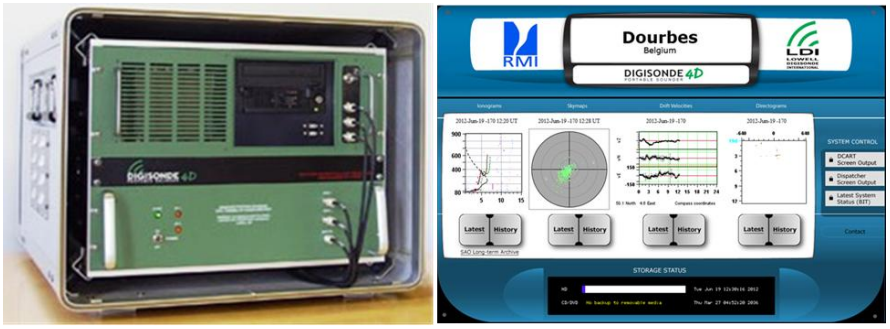

*Figure 54: The RMI Dourbes' new digital ionosonde (left) and its website (**http://digisonde.oma.be/**).*

the digisonde is operated in a high time resolution mode, one sounding every 5 minutes. Sounding data is available online at http://digisonde.oma.be/ for registered users.

One of the key tasks in the past few months since the beginning of the digisonde's operation was to obtain experience in the sounder's technicalities, operability, and the novel functionalities it offers. For this purpose, the ionospheric behavior during the evolution of three geomagnetic storms within the month of September 2011 has been investigated. The storms were occurring on 9, 17 and 26 September 2011 as the first prominent storm sequence at the early stage of the new solar cycle number (Figure 55).

The emphasis was on the geomagnetic storm effects in the ionospheric F2-layer. To specify the ionospheric behavior for each storm, the critical frequency of the F2-layer (foF2), the F2-layer density peak height (hmF2), and the propagation factor (M(3000)F2), from ground-based ionosonde measurements were used. foF2 is the ordinary-wave critical frequency of the highest stratification in the F-region. The propagation factor M(3000)F2 is a conversion factor applied to the ionospheric critical frequency at vertical incidence to obtain the maximum frequency usable for a given oblique propagation over a distance of 3000 km.

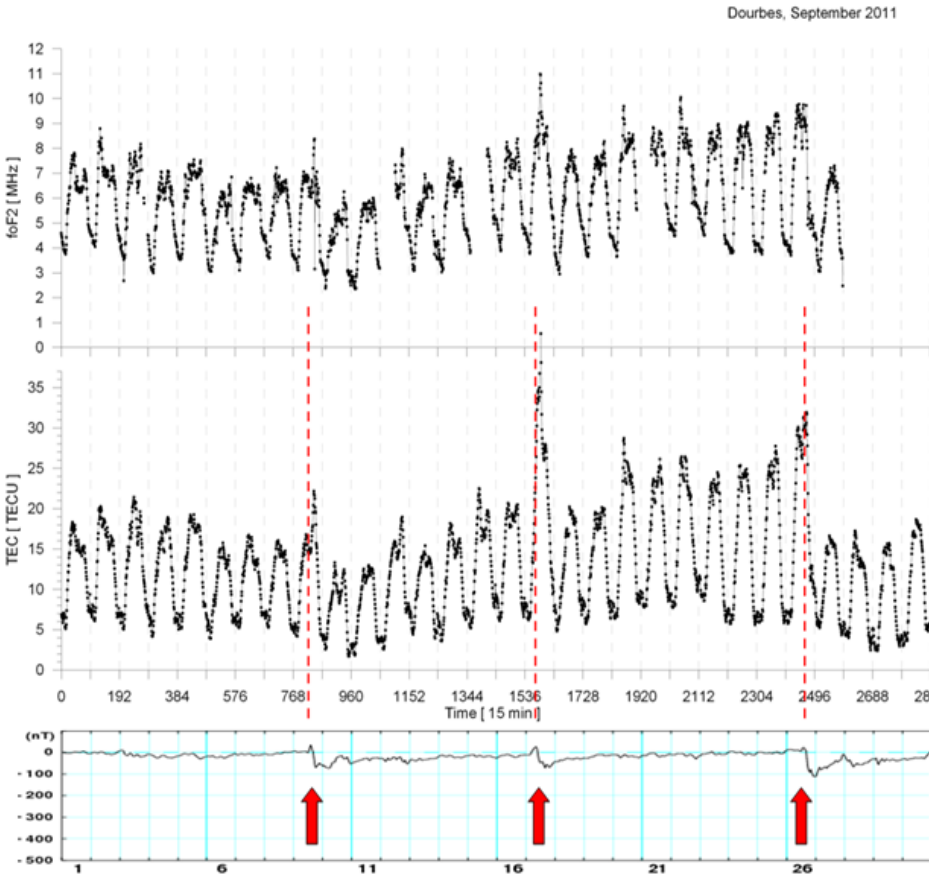

Figure 55: Ionospheric storms in September 2011 as observed at Dourbes: foF2 (top panel) and TEC (middle panel). The Dst index is plotted in the bottom panel.

Data was obtained from the digisondes at Dourbes (4.59°E, 50.09°N) and Chilton (358.67°E, 51.70°N) and from the co-located ground-based Global Positioning System (GPS) receivers at DOUR (4.59°E, 50.09°N) and HERS (0.33°E, 50.86°N).

Additionally, the ionospheric slab thickness, τ (TEC/NmF2), was also calculated and used for the study. The storm response of all considered ionospheric parameters foF2, hmF2, M(3000)F2, VTEC and τ was extracted from the time series data as departure from the quiet periods defined in terms of the monthly medians. The daily foF2 variations were compared with the corresponding VTEC variations during the three storm periods. Note the sharp increase in both TEC and foF2 values, about 100%, during the initial phase of the storms on 9, 17, and 26 September and the severely depleted ionosphere during the recovery phase from 27-30 September.

- Other developments

In the frame of a new collaboration with I. Tsagouri (NOA, Greece), we developed tools to provide the VTEC for several days in 2002 over Millstone region (USA) to perform comparison with models based on ionosonde data.

We compared the VTEC extracted from the ROB maps with the VTEC values delivered by the RMI-tool SWANS (http://swans.meteo.be/) for the 30 days of September, 2011 for the Dourbes and Brussels locations. The differences are of the order of 0.0±1.0 TECU for Brussels and 0.8±1.0 TECU for Dourbes. If the differences are negligible for Brussels, the bias over Dourbes is significant and might be due to the different approach of ROB (use of ~120 GPS stations and interpolation) and SWANS (use of one GPS station) to estimate the VTEC. The use of a station network and the interpolation performed by ROB to estimate the VTEC allows avoiding any bias compared to the use of only one station.

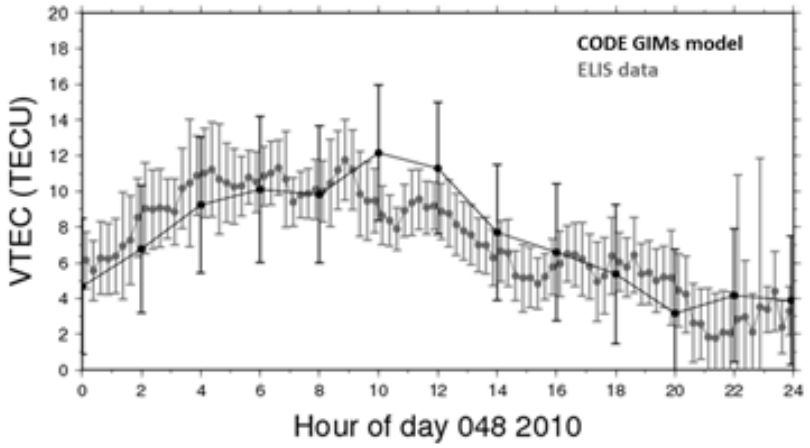

Figure 56: VTEC estimated every 15 minutes above the Princess Elisabeth polar base from ELIS GNSS station (gray). In black the CODE Analysis Center estimation based on a global model (estimate every 2 hours).

We continued to develop a method in order to obtain VTEC based on the observations from the permanent GPS station that we installed at the Princess Elisabeth station (ELIS) in Antarctica. The results, for one day of 2010, show differences of 0.1±1.7 TECU with respect to the global ionospheric model provided by the CODE Analysis Center (see Figure 56) which confirms that our method to obtain VTEC is robust at first order.

Software for determining ionospheric positioning error based on GNSS-data

Nowadays, GNSS signals are widely used to measure positions in real-time with a few cm precision. Such a level of precision can be obtained in "differential mode". In this positioning mode, "differential" corrections broadcast by reference stations are used in order to improve the positioning precision. At the present time, the ionospheric effect on GNSS radio signals remains the main factor which limits the accuracy and the reliability of differential positioning. GNSS differential applications are based on the assumption that the measurements made by the reference station and by the mobile user are affected in the same way by the different error sources, in particular, by the ionospheric effect. The validity of this assumption depends on the distance between the user and the reference station which is called "baseline": on shorter baselines, ionospheric residual effects are smaller than on larger baselines. In practice, these applications will not be affected by the "absolute" TEC but by gradients in TEC between the reference station and the user. For this reason, local variability in the ionospheric plasma can be the origin of strong degradations in positioning precision. Strong variability in the ionospheric electron concentration (and in TEC) is mainly due to space weather events such as geomagnetic storms. GNSS real-time users who experience degradation of their measurement accuracy are not necessarily aware about this problem. This is an important limitation to the reliability of GNSS, e.g. in the so-called "safety-of-life" applications. Therefore, it is important to develop services allowing to monitor the GNSS "integrity" with respect to ionospheric threats and to warn GNSS users against such events.

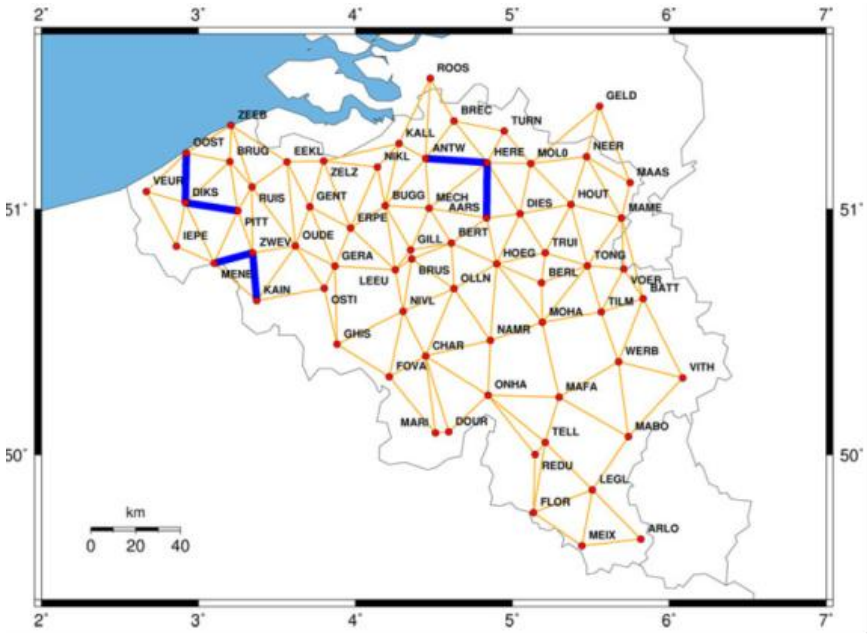

Figure 57: The active geodetic network with baselines selected for the orientation analysis (thick lines).

The Software for Determining Ionospheric Positioning Error on RTK (SoDIPE-RTK) has been described in more detail in the previous STCE reports, with main results published in Lejeune et al (2012). This software uses RINEX (Receiver Independent Exchange Format) observation and navigation files to compute, for a given baseline, the part of the positioning error which is only due to the ionosphere. The software processes GNSS data in three main steps. The first one consists in forming double differences like in classic RTK. Then, using geometry-free phase combination, we compute the differential ionospheric effect, which is used in the third step to extract the ionospheric positioning error. The software needs to be permanently updated to take into account changes in network characteristics (receiver and antenna types, number and maintenance of stations, etc.). The validation uses the Belgian

Active Geodetic Network (AGN) consisting of 66 dual-frequency GPS stations operated by three different institutions: FLEPOS (Flemish part, 40 stations), WALCORS (Walloon part, 23 stations), and the Royal Observatory of Belgium, ROB (3 stations), with 160 baselines in total (Figure 57).

In order to identify the effects of ionospheric structures on relative positioning, three particular days, based on their typical ionospheric conditions, were analyzed in detail and presented here: DOY 310/2008 (quiet), DOY 359/2004 (active), and DOY 324/2003 (disturbed), see Figure 58.

We selected November 5, 2008, as a reference day. This day is characterized by a quiet TEC background of less than 10 TECU and quiet geomagnetic activity with Kp value of 0.3. Furthermore, nearly no ionospheric events were detected by the single-station method. This technique allows detection of small-scale structures in ionospheric plasma by analyzing the geometry-free combination at a given GPS station. High-accuracy GNSS-based positioning in real-time is referred to as RTK (Real-Time Kinematic) positioning. RTK positioning involves a reference receiver transmitting its raw measurements (or observation corrections) to a rover receiver. The ionosphere varies with different intensity that generally increases during ionospheric events (disturbances, storms) leading to increased positioning errors. When such variability is present, SoDIPE-RTK is able to detect the so-called ionospheric event (with its associated intensity) that is called "RTK intensity". DOY 310/2008 is therefore considered as representative of a quiet ionosphere.

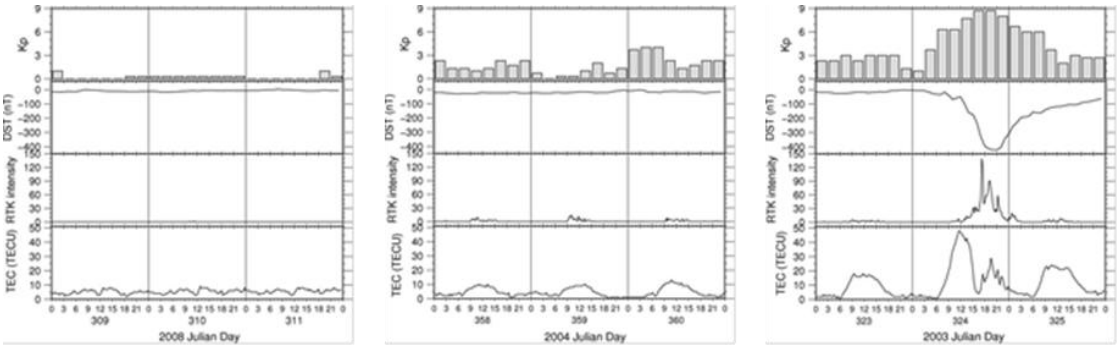

Figure 58: Geomagnetic and ionospheric conditions during DOYs 310/2008, 359/2004 and 324/2003.

While the occurrence of medium-scale TID (MSTID) is relatively common around noon in winter, we chose the day for which the intensity of the events presents the largest values. On 24 December 2004, a medium-scaled traveling ionospheric disturbance occurred lasting from 09:00 to approximately 15:00. Maximal value of RoTEC (rate of TEC), which is actually the TEC time derivative, was about 0.8 TECU/min around noon at BRUS. As this kind of TID is generally not linked to geomagnetic activity, the geomagnetic indices for this day show, as expected, very quiet conditions (Kp_{max} = 2 and Dst_{min} = -26 nT). The background TEC for DOY 359/2004 is also quiet, with a maximum of about 10 TECU, which corresponds to solar quiet conditions (sunspot number Ri = 17.9). As the TID occurred between 09:00 and 15:00, we will only consider this time period in further computations.

On 20 November 2003, a huge coronal mass ejection coming from a giant sunspot group hit the Earth's magnetosphere, which resulted in a severe geomagnetic storm. It was one of the most powerful geomagnetic storms observed since the beginning of GPS recording. Indeed, Dst values reached -422 nT around 20:00, while the Kp index was 8.7 during more than 6 hours. The ionospheric background of DOY 324/2003 was relatively high, partially due to the high value of the sunspot number (Ri = 67.3): A

maximum of about 50 TECU was observed around noon, which is more than 150% above the TEC background of the previous day. A secondary maximum of about 30 TECU was also observed around 20:00, in phase with a large increase of RTK intensity and increasing geomagnetic activity. The maximum RoTEC value at BRUS was about 9 TECU/min at 19:00.

An important issue is the effect of ionospheric small-scale disturbances on precise relative positioning. For the purpose, we analyzed the influence of the baseline length during disturbed conditions. In addition, we investigated the effect of the baseline orientation on the positioning error to highlight a potential influence of the direction of propagation of ionospheric disturbances.

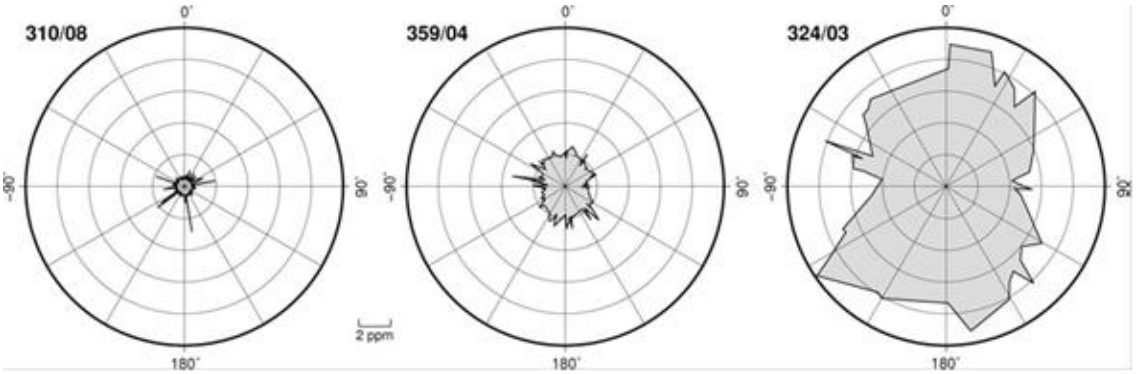

Figure 59: Standard deviation of distance component normalized by the baseline length (ppm) for DOYs 310/2008, 359/2004, and DOY 324/2003, for all AGN baselines.

In conclusion, we showed that geomagnetic storms induce the largest positioning error (more than 2 m for a 20 km baseline) and that the positioning error depends on the baseline orientation. Baselines that are oriented parallel to the propagation direction of the ionospheric disturbances are more affected than others. Since the accuracy is also a function of baseline orientation, errors are larger for baselines with a north–south orientation. We observed in these cases that the degradation is due to the preferential direction of TID's propagation. It is therefore important to offer to GNSS users an integrity monitoring service which can help them to take into account the influence of such moving structures. While users are generally aware of the impact of these ionospheric perturbations, they are not especially informed about the propagation of these atmospheric structures. The positioning error due to ionospheric small-scale structures can be so identified by our method, which is not always the case with the modern ionosphere mitigation techniques. In the future, this ionospheric impact formulation could be considered in the development of an integrity monitoring service for GNSS relative positioning users.

GNSS-based monitoring and modeling of the Earth's troposphere

- GNSS observation network

As GNSS signals travel through the Earth's atmosphere, they contain information on the state of the ionosphere and the troposphere. To extract this information from GNSS signals, networks of continuously observing GNSS stations, with well-known positions, are used. For that purpose, the ROB GNSS team maintains a network of continuously observing GNSS stations and contributes actively to the elaboration and extension of the European GNSS network, known as the EUREF Permanent Network (EPN). In a second step, the GNSS data from these networks are used to compute information on the state of the Earth's ionosphere and troposphere.

In the upcoming years, GNSS will be facing a changing landscape with new heterogeneous navigation systems (Galileo, COMPASS), signals and frequencies. How to analyze the data of these new systems as one homogeneous system is a major challenge. What new products should be delivered to the users and how to upgrade the GNSS tracking networks without compromising products and the long-term stability, are some of the questions that we will need to answer in the following years.

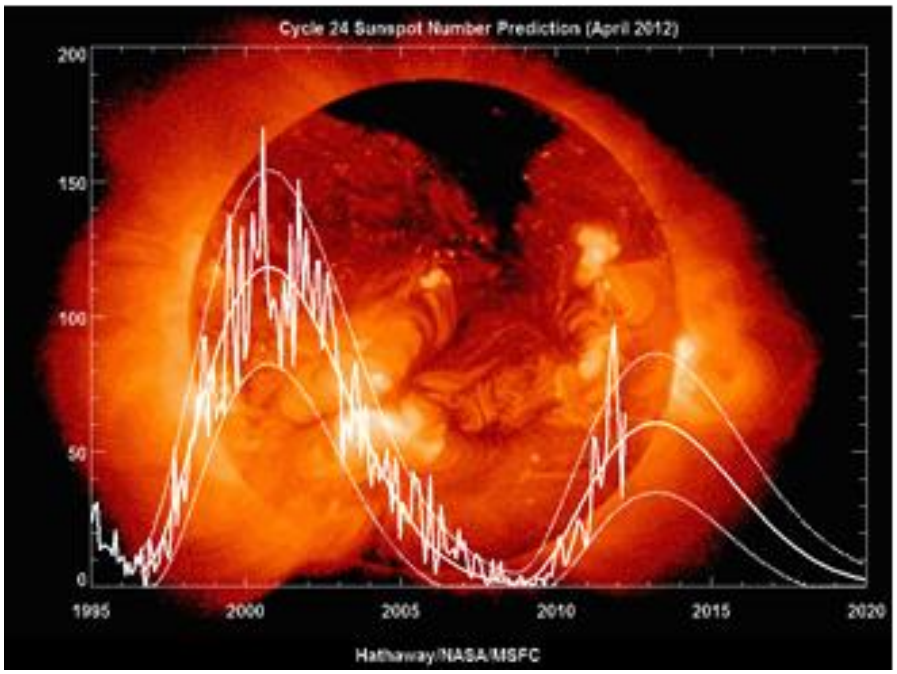

Figure 60: Solar cycle 23 and 24 based on the Sunspot Number. Also shown is the prediction until 2020. The most recent prediction for Sunspot Cycle 24 by NASA/MSFC gives a smoothed sunspot number maximum of about 61 in the spring of 2013. Source: http://solarscience.msfc.nasa.gov/predict.shtml

In addition, radio wave propagation problems due to the ionosphere for applications such as GNSS positioning, amateur radio, intercontinental communications…) may increase in the next few years due to the increase of the solar activity with a maximum predicted in mid-2013 (Figure 60) . Consequently it is important to monitor and to better understand the meteorological and climatological effects which affect this layer of our upper atmosphere.

We are in charge of the daily management of the EUREF Permanent GNSS network (EPN) consisting of almost 250 GNSS stations located all over Europe. Within that framework, we maintain and continuously update the EPN Central Bureau (CB) web site (http://epncb.oma.be/). In 2011, the site received about 1.7 million hits. Also, three new tracking stations were added to the EPN, one in Denmark (Faroe Islands), one in Greece and one in Greenland.

The quality of the ionospheric and tropospheric monitoring will improve if more satellite signals traversing the Earth's atmosphere will become available. For that purpose, encouraging EPN stations to switch from GPS-only to GPS+GLONASS (Russian counterpart of GPS) or GPS+GLONASS+Galileo (future European navigation system) is one of our top priorities. As a result, 68% of the EPN GNSS receivers track now GLONASS satellites in addition to GPS, which is a 10% increase with respect to last year. Moreover, 16% of the EPN stations are now already Galileo-capable.

In 2011, we purchased and partially installed new equipment for the ROB GNSS stations. During the year 2012, all of these stations will switch from GPS-only to GPS/GLONASS/Galileo tracking.

Figure 61: European stations for which ROB collects real-time GNSS observations (Status: 6 February 2012, some stations are located outside the region represented by the map)

The generation of GNSS-based near real-time and real-time ionospheric and tropospheric maps and products requires the availability of real-time GNSS data from stations all over Europe. We maintain an EPN relay broadcaster providing real-time access to all EPN data from stations streaming real-time data. Over time, this relay caster is gradually evolving into a (redundant) top caster: The streams relayed from the NTRIP caster at the Bundesamt für Kartographie und Geodäsie (BKG) are progressively replaced by streams accessing directly the station instead of via the caster of BKG. In addition, we have developed procedures and programs to monitor the real-time data acquisition and to generate RINEX observations, SP3 orbit and CLK clock files from these real-time GNSS observations and real-time IGS orbit and clock corrections streams. In 2011, the real-time GNSS observation acquisition procedures have been enhanced and extended to new GNSS sites from several networks, in total 248 stations (125 EPN stations, 68 IGS observations, 20 stations from the French RGP network, 12 stations from the UK Ordnance Survey network, and 23 stations from the Belgian WALCORS network - see Figure 61).

- Monitoring of the Earth's troposphere

We have developed and maintained tools to monitor the European wet tropospheric delay estimated from GNSS observations and provided by the near real-time "EUMETNET EIG GNSS water VApour Program" (E-GVAP) service running at the ROB. This service is used by Meteorological Agencies all over Europe in order to enhance Numerical Weather Prediction (NWP). In that context, about 15 new GNSS stations have been added in 2011 to the near real-time solution provided to E-GVAP members. 80 GNSS stations have been added to the precise monitoring of the European troposphere (post-processing analysis) mainly used for validation purposes and re-analysis applications.

Based on the tropospheric delay information provided to E-GVAP, we are developing tools to create a web-based interface with dynamic maps of the wet tropospheric delay data over Europe. This includes

the testing of several interpolation techniques to calculate the tropospheric delay grid over Europe and the development of a web-based user interface to provide access to interactive products (e.g. static maps, movies, values of the tropospheric delay). These maps and products are presently in their validation phase and release to the public is expected in 2012.

End 2011, new IT infrastructure was installed at ROB to sustain and maintain the E-GVAP activities. All programs related to the E-GVAP service have been adapted and optimized to run on this new infrastructure. It resulted in a 44% increase in the number of stations included, while speeding up the processing (at least) by a factor of 2 (the processing time was decreased from 10-25 min to 5-8 min) and keeping the same level of precision. Since November 2011, this new service is run in parallel to the old one in order to carry out extensive comparisons and validations (see Figure 62) and provides a test solution to meteorologists participating in E-GVAP. This step is mandatory before the new service can become the official ROB solution within E-GVAP during 2012.

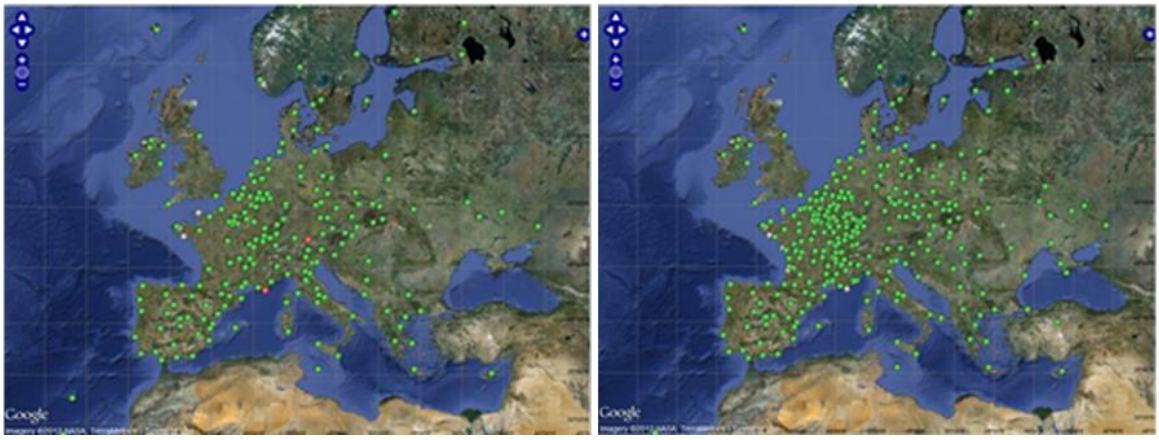

Figure 62: GNSS network processed in near-real time in the framework of E-GVAP. Left: Official service solutions. Right: New service solutions under validation. (Status: 6 February 2012). Please note some stations are located outside the region represented by the map.

A collaboration between RMI and ROB concerning the E-GVAP activities and concerning the possible exploitation of GNSS observations for climate applications has been started.

- Tropospheric Climatological Modeling

Water vapor plays a dominant role in the climate change debate. However, observing the atmospheric water vapor over climatological timescales in a homogeneous and consistent manner is challenging. The STCE is in a unique situation allowing the comparison of different techniques providing access to observations of the atmospheric water vapor. Indeed, ROB, RMI and BISA have each of them an expertise in different ground-based, in-situ and satellite-based techniques to measure the atmospheric water vapor. Based on this knowledge, a new STCE collaboration was set up in 2011 with the goal to assess the potential of each technique to observe water vapor for climatological applications, with a focus on inter-technique comparisons and the applicability of the derived datasets for water vapor time series analysis.

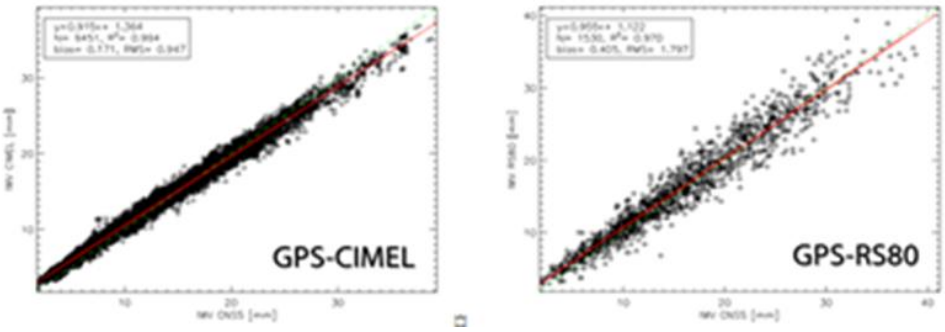

Figure 63: Scatter plots of simultaneous IWV measurements of the different instruments with the GNSS device. Left: GPS and CIMEL IWV, Right: GPS and radiosonde (RS80) IWV.

In 2011, we started the inter-comparison of atmospheric water vapor data derived from the observations of several ground-based, in-situ and satellite-based techniques focused on the Uccle station (which shares all techniques and for which we dispose of all the necessary meta-data). Particularly, we derived Integrated Water Vapor (IWV) time series for the period 2000-2011 from ground-based reprocessed GNSS observations (provided by ROB), radiosondes measurements (provided by RMI), and CIMEL (French manufacturer) and IASI measurements (provided by BISA). This study demonstrated that the CIMEL sun-photometer, the radiosonde and the GNSS technique have a very good agreement with a small bias (below 0.6 mm of IWV) and an RMS below 1.9 mm of IWV (see Figure 63). However, the satellite-based observations from IASI and the GNSS-based measurements, do not agree at the same level (bias of 5.4 mm and RMS of 9.5 mm of IWV, see Figure 64). In 2012, this inter-comparison will be extended to about 30 sites worldwide having technique colocation (max. separation distance of 30 km) of GNSS (provided by ROB), radiosondes (provided by RMI) and CIMEL, IASI/GOME/GOME2/SCIAMACHY (provided by BISA and the Max Planck Institute for Chemistry).

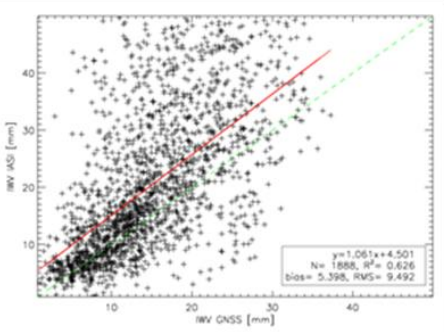

Figure 64: Scatter plots of simultaneous IWV measurements of the IASI instrument with the GNSS device.

GNSS-based early identification of deep convection

In 2010, a workgroup on water vapor and GNSS research was created within the STCE, involving teams from the three institutes at the Space Pole. Using accurate GNSS, one of our main goals has been to develop a strategy to detect initiation of deep convection using accurate GNSS measurements of the Belgian Dense Network. Deep convection is associated to the creation of convective cells (and clouds with high vertical extension) which create (heavy) rain.

The objective of this work is to show the interest of GNSS observations for weather forecasts, especially for nowcasting. We focused on GPS observations of Zenith Total Delay of the neutrosphere (ZTD) and horizontal gradients of delay and try to answer to the following question: "Can the detection of water vapor by GNSS allow us to establish typical configurations of humidity fields which characterize convective systems and particularly which supply forerunners of their initialization associated to deep convection?"

We based this study on the rainfall event of 28-29 June 2005. From the afternoon of 28 to the evening of 29 June 2005, consequent precipitation has been observed over the main part of Belgium. Neméghaire and Brenot (2010) give a precise description of this meteorological event. Using the Belgian synoptic network and near real-time meteorological observations (Radar, SAFIR, METEOSAT), forecast of rainfalls induced by the several convective systems which took place was not a success for such a tricky situation.

The neutral atmosphere represents an element of uncertainty of GNSS positions because water vapor decreases speed of propagation of radio waves. This is why tropospheric parameters, called ZTD and horizontal gradient of delay, have been introduced in geodetic software to improve positioning solutions. When positions of stations are well established, precise ZTD measurements (strongly linked to the humidity field variations) and horizontal gradient of water vapor around a station can be estimated by a least-square adjustment which uses double difference of delays of the ionosphere-free combination (Brenot et al., 2006; Brenot and Warnant, 2008).

Our study of the rainfall event of June 2005 has shown that the meteorological situation and the location of water vapor bubbles observed by GNSS are in a good agreement with Radar precipitations. Strong horizontal GNSS gradients are observed when significant hourly precipitations are recorded by meteorological Radar. This is evidence that strong anisotropy of the humidity field took place during this period. For this reason we have combined ZTD and gradients to improve spatial resolution of our humidity field assessments (Brenot et al, in preparation). In Figure 65, we can clearly see an improvement of the resolution of humidity field with this technique.

The next step of our study has been to implement H2O alerts according to a specific configuration of the GNSS humidity field. A meticulous observation of ZTD and gradients time series have shown that for some regions a typical configuration can be observed before initiation of deep convection. This configuration is described by an important local decrease of ZTD (drier region) followed by a strong increase of ZTD (wetter region). This dry/wet contrast evolution is illustrated in Figure 65b.

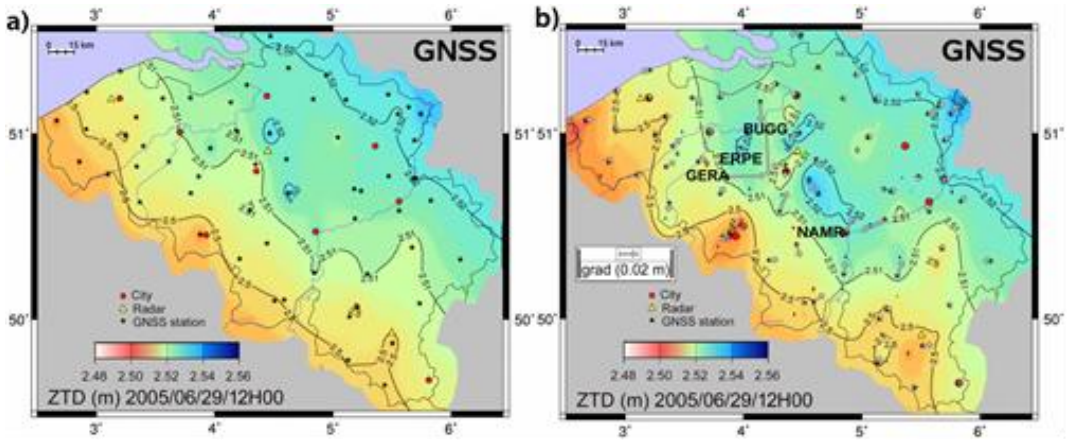

Figure 65: a) imaging of the 2D field of ZTD with a classic interpolation (stations are plotted by black stars); b) improvement of this field by GNSS gradients. These gradients are plotted by gray arrows at each GNSS site. BUGG, ERPE, GERA and NAMR stations are plotted. Locations of 9 major cities (red circles) and meteorological Radars (yellow triangles) are also plotted on these 2D maps.

The conditions to obtain a H2O alert at the time T are the following:

ZTD decrease of 0.008 m from T – 30 min to T – 15 min

ZTD increase of 0.015 m from T – 15 min to T

To validate our H2O alert, we considered two external meteorological indicators of deep convection. The first one uses C-band weather Radar (5.64 GHz frequency) and echoes tops measurements of precipitation with reflectivities larger or equal to 38 dBZ. We estimate that an altitude of the highest 38 DbZ radar echo higher than 5 km represents a good indicator of deep convection for this location. The second indicator of deep convection that we use, is infrared radiance from the SEVIRI (Spinning Enhanced Visible and Infrared Imager) instrument on METEOSAT Second Generation. If effective radiance (channel 09) is less than 200W/m^2 we consider that deep convection took place.

To estimate the score of our H2O GNSS alerts we consider that an alert is validated if an indicator of deep convection (by Radar and/or by SEVIRI) is observed during the next 45 minutes. Using ZTD and gradients measurements, a grid of H2O alert has been estimated with a resolution of 3 km × 3.5 km (resolution required to detect convective

Periods	Number of H_2O alert	Score (Radar)	Score (SEVIRI)	Final Score
2005/06/26	0 (0)	/	/	/
2005/06/27	0 (0)	/	/	/
2005/06/28	798 (1853)	34% (31%)	70% (71%)	78% (75%)
2005/06/29	2821 (6384)	48% (44%)	82% (84%)	89% (87%)
2005/06/30	0 (0)	/	/	/
2005/07/01	0 (0)	/	/	/
2005/07/02	0 (0)	/	/	/
All days	3619 (8237)	45% (41%)	79% (81%)	86% (84%)

Figure 66: Statistical results and score of our H2O alerts (GNSS observations from 26 June 2005 till 2 July 2005). Time resolution of GNSS observations is 15 minutes. Shown in brackets are the results when GNSS observations are interpolated linearly every 5 minutes.

cells). To validate our H2O alert, 38 dBZ Radar echo tops and infrared radiance of SEVIRI have been established for the same grid.

To resume, analysis of this period (from 26 June 2005 till 2 July 2005) shows that GNSS H2O alerts are the result of dry-wet contrasts in time (strong increase and decrease) and dry/wet contrasts in space (dipole). That means a dry region is close to a wet region and there is a transfer of water vapor in this region. We have observed strong amplitudes of horizontal gradients pointing wet area with strong instability. This shows the interest of these observations for nowcasting. Statistical results and validation of our GNSS H2O alerts detected are shown in Figure 66. When no meteorological activity and deep convection is present, no alert is detected. More than 80% of our alerts are validated by Radar and SEVIRI. We have estimated linearly ZTD and gradients measurements for a time-resolution of 5 minutes. We can follow precisely the evolution of the humidity field and the interest of our GNSS alerts for nowcasting. In fact, the number of alerts increased and for some cases, the alerts took place earlier.

We have shown the key role of GNSS horizontal gradient to detect water vapor bubbles and associated contrasts of humidity which are forerunners of deep convection. Nevertheless our study considers post-processed observations with a high sensitivity to humidity.

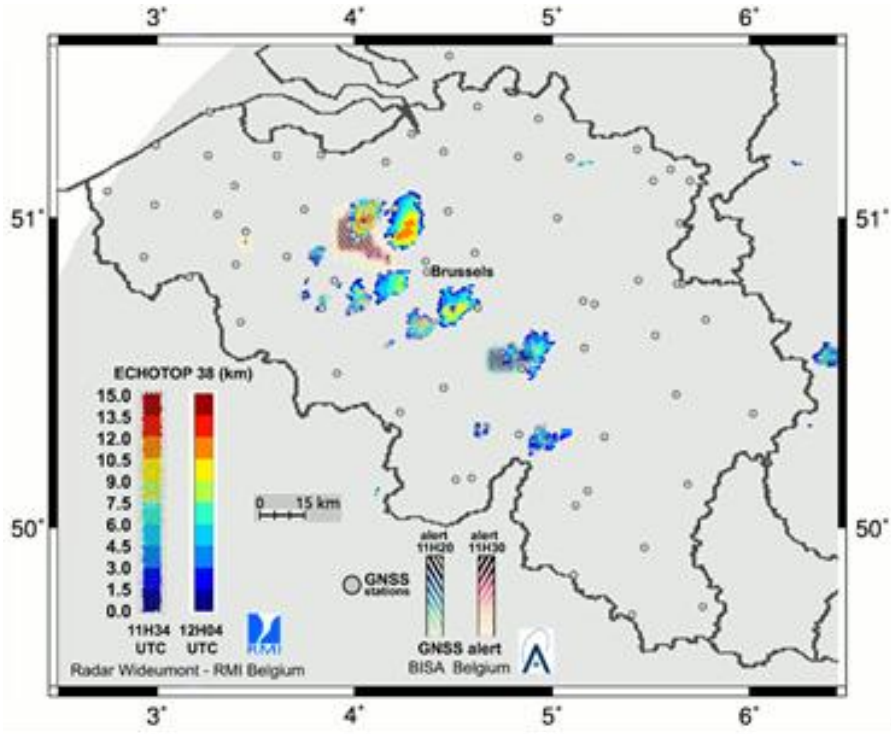

Figure 67: GNSS H2O alert (11:20 and 11:30 UTC) and 38 dBZ Radar echo tops (11:35 and 12:05 UTC) on June 29, 2005.

A poster of this study has been presented at EGU in Vienna (April 2011) and in the final meeting of Water Vapor in the Climate System (WAVACS) COST action. A draft of this publication is in review by co-authors and will be submitted as soon as possible to a special issue of Atmospheric Chemistry and Physics dedicated to WAVACS.

The influence of ozone and aerosol on climate and UV radiation

- Ozone

Through comparisons with data from other European ozone sonde stations and from aircraft measurements, Logan et al. 2012 pointed out that our Uccle ozone sonde station is measuring too much tropospheric ozone during recent years. As a matter of fact, we compared our dataset with quasi-simultaneous observations at the nearby ozone sonde station of De Bilt (see Figure 68) and we found a positive tropospheric ozone bias in our data in the period mid-2007 to the end of 2009. On the other hand, no bias is observed between both stations for the boundary layer and stratospheric ozone data.

The beginning of the deviation period coincides with the change of the radiosounding equipment (and consequently, radiosonde and ozone interface type change) which affects the measurements of the vertical profiles of temperature – both the temperatures inside and outside the isolation box which contains the ozone sonde –, relative humidity and pressure. Of these variables, the box temperature is the only one that is directly related to the ozone measurements. The new temperature sensors report consistently lower temperatures in the isolation box, throughout the entire vertical profile, but a temperature difference of 5°C affects the measurement result (ozone in ppb) only to about 1.5 to 2 % of the calculated value throughout the profile. With the installation of the new radiosounding equipment hardware, also the software for calculating the ozone amounts from the raw data values changed. The impact of this new software on the resulting ozone amount should be marginal, but we nevertheless decided to extract the raw data values from the dataset and to do the conversion ourselves, in order to be fully independent of the manufacturer's conversion and correction algorithms. This is a very time consuming task and is actually still ongoing.

Another possible cause for the detected bias in the tropospheric ozone measurements at the Uccle station are the ozone sondes themselves. As the problem arises only in the free troposphere (the region in which the ozone amounts are lowest), the deviation could be traced back to the sensitivity of the ozone sondes. In particular, the influence of the background current, measured in the labo before the ozone sonde launch and subtracted afterwards from every single raw ozone measurement, is largest in this atmospheric region.

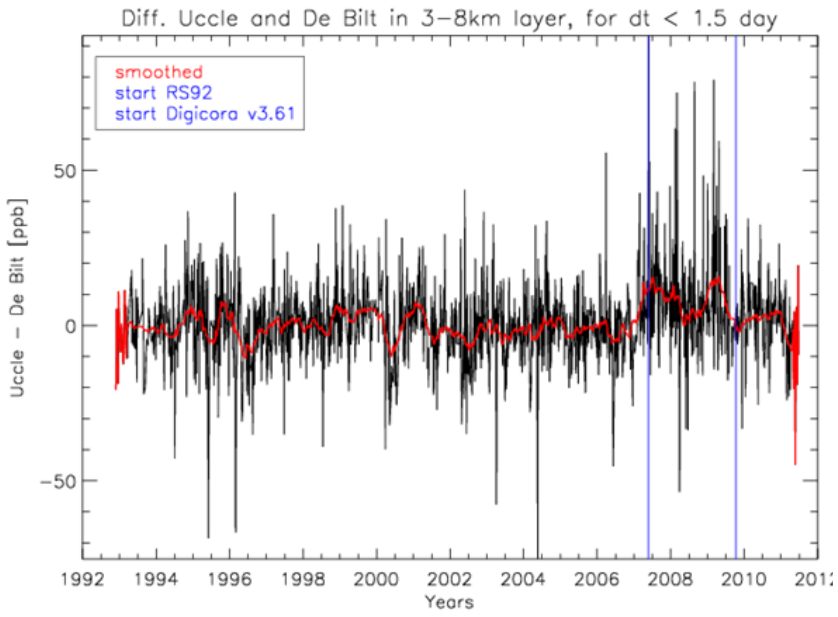

Figure 68: Difference in the total amount of ozone (in ppb), calculated in a layer between 3 and 8 km, measured with ozone sondes launched at Uccle and De Bilt at identical or consecutive days. The red curve shows a smoothed version (running mean) of this difference and the vertical blue lines denote the change of the radiosounding equipment and an update of the sounding software, respectively.

However, the time series of background currents measured at Uccle does not reveal any discrepancy in the 2007-2009 timeframe. As a matter of fact this period is characterized by a very small variability in the background current. Other properties of the ozone sondes also do not show any deviating trend or bias during 2007-2009. It is nevertheless striking that the beginning and the end of the "bad period" coincide with the use of certain batches of ozone sondes. Or to put it in another way: 3 batches of ozone sondes show much stronger deviations from the quasi-simultaneous ozone sondes at De Bilt than the batches we received before and afterwards from our manufacturer. Could it be that, 3 years in a row, we received batches of minor quality? But why do these same batches of ozone sondes perform better when launched (a second time) after November 2009?

To conclude, the origin of the positive bias in tropospheric ozone, as measured at the Uccle ozone sonde station, is still unclear and needs further investigation. Probably, different causes play a role. As Uccle holds one of the three longest records of ozone sonde observations in the world, we need to deal with this issue and we need to provide answers to the community that is frequently using our data.

- Aerosol optical properties

Data from the Brewer spectrophotometer can be used to retrieve the Aerosol Optical Depth (AOD) in the UV. The Cimel sunphotometer is a standard instrument widely uses in the AERONET network to obtain AODs mainly in the visible and the infrared.

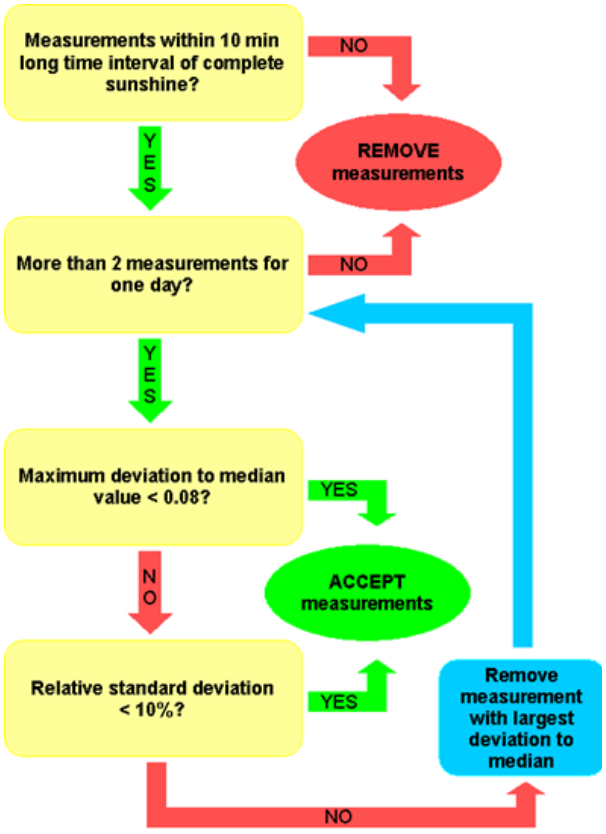

Figure 69: Overview of the improved cloud screening method.

It has been shown that Brewer sun scan measurements can be used to derive AOD values at 340nm (De Bock et al. 2010). Together with this retrieval method, a cloud screening algorithm was developed. However, analysis of the cloud screened values AOD (i.e. data affected by clouds are filtered out) showed that the applied cloud screening technique was not optimal. Therefore, a new cloud screening algorithm had to be developed.

This new algorithm makes use of sunshine duration data (from 4 pyrheliometers at Uccle) and is also based on the assumption that the variability of the AOD in the course of one day is either lower than 10% or lower than 0.08 AOD units. Figure 69 gives a schematic overview of the improved cloud screening technique. The advantages of this new method are the removal of the arbitrary maximum level of AOD values and that it runs completely automatic (whereas the old one needed manual verification afterwards).

The AODs obtained with the improved cloud

screening method are compared to quasi-simultaneous Cimel level 2.0 values (with a maximum time difference of 3 minutes). Due to the delays in the availability of the Cimel data, the period of comparison is limited to a period from 1 September 2006 until 1 September 2010. For this period, 665 individual AOD values were compared and the correlation coefficient, slope and intercept of the regression line are 0.9760, 0.9816 +/- 0.0085 and 0.0776 +/- 0.0030 resp. This shows that the cloud screened Brewer AOD agree very well with the Cimel data.

Figure 70: Lidar Ceilometer installed in Uccle

We also investigated the temporal variability of the cloud screened AOD. The highest AOD values occur in spring, whereas in autumn and winter, the AOD are clearly lower.

In 2011 a LIDAR/Ceilometer (Figure 70) was installed in Uccle. This instrument is designed to measure the height of the cloud base. It consists of an infrared laser which sends short pulses into the atmosphere. The backscattered signal delivers information on the vertical structure of the atmosphere. From this, not only the height of the clouds can be detected, but also the height of the mixing layer, large pollution events and the possible presence of volcanic debris. In the coming periods the data will be analyzed in detail.

- UV radiation

On 9 November 2011, Brewer 178 spectrophotometer of RMI was brought to the calibration laboratory of BISA. Reason was that there were doubts about the validity of the so-called cosine response of the instrument. The Brewer measures the solar light intensity in the UV (286-363nm) on a horizontal surface. Ideally the response should follow the cosine of the angle of the incident light with the vertical. If this is not the case and the deviation is known, measurements can be corrected. Therefore a laboratory setup at BIRA was used to measure the deviation for this particular instrument.

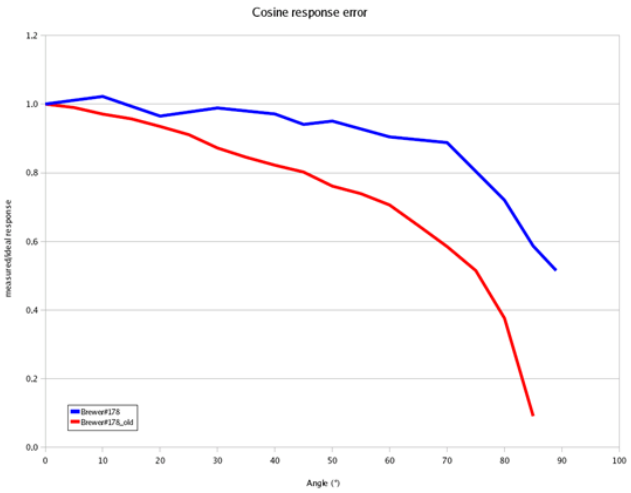

Figure 71: Result of the cosine response error campaign. The red line represents the old cosine response function as provided by the manufacturer. The blue line shows the actual measured cosine response error of Brewer#178.

Figure 71 shows that the cosine response given by the manufacturer is no longer valid. In further analyses, the newly measured one will be used. With the good knowledge of the cosine response, we will try to retrieve the Single Scattering Albedo (SSA) of the aerosol particles by inverse modeling. This is an important parameter for the estimation of the radiative effect of aerosols.

User web applications

- Further development of the SWANS website

In 2008, RMI launched in the frame of the STCE the project Space Weather And Navigation Systems (SWANS). The project was primarily concerned with monitoring and research of space weather phenomena and their effects on GNSS-based applications. In 2011, the Royal Observatory (ROB) also joined the project and focused on the development of GNSS-based services. Most measurements are carried out at the RMI Geophysical Centre in Dourbes (CPG) and the Royal Observatory (ROB).

Several developments have already been released and are now available on the SWANS website (http://swans.meteo.be/) in 2 main areas: Space Weather effects on GNSS-based applications, and Space Weather monitoring services.

Figure 72: The STCE Space Weather and Navigation Systems website with services available to the users.

- LIEDR: Award winning best paper

The availability of the Dourbes comprehensive ionosonde database and the immediate access to high-quality digisonde measurements allowed the STCE scientists to do valuable research and developments.

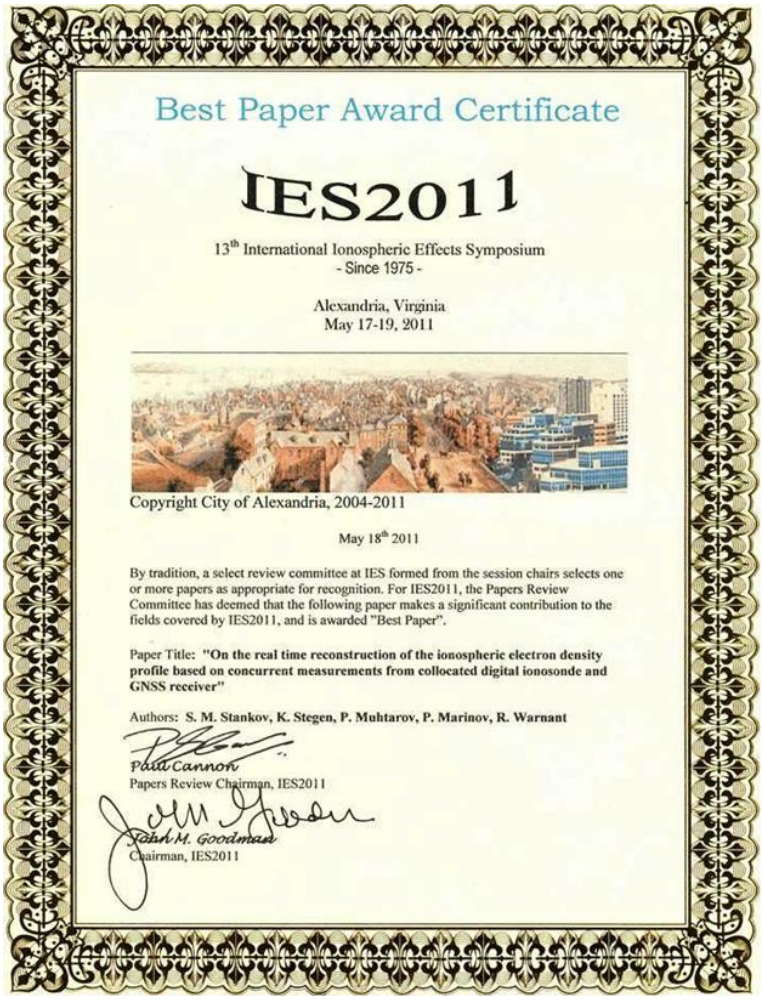

Best Paper Award Certificate

IES2011

13th International Ionospheric Effects Symposium
- Since 1975 -

Alexandria, Virginia
May 17-19, 2011

Copyright City of Alexandria, 2004-2011

May 18th 2011

By tradition, a select review committee at IES formed from the session chairs selects one or more papers as appropriate for recognition. For IES2011, the Papers Review Committee has deemed that the following paper makes a significant contribution to the fields covered by IES2011, and is awarded "Best Paper".

Paper Title: **"On the real time reconstruction of the ionospheric electron density profile based on concurrent measurements from collocated digital ionosonde and GNSS receiver"**

Authors: **S. M. Stankov, K. Stegen, P. Muhtarov, P. Marinov, R. Warnant**

Paul Cannon
Papers Review Chairman, IES2011

John M. Goodman
Chairman, IES2011

Figure 73: The IES-2011 Best Paper Award certificate.

For example, we developed a novel operational system based on measurements from the collocated Digisonde and a GNSS receiver in Dourbes. The system, dubbed LIEDR (Local Ionospheric Electron Density profile Reconstruction), acquires and promptly processes the incoming measurements, computes the full-height ionospheric electron density profile, and displays the resulting profilograms. LIEDR is designed to operate in continuous real-time mode for service applications and to provide historical data/plots for research applications and further developments of the system. The work was well accepted by the international research community and a publication reporting on this development won the best paper award (Figure 73) at the prestigious International Ionospheric Effects Symposium, held May 2011 in Washington, USA. The International Ionospheric Effects Symposium (IES), is a triennial symposium inaugurated in 1975 (http://www.ies2011.com/), with the objective of bridging the gap between applications and research involving ionospheric and space weather disciplines. Every three years, the event covers the effects of ionosphere and space weather on military and commercial telecommunication and satellite systems.

- Monitoring of the Earth's ionosphere

A new web product to monitor the ionosphere in near real-time over Europe using GPS observations was put into operation. The service is available from the GNSS website (http://gnss.be/Atmospheric_Maps/ionospheric_maps.php) and has been integrated into the SIDC web portal (http://sidc.oma.be/LatestSWData/LatestSWData.php). These European near real-time ionospheric VTEC maps are based on the real-time GPS data available from the EPN. Two different products are proposed to the user community: (1) an interactive product (e.g. movies, VTEC values); (2) a static product with statistics (e.g. differences with respect to the previous 15 days ionospheric activity).

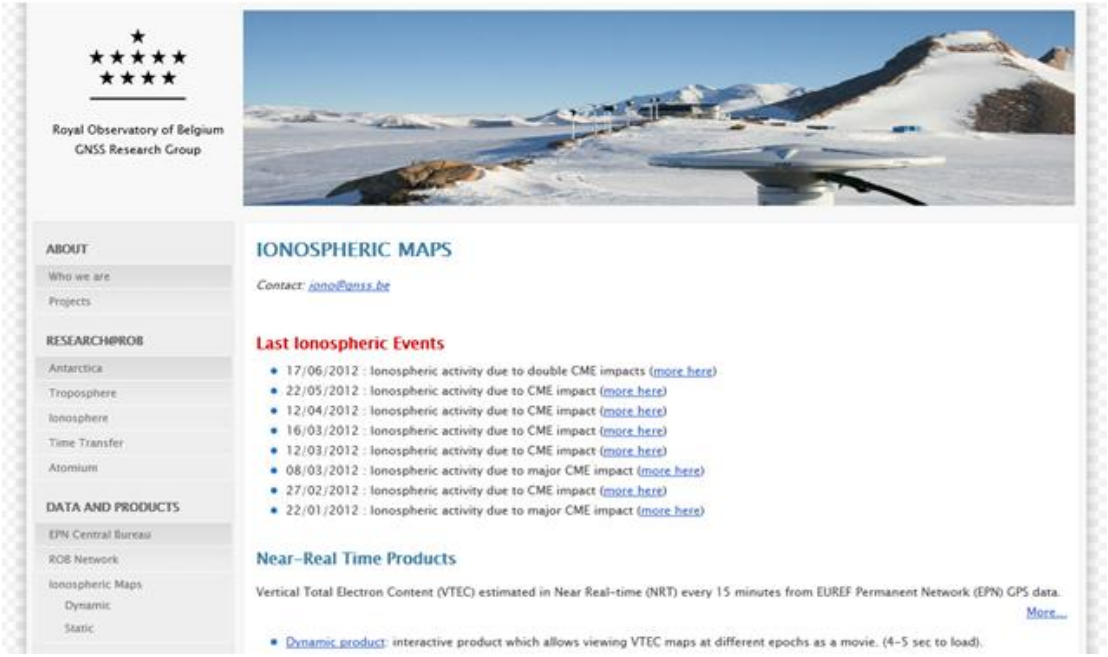

Figure 74: The new website for monitoring the Earth's ionosphere

- Ground-based solar radiation measurements

The main objective of ground-based solar radiation measurements is to exploit, upgrade, and/or make publicly available the existing UV measurements at the 6 stations of the IASB-BIRA network (at Uccle, Redu, Oostende, Virton, Mol and Mont-Rigi) and IASB-BIRA calibration facilities.

During 2011, a new station has been deployed in Mont-Rigi (Hautes Fagnes) and is fully operational since November 2011 (see Figure 75 left).

The stations (Uccle, Redu, Oostende, Virton, Mol, Mont-Rigi and Diekirch) provide UV-B, UV-A, and Visible datasets of the solar irradiance reaching the Earth's surface. Ancillary meteorological data (temperature, relative humidity, pressure, wind speed and direction, pluviometry, cloud cover) complete the data set (Figure 75 right). All the data are available on our new web site: http://uvindex.aeronomie.be/

We will continue to support our ground network for measurement of the solar irradiance in UV-VIS-IR. Some refurbishments are planned to replace the older instruments, more than 6 years of use, by new ones. Installation of a UV-Visible set of instruments is planned at the Princess Elisabeth Station (Antarctica) in October 2012.

Figure 75: At left, the instruments at the Mont-Rigi station. At right the UV network in Belgium with daily measurements, as available at the BISA's UV-index website.

- Space Environment Information System (SPENVIS)

The Space Environment Information System (SPENVIS) is a web-based interface for assessing the space environment and its effects on spacecraft systems and crews. The SPENVIS system has been developed and maintained for the European Space Agency and is used for mission analysis and planning. It includes several empirical models of the space environment covering mainly cosmic rays, solar energetic particles, natural radiation belts, magnetic fields, space plasmas and the upper atmosphere, and, several engineering models to assess the effects of the space environment on spacecraft such as surface and internal charging, energy deposition, solar cell damage and single event upset rates. The SPENVIS system also includes extensive background information on the space environment, the implemented models and the related standards.

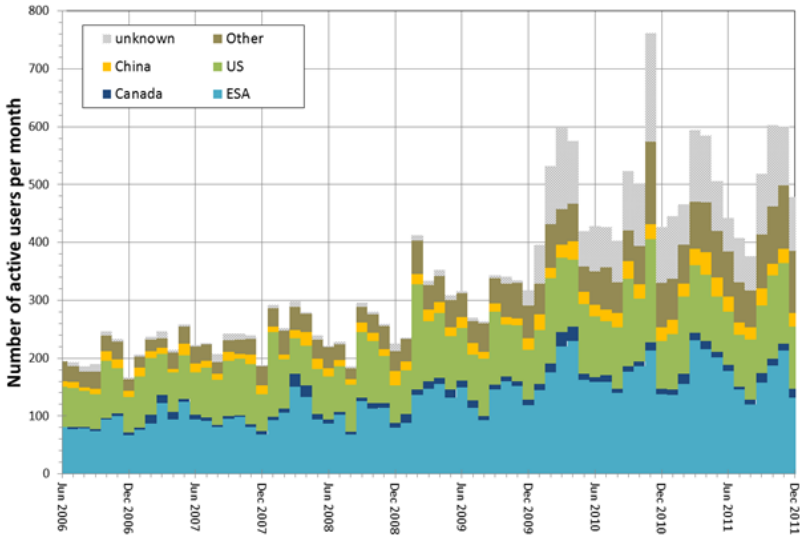

Figure 76: Progression of the active users of the Space Environment Information System (SPENVIS) since mid-2006 and their geographical repartition. For each month the statistic shows the repartition of users having accessed the system and requested the execution of at least one model.

Since 2010, the SPENVIS system is actively used by about 3000 people per year with an average of 500 active users per month. An overview of the geographic repartition of those users and its evolution in time is provided on Figure 76. An upgraded version (4.6.5) of the SPENVIS system has been released on September 19, 2011, including some new models or tools such as the Meteoroid and Space Debris Terrestrial Environment Reference (MASTER) or the Jupiter Radiation Environment and Effects Models and Mitigation (JOREM). The SPENVIS system can be accessed from URL http://www.spenvis.oma.be/

- European Space Weather Portal (ESWP)

The European Space Weather Portal (ESWP) is an integrated website providing a centralized access point to the space weather community to share their knowledge and results. Initiated under the COST 714 action and hosted by the Belgian Institute for Space Aeronomy, the ESWP is being further developed in the framework of the COST ES0803 action. The portal has a large section devoted to education and outreach, but it is also a platform to run local and remote models and to access their results both in graphical and various numerical forms.

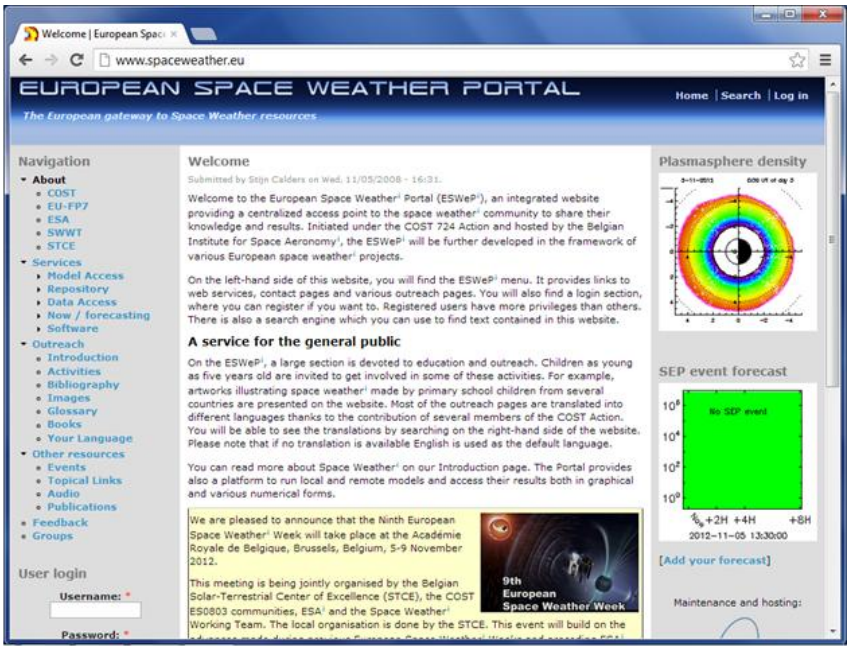

Figure 77: Welcome page of the European Space Weather Portal

The ESWP portal is also gathering some results from other European initiatives such as the Space Weather Working Team (SWWT) and the FP7 projects SOTERIA and eHEROES. The ESWP portal is accessible from the URL http://www.spaceweather.eu/.

Publications

This list of publications consists only of the peer-reviewed articles and the presentations and posters at conferences. Adding all the non-refereed articles, the press releases, the daily, weekly and monthly bulletins that are published for the whole series of solar-terrestrial parameters, the public outreach texts,… would simply take too much space in this report. These data are available at the STCE-website http://stce.be/index.php or upon request.

Peer reviewed articles

1. Q. Baire, C. Bruyninx, P. Defraigne, J. Legrand
Precise Point Positioning with ATOMIUM using IGS Orbit and Clock Products: First Results
Bulletin of Geodesy and Geomatics, 69 (2-3), pp.391-399

2. M.R. Bareford, P.K. Browning, R.A.M. Van der Linden
The Flare-energy Distributions Generated by Kink-unstable Ensembles of Zero-net-current Coronal Loops
Solar Physics, 273, pp.93-115

3. N. Bergeot, C. Bruyninx, P. Defraigne, S. Pireaux, J. Legrand, E. Pottiaux, Q. Baire
Impact of the Halloween 2003 Ionospheric Storm on Kinematic GPS Positioning in Europe
GPS Solutions, doi: 10.1007/s10291-010-0181-9, Volume 15, Issue 2, pp.171-180, April 2011

4. B. Bidaine, R. Warnant
Ionosphere modeling for Galileo single frequency users: illustration of the combination of the NeQuick model and GNSS data ingestion
Advances in Space Research, Vol.47, pp.312-322, doi:10.1016/j.asr.2010.09.001

5. K. Bonte, C. Jacobs, E. Robbrecht, A. De Groof, D. Berghmans, S. Poedts
Validation of CME detection software (CACTus) by means of simulated data & analysis of projection effects on CME velocity measurements
Solar Physics, 270 (1), pp.253

6. C. Bruyninx, W. Aerts, J. Legrand
GPS, Data Acquisition and Analysis
Encyclopedia of Solid Earth Geophysics, Earth Science Series, Springer, 2011, pp.420-431, doi: 10.1007/978-90-481-8702-7

7. P. Chainais, V. Delouille, J.-F. Hochedez
Scale invariant images in astronomy through the lens of multifractal modeling
Proceedings, IEEE International Conference on Image Processing, pp.1309-1312

8. F. Clette
Past and future sunspot indices: New goals for SoTerIA
Journal of Atmospheric and Solar-Terrestrial Physics, 73, Issue 2-3, pp.182-186

9. L. Dolla, A.N. Zhukov
On the nature of the spectral line broadening in solar coronal dimmings
Astrophysical Journal, 730, pp.113

10. L. Dolla, C. Marqué, D.B. Seaton, T. Van Doorsseleare, M. Dominique, D. Berghmans, C. Cabanas Parada, A. De Groof, W. Schmutz, Andrea Verdini, M. West, J. Zender, A.N. Zhukov
Time delays in quasi-periodic pulsations observed during the X2.2 solar flare on 15 February 2011 Astrophysical Journal, , pp., accepted

11. U. Feldman, I.E. Dammasch, G.A. Doschek
Redshifts, widths, and radiances of spectral lines emitted by the solar transition region
Astrophysical Journal, 743, pp.165-188

12. S. Gunár, S. Parenti, U. Anzer, P. Heinzel, J. C. Vial
Synthetic differential emission measure curves of prominence fine structures: II. The SOHO/SUMER prominence of 8 June 2004
Astronomy and Astrophysics, 535, pp.id.A122

13. M.E. Innocenti, G. Lapenta, B. Vrsnak, F. Crespon, C. Skandrani, M. Temmer, A. M. Veronig, L. Bettarini, S. Markidis, M. Skender
Improved forecasts of solar wind parameters using the Kalman filter
Space Weather, 9, pp.S10005

14. R. Jurdana-Sepic, R. Brajsa, H. Woehl, A. Hanslmeier, I. Poljancic, L. Svalgaard, S. Gissot
A relationship between the solar rotation and activity in the period 1998-2006 analysed by tracing small bright coronal structures in SOHO-EIT images
Astronomy and Astrophysics, 534, pp.A17

15. S.T. Kumara, R. Kariyappa, M. Dominique, D. Berghmans, L. Damé, J.-F. Hochedez, V.H. Doddamani, L.P. Chitta
Preliminary Results on Irradiance Measurements from Lyra and Swap
Advances in Astronomy, 2012, pp.1--5

16. H. Lamy, S. Ranvier, J. de Keyser, S. Calders, E. Gamby, C. Verbeeck
BRAMS: the Belgian RAdio Meteor Stations
In "Meteoroids: The Smallest Solar System Bodies" (eds. W.J. Cooke, D.E. Moser, B.F. Hardin, D. Janches; Breckenridge, Colorado, USA, May 24-28, 2010), p. 351.

17. S. Landi, L. Bettarini
Three-Dimensional Simulations of Magnetic Reconnection with or Without Velocity Shears
Space Science Reviews, Online First, doi: 10.1007/s11214-011-9824-6

18. G. Lapenta, L. Bettarini
Spontaneous transition to a fast 3D turbulent reconnection regime
Europhysics Letters, 93, pp.65001

19. G. Lapenta, L. Bettarini
Self-consistent seeding of the interchange instability in dipolarization fronts
Geophysical Research Letters, 38, pp.CiteID L11102

20. M. Lazar, V. Pierrard, R. Schlickeiser, S. Poedts
Modeling space plasma dynamics with anisotropic Kappa distributions
Astrophysics and Space Science, 2012 (in press)

21. L. Lefèvre, F. Clette
A global small-sunspot deficit at the base of the index anomalies of solar cycle 23
Astronomy and Astrophysics, 536, pp.L11

22. J. Legrand, C. Bruyninx, N. Bergeot
Results and Comparisons of a Local and a Regional Reprocessed GNSS Network
Bulletin of Geodesy and Geomatics, 69 (2-3), pp. 257-267, 2011

23. S. Lejeune, G. Wautelet, R. Warnant
Ionospheric effects on relative positioning within GPS dense network
GPS Solutions, Vol.16, No.1, pp.105-116, doi: 10.1007/s10291-011-0212-1

24. P. Malinowski, J.-Y. Duboz, P. de Moor, J. John, K. Minoglou, N. Srivastava, F. Semond, E. Frayssinet, B. Giordanengo, A. BenMoussa, U. Kroth, C. Laubis, R. Mertens, C. Van Hoof
AlGaN-on-Si-based 10 μm pixel-to-pixel pitch hybrid imagers for the EUV range
Electron Device Letters, 32, pp.1561-1563

25. P. Malinowski, J.-Y. Duboz, P. de Moor, K. Minoglou, J. John, B. Giordanengo, A. BenMoussa, R. Mertens, C. Van Hoof
Extreme ultraviolet detection using AlGaN-on-Si inverted Schottky photodiodes
Applied Physics Letters, 98, pp.14104

26. A. Mangold, H. De Backer, B. De Paepe, S. Dewitte, I. Chiapello, Y. Derimian, M. Kacenelenbogen, J.-F. Léon, N. Huneeus, M. Schulz, D. Ceburnis, C. D. O'Dowd, H. Flentje, S. Kinne, A. Benedetti, J.-J. Morcrette, O. Boucher
Aerosol analysis and forecast in the ECMWF Integrated Forecast System: 3. Evaluation by means of case studies
Journal of Geophysical Research, 116, D03302, doi: 10.1029/2010JD014864, 2011

27. S. Markidis, G. Lapenta, L. Bettarini, M. Goldman, D. Newman, L. Andersson
Kinetic simulations of magnetic reconnection in presence of a background O+ population
Journal of Geophysical Research, 116, pp.CiteID A00K16

28. M. Mierla, I. Chifu, B. Inhester, L. Rodriguez, A.N. Zhukov
Low polarised emission from the core of the 31 August 2007 CME
Astronomy and Astrophysics, 530, L1, 2011

29. M. Mierla, B. Inhester, L. Rodriguez, S. Gissot, A.N. Zhukov, N. Srivastava
On 3D Reconstruction of Coronal Mass Ejections: II. Longitudinal Width Analysis of 31 August 2007 Event
J. Atmos. Sol.-Terr. Phys., 73, pp.1166-1172

30. M. Mierla, D.B. Seaton, D. Berghmans, I. Chifu, A. De Groof, B. Inhester, L. Rodriguez, G. Stenborg, A.N. Zhukov
Study of a Prominence Eruption using SWAP/PROBA2 and EUVI/STEREO Data
Solar Physics, , pp., accepted

31. J.M. Pasachoff, V. Rusin, H. Druckmullerova, M. Saniga, M. Lu, C. Malamut, D.B. Seaton, L. Golub, A. J. Engell, S. Hill, R. Lucas
Structure and Dynamics of the 2010 July 11 Eclipse White-light Corona
Astrophysical Journal, 734, pp.114 (10pp)

32. J.M. Pasachoff, E.D. Tingle, I.E. Dammasch, A. Sterling
Simultaneous Observations of the Chromosphere with TRACE and SUMER
Solar Physics, 268, pp.151-163

33. H. Peter, et al., incl. S. Parenti
Solar magnetism eXplorer (SolmeX)
Experimental Astronomy, doi: 10.1007/s10686-011-9271-0

34. V. Pierrard
A numerical method to determine the particle velocity distribution functions in space
Astronum2010 Proceedings, Numerical Modeling of Space Plasma Flows, Astronomical Society of the Pacific Conference series, Edited by N. V. Pogorelov, E. Audit and G. P. Zank, vol. 444, 166-176, 2011b

35. V. Pierrard
Effects of suprathermal particles in space plasmas
ICNS Annual International Astrophysics Conference Proc., American Institute of Physics, 2012b (in press)

36. V. Pierrard
Kinetic models for solar wind electrons, protons and ions
"Exploring the solar wind", 221-240, Intech, Edited by M. Lazar, ISBN 978-953-51-0339-4, 2012a

37. V. Pierrard
Solar wind electron transport: interplanetary electric field and heat conduction
Space Science Review (solar wind), 2011a, doi: 10.1007/s11214-011-9743-6.

38. V. Pierrard, K. Borremans
Fitting the AP8 spectra to determine the proton momentum distribution functions in space radiations
Radiation Measurements, 47, 401-405, 2012a, doi: 10.1016/j.radmeas.2012.04.002

39. V. Pierrard, K. Borremans
The ionosphere coupled to the plasmasphere and polar wind models
Astronum2011 Proceedings, ASP Conference series, 2012b (in press)

40. V. Pierrard, M. Lazar, R. Schlickeiser
Evolution of the electron distribution function in the wave turbulence of the solar wind
Solar Physics, 269, 2, 421-438, 2011, doi: 10.1007/s11207-010-9700-7

41. V. Pierrard, M. Voiculescu
The 3D model of the plasmasphere coupled to the ionosphere
Geophysical Research Letters, 38, L12104, 2011, doi: 10.1029/2011GL047767

42. T. Podladchikova, R.A.M. Van der Linden
Peak Sunspot Number for Solar Cycle 24
Journal of Space Weather and Space Climate, 1, pp.A01

43. O. Podladchikova, A. Vuets, P. Leontiev, R. A. M. Van der Linden
Recent Developments of NEMO: Detection of EUV Wave Characteristics
Solar Physics, 276 (1-2) , 2012, 479-490

44. E. Pottiaux, E. Brockmann, C. Bruyninx, W. Söhne
The EUREF-EUMETNET Collaboration: First Experience and Potential Benefits
Bulletin of Geodesy and Geomatics, Vol. LXVIII, N°3, pp.269-288

45. H. Rieder, L.M. Jansco, S. Di Rocco, J. Stähelin, J.A. Maeder, T. Peter, M. Ribatet, A.C. Davison, H. De Backer, U. Köhler, J. Krzyścin, K. Vaníček
Extreme events in total ozone over the Northern mid-latitudes: An analysis based on long-term data sets from five European ground-based stations
Tellus B, 63B, 5, 860–874, doi: 0.1111/j.1600-0889.2011.00575.x, 2011

46. L. Rodriguez, M. Mierla, A.N. Zhukov, M. West, E. Kilpua
Linking remote-sensing and in situ observations of coronal mass ejections using STEREO
Solar Physics, 270, pp.561-573

47. D.B. Seaton, M. Mierla, D. Berghmans, A.N. Zhukov, L. Dolla
SWAP-SECCHI Observations of a Mass-loading Type Solar Eruption
Astrophysical Journal Letters, 727 (Iss 1), pp.L10 (5pp)

48. Y.S. Shugai, I.S. Veselovsky, D.B. Seaton, D. Berghmans
Hierarchical approach to forecasting recurrent solar wind streams
Solar System Research, 45 (Issue 6), pp.546-556

49. R. Soler, J.L. Ballester, S. Parenti
On the stability of thermal modes in cool prominence plasmas
Astronomy and Astrophysics, 2012, 540, A7

50. J. Spits, R. Warnant
*Total Electron Content Monitoring using triple frequency GNSS: results with Giove-A/-B d*ata
Advances in Space Research, Vol.47, No.2, pp.296-303, doi: 10.1016/j.asr.2010.08.027

51. S. Stankov, K. Stegen, P. Muhtarov, R. Warnant
Local ionospheric electron density profile reconstruction in real time from simultaneous ground-based GNSS and ionosonde measurements
Advances in Space Research, Vol.47, No.7, pp.1172-1180, doi: 10.1016/j.asr.2010.11.039

52. S. Stankov, K. Stegen, R. Warnant
K-type geomagnetic index nowcast with data quality control
Annals of Geophysics, Vol.54, No.3, pp.285-295, doi: 10.4401/ag-4655

53. L. Teriaca, et al. incl. S. Parenti
LEMUR: Large European Module for solar Ultraviolet Research
Experimental Astronomy, doi: 10.1007/s10686-011-9274-x

54. T. Van Doorsseleare, A. De Groof, J. Zender, D. Berghmans, M. Goossens
LYRA Observations of Two Oscillation Modes in a Single Flare
Astrophysical Journal, 740 (Issue 2), pp.90

55. C. Verbeeck, P. Higgins, T. Colak, F. Watson, V. Delouille, B. Mampaey, R. Qahwaji
A multi-wavelength analysis of active regions and sunspots by comparison of automatic detection algorithms
Solar Physics, pp.1-29

56. C. Verbeeck, G.O. Ryabova
Calculation of the incident flux density of meteors by numerical integration: Improved geometrical approach
Journal of Atmospheric and Solar-Terrestrial Physics, 73, 9, 901-903, doi:10.1016/j.jastp.2010.10.005

57. Andrea Verdini, Roland Grappin, Marco Velli
Coronal heating in coupled photosphere-chromosphere-coronal systems: turbulence and leakage
Astronomy and Astrophysics, 538, pp. A70 (2012)

58. Y. Voitenko, J. De Keyser
Turbulent spectra and spectral kinks in the transition range from MHD to kinetic Alfvén turbulence
Nonlinear Processes in Geophysics, 18, 587-597, 2011

59. Y.M. Wang, R. Grappin, E. Robbrecht, N.R. Sheeley, Jr
On the nature of the solar wind from coronal pseudostreamers
Astrophysical Journal, 749, pp.182-195 (2012)

60. Y.M. Wang, E. Robbrecht
Asymmetric Sunspot Activity and the Southward Displacement of the Heliospheric Current Sheet
Astrophysical Journal, 736, pp.136-147

61. Y.M. Wang, E. Robbrecht, K. Muglach
The Evolution of Dark Canopies Around Active Regions
Astrophysical Journal, 733, pp.20-27

62. M. West, A.N. Zhukov, L. Dolla, L. Rodriguez
Coronal seismology using EIT waves: estimation of the coronal magnetic field strength in the quiet Sun
Astrophysical Journal, 730, pp.122

63. A.N. Zhukov
EIT Wave Observations and Modeling in the STEREO Era
J. Atmos. Sol.-Terr. Phys., 73, pp.1096-1116

Presentations and posters at conferences

1. F. Auchère, S. Parenti, D. Berghmans, S. Gissot, L. Harra & the EUI team
EUI Beacon Data
4th Solar Orbiter Workshop, Telluride, Colorado, USA, March 27-31, 2011

2. Q. Baire, E. Pottiaux, C. Bruyninx, P. Defraigne, J. Legrand, N. Bergeot
Comparison of receiver antenna calibration models used in the EPN
EUREF Annual Symposium 2011, 24-27 May 2011, Chisinau, Moldova

3. A. BenMoussa, I.E Dammasch and M. Dominique
Status of the diamond detectors onboard LYRA, the Solar VUV radiometer
International Conference on New Diamond and Nano Carbons 2011, 16-20 May 2011

4. A. BenMoussa, B. Giordanengo, S. Gissot
Development of EUV photodetectors for EUI onboard Solar Orbiter
International Conference on New Developments In Photodetection – NDIP2011 - 04-08 July 2011, Lyon, France

5. A. BenMoussa, B. Giordanengo, S. Gissot et al.
Characterization of (E)UV CMOS APS for EUI onboard Solar Orbiter
CALCON Technical Conference: Conference on Characterization and Radiometric Calibration for Remote Sensing 29 August 2011, Logan, UT, USA

6. A. BenMoussa
Developments of detectors for Extreme Ultraviolet Imager telescopes (EUI) onboard Solar Orbiter
PTB seminar, 262nd EUV metrology, 27-28 October 2011, Berlin, Germany (invited talk)

7. A. BenMoussa, B. Giordanengo, S. Gissot et al.
Developments of back side illuminated CMOS APS for EUV Solar Observations
CNES CMOS image sensor Workshop, EUV metrology, 06-07 December 2011, Toulouse, France

8. N. Bergeot, J.-M. Chevalier, L. Benoit, C. Bruyninx, J. Legrand, E. Pottiaux, Q. Baire, P. Defraigne
Near Real-Time Ionospheric Models from European Permanent Network GPS Data
EUREF Annual Symposium 2011, 24-27 May 2011, Chisinau, Moldova

9. N. Bergeot, J. Legrand, R. Burston, C. Bruyninx, P. Defraigne, J.-M. Chevalier, F. Clette, C. Marque, L. Lefevre
Ionospheric Response to Solar Activity during the 23rd Solar Cycle
COST ES0803 workshop "Assessment and validation of space weather models", Alcala Spain, 16-17 March, 2011

10. N. Bergeot, J. Legrand, S. Le Maistre, C. Bruyninx, P. Defraigne. J.-M. Chevalier
Relation between the Earth's Daily Mean Ionospheric Electron Content and Solar Parameters: Experience from the 23rd Solar Cycle
Space Weather Workshop 2011, April 26-29 2011, Boulder, US

11. N. Bergeot
Relation between the Earth's Mean Daily Ionospheric Electron Content and Solar Parameters: Experience from the 23rd Solar Cycle
Splinter "Climatology and long-term changes of the ionosphere" of the Eighth European Space Weather Week - Namur, Belgium, November 28 - December 02, 2011

12. D. Berghmans
Flare Reporting by PROBA2 [link]
Talk in Plenary Session of 8th European Space Weather Week, November 28 2011, Namur (Belgium)

13. D. Berghmans + SWAP team
SWAP Status [link]
PROBA2 SWT at 8th European Space Weather Week, November 28 2011, Namur (Belgium)

14. D. Berghmans
Oscillations during Occultations [link]
STCE Meeting on Occultations & Eclipses, May 5 2011, Brussels (Belgium)

15. D. Berghmans, L. Dolla, D. Seaton, M. Dominique, C. Marque, A. De Groof, J. Zender, T. Van Doorsselaere
Quasi-periodic oscillations observed by LYRA and other instruments [link]
SOTERIA Third Annual Meeting, Leuven, May 30 2011

16. D. Berghmans, PROBA2 Science Consortium & Guest Investigators
PROBA2 Space Weather Services [link]
ESA Space Weather Working Team (SWWT) plenary meeting, Brussels, June 28 2011

17. D. Berghmans, K. Bonte and EUI consortium
Towards eruption detection onboard Solar Orbiter [link]
Solar Orbiter Workshop, March 27 2011, Telluride (Colorado, US)

18. D. Berghmans
EUI operations
Science Operations Working Group Kick-Off, Solar Orbiter Workshop 4, 27 March 2011, Telluride

19. D. Berghmans, K. Bonte
Towards eruption detection onboard Solar Orbiter
Solar Orbiter Workshop 4, Telluride, 28 March 2011

20. D. Berghmans, V.M. Pillet
Report from Remote Sensing WG
Science Working Team, Solar Orbiter Workshop 4, Telluride, 28 March 2011

21. K. Borremans and V. Pierrard
3D dynamic model and animations of the plasmasphere
10th International School/symposium for space simulations (ISSS10), Alberta, Canada, 24-31 July 2011 (poster)

22. V. Bothmer, R. Van der Linden, C. Verbeeck, A. Parnowski, R. Brunner, C. Hall, N. Jakowski, C. Borries, W. Pfeffer, R. Viereck and the AFFECTS team
Advanced Forecast For Ensuring Communications Through Space (AFFECTS)
Astronomy and Space Physics, Kyiv, Ukraine, May 24-27, 2011.

23. D. Boyes, B. Mampaey, V. Delouille
Wissdom: Data for Space Weather and Research from the Belgian SDO data center
European Space Weather Week 8, Belgium, November 28-December 2, 2011 (poster)

24. H. Brenot, J. Neméghaire, L. Delobbe, N. Clerbaux
Development of deep convection and identification of preliminary signs in water vapour structures by GNSS
EGU2011-7939, vol 13, April 2011, Vienna, Austria

25. H. Brenot, J. Neméghaire, L. Delobbe, N. Clerbaux
Initiation of deep convection detected by GNSS measurements
Atmospheric Water Vapour in the Climate System (WaVaCS) Final Workshop, 26-28 September 2011, Paris, France

26. H. Brenot, J. Neméghaire, L. Delobbe, N. Clerbaux
Development of deep convection and identification of preliminary signs by GNSS
STCE Workshop 2011: Water Vapour, Meteorology and Climate, 19 May 2011, Brussels, Belgium

27. C. Bruyninx, Q. Baire, J. Legrand, F. Roosbeek
The EUREF Permanent Network (EPN): Recent Developments and Key Issues
EUREF Annual Symposium 2011, 24-27 May 2011, Chisinau, Moldova

28. C. Bruyninx, J. Legrand, N. Bergeot, E. Pottiaux
Measuring long-term ground velocities using GNSS: Experiences from the EPN
EGU General Assembly 2011, April 3-8, 2011, Vienna, Austria (invited)

29. C. Bruyninx
Maintenance of the ETRS89 using EUREF's Permanent GNSS Service
CROPOS Conference, April 8, 2011, Zagreb, Croatia (invited)

30. C. Bruyninx
Main Activities and New Initiatives of the EUREF Technical Working Group
EUREF Symposium 2011, May 25-28, 2011, Chisinau, Moldavia

31. C. Bruyninx, J. Legrand, J. Dawson, J. Griffiths, A. Kenyeres, L. Sánchez, A. Santamaria-Gomez, Z. Altamimi, M. Becker, M. Craymer, L. Combrinck, R. Dietrich, R. Fernandes, T. Herring, R. King, C. Kreemer, D. Lavallée, G. Sella, Z. Shen, G. Wöppelmann
Efforts Towards a Dense Velocity Field Based on GNSS Observations
XXV IUGG General Assembly, 28 June - 7 July 2011, Melbourne, Australia

32. P. Chainais, V. Delouille, J.-F. Hochedez
Scale invariant images in astronomy through the lens of multifractal modeling
IEEE International Conference on Image Processing, Bruxelles, Belgium, 11-14 September 2011

33. E. Dammasch, M. Dominique & the LYRA Team
LYRA Data: getting them and exploiting them
SOTERIA Capacity Building Workshop, Brussels

34. E. Dammasch
LYRA Calibration, Data Products, Cross-Calibration
EUV Irradiance Workshop, Boulder

35. E. Dammasch, M. Dominique, M. Kretzschmar, P. C. Chamberlin
Components of soft X-ray and extreme ultraviolet in flares observed by LYRA on PROBA2
8th European Space Weather Week, Namur (Poster, plus talk on SCSL splinter)

36. F. Darrouzet, J. De Keyser, V. Pierrard, H. Matsui and N. Ganushkina
The dynamics of the plasmasphere
International Symposium on Recent Observations and Simulations of the Sun-Earth System II, Borovets, Bulgaria, September 11-16, 2011 (oral)

37. F. Darrouzet, V. Pierrard, N. Ganushkina, J. De Keyser
Relation between the Position of the Plasmapause and the Inner Edge of the Outer Radiation Belt
IUGG Conference, Melbourne, Australia, 28 June - 7 July 2011 (oral)

38. V. De Bock, H. De Backer and A. Mangold
Improved cloud screening for Aerosol Optical Depth measurements with a Brewer spectrophotometer, Poster at European Aerosol Conference, Manchester, United Kingdom, 4-9 September 2011

39. P. Defraigne, M.C. Martinez, Q. Baire
Using Galileo E5 for Time and Frequency Transfer
3rd colloquium Scientific and Fundamental Aspects of the Galileo Program, Copenhague, September 2011

40. P. Defraigne, A. Harmegnies, G. Petit
Time and frequency transfer combining GLONASS and GPS data,
EFTF-IFCS, San Francisco, 2011

41. P. Defraigne
GNSS Time and Frequency Transfer: state of the art and possible evolution,
Workshop on Development of Advanced Time and Frequency Transfer Techniques, Paris, June 2011 (invited)

42. De Groof & PROBA2 Science Center Team
SWAP, a pioneering CMOS detector for Solar Physics [link]
Solar Orbiter Workshop, March 27 2011, Telluride (Colorado, US)

43. De Groof & PROBA2 Science Center Team
PROBA2/SWAP & LYRA: Opportunities for Solar Physics and First Results [link]
4th SOLAIRE network meeting, Teistungen, Germany, May 9-13, 2011

44. De Groof, PROBA2 Science Consortium
Proba2/swap & lyra: First Results & Opportunities for Solar Physics and Space Weather[link]
European Solar Physics Meeting (ESPM13), Rhodos (Greece), 2011-09-12

45. Delcloo, R. Van Malderen, H. De Backer,
Trends in ozone concentrations at the ozone sonde station of Uccle,
Second Workshop on tropospheric ozone changes Toulouse, France, 11-14 April, 2011

46. V. Delouille, B. Mampaey, C. Verbeeck
Detection and tracking of coronal holes using AIA
ISSI meeting "Mining and Exploiting SDO data in Europe", Bern, Switzerland, May 30-June 1, 2011

47. V. Delouille, B. Mampaey, C. Verbeeck, M. Kretzchmar
Coronal hole detection with SDO-AIA 19.3nm
European Space Weather Week 8, Belgium, November 28-December 2, 2011 (poster)

48. V. Delouille, B. Mampaey, C. Verbeeck
Detection and tracking of coronal holes using AIA
ISSI meeting "Mining and Exploiting SDO data in Europe", Bern, Switzerland, May 30-June 1, 2011

49. E. D'Huys and the P2SC team
PROBA2 (Running Presentation)
Paris Air Show – Le Bourget, STCE stand, June 20 - 26, 2011, Paris, France

50. E. D'Huys, D. Seaton, A. De Groof, C. Jacobs, S. Poedts
Joint AIA-SWAP Observations of Reconnection-Related Processes During Coronal Eruptions
The Sun 360: Stereo-4/SDO-2/SOHO-25 Workshop, July 25-29, Kiel, Germany (Poster)

51. E. D'Huys, D. Seaton, A. De Groof, C. Jacobs, S. Poedts
Multi-Spacecraft Analysis and Modeling of a Solar Eruption on August 14, 2010
Sun-360/SDO-2/STEREO-4/SOHO-25 Meeting, Kiel, Germany (Poster)

52. L. Dolla, C. Marqué, D. Berghmans, C. Cabanas, M. Dominique, A. De Groof, D. Seaton,
T. Van Doorsselaere, A. Verdini, M. West, J. Zender,
A. Zhukov
A comparison of quasi-periodic pulsations in different wavebands
BUKS 2011 Workshop, 27-29 June 2011, Palma de Mallorca, Spain

53. L. Dolla, C. Marqué, D. Berghmans, C. Cabanas, M. Dominique, A. De Groof, D. Seaton, T. Van Doorsselaere, A. Verdini, M. West, J. Zender, A. Zhukov
A comparison of quasi-periodic pulsations in solar flares observed in different wavebands
"The Sun 360", Stereo-4/SDO-2/SOHO-25 Workshop, 25-29 July 2011, in Kiel, Germany

54. L. Dolla and A. Zhukov
Multi-component spectral line profiles in active region loops
The Fifth Coronal Loops Workshop, 29 June – 2 July 2011, in Palma de Mallorca, Spain

55. L. Dolla and A. N. Zhukov
Spectroscopic Diagnostics of Alfvén Waves in the Solar Corona (oral presentation)
STCE Workshop on Alfvén waves, ROB, Brussels, Belgium, May 31

56. M. Dominique + LYRA team
LYRA status [link]
PROBA2 workshop, Feb 12-18 2011, Brussels, Belgium

57. M. Dominique + LYRA team
LYRA on-board PROBA2
Solar EUV Irradiance Inter-Calibration and Validation, October 25-27 2011, Boulder (USA)

58. M. Dominique, A. Shapiro, D. Berghmans
LYRA and SWAP, the two Solar Instruments on-board PROBA2
AGU (Poster), December 02 2011, San Francisco (USA)

59. M. Dominique
LYRA occultations [link]
STCE Meeting on Occultations & Eclipses, May 5 2011, Brussels (Belgium)

60. M. Domimique+ LYRA team
Status and Last Results [link]
PROBA2 SWT at 8th European Space Weather Week, Nov 28 2011, Namur (Belgium)

61. M. Domimique+ LYRA team
Flare tracking campaigns with LYRA [link]
PROBA2 SWT at 8th European Space Weather Week, Nov 28 2011, Namur (Belgium)

62. S. Gissot, A. BenMoussa, B. Giordanengo
Development of (E)UV imaging system for solar space missions
2nd EIROforum School on Instrumentation (ESI 2011), Grenoble, France, 18 May 2011

63. R. Grappin, A. Verdini, W-C Müller
Anisotropy in MHD turbulence with mean field: zero parallel cascade?
Oral contribution, EGU 2011, 08 April 2011, Vienna, Austria, 08 April 2011

64. C. Guennou, F. Auchère, K. Bocchialini, S. Parenti, N. Barbey
An optimal multi-thermality for solar plasma: application to SDO/AIA
The Fifth Coronal Loop Workshop, Palma de Mallorca, 29 June – 2 July 2011

65. P. Heinzel, B. Schmieder, S. Parenti and L. Golub
On the visibility of solar prominences in SDO/AIA channels
5th Hinode meeting, poster

66. R. Kariyappa, S. T. Kumar, M. Dominique, D. Berghmans, L. Dame, C.L. Pradeep
First Results on Solar Irradiance Variability from PROBA2/LYRA/SWAP [link]
PROBA2 workshop, February 17 2011, Brussels (Belgium)

67. A. Kenyeres, C. Bruyninx, A. Caporali and G. Stangl
EPN- based products and services in support of ground deformation monitoring (invited)
Technical Workshop on Satellite Altimeter Calibration & Deformation Monitoring with GNSS, January 20-21 2011, Chania, Greece

68. M. Kretzschmar, I. E. Dammasch, M. Dominique
Monitoring Solar Flares: a Comparison of Observations from GOES and PROBA2/LYRA
8th European Space Weather Week, Namur (Poster)

69. M. Kretzschmar, M. Dominique, I. E. Dammasch
Solar Irradiance Variations as Observed by the LYRA Radiometer onboard PROBA2
8th European Space Weather Week, Namur

70. M. Kretzschmar + LYRA team
Status and Last Results [link]
Solar EUV Irradiance Inter-Calibration and Validation, October 25-27 2011, Boulder (USA)

71. M. Kretzschmar + LYRA team
Solar flux variations observed by LYRA: From Space Weather to Space Climate [link]
Talk in Plenary Session of 8th European Space Weather Week, November 28 2011, Namur (Belgium)

72. M. Lazar and V. Pierrard
Modeling space plasma dynamics with Kappa distributions
International Astrophysics Forum Alpbach, IAFA 2011, Frontiers in Space Environment Research, Congress Center Alpbach, Tirol, Austria, June 20-24, 2011 (oral, invited)

73. G. Lechat, H. Lamy, V. Pierrard, N. Meyer-Vernet, K. Issautier, I. Zouganelis
New developments in exospheric theory of the solar wind
ESPM-13, Rhodes, 13th European Solar Physics Meeting Rhodes, Greece, 12-16 September 2011 (poster)

74. L. Lefèvre (Oral Presentation)
Sunspot catalog Survey and Merging Work
Capacity Building Workshop, SOTERIA, February 2011

75. L. Lefèvre. F. Clette, L. Wauters (POSTER)
Towards advanced sunspot-based indices and solar forcing proxies
European Geophysocal Union, Vienna April 2011

76. L. Lefèvre, F. Clette (Oral Presentation)
A small sunspot deficit in cycle 23
Sunspot Workshop, September 19th – 22nd , Sunspot NM, 2011

77. L. Lefèvre, F. Clette (Oral Presentation)
A small Sunspot deficit in Cycle 23: a possible proxy breakdown.
ESWW8, Namur, Splinter Session: Climatology and long-term changes in the ionosphere, November 29th 2011

78. L. Lefèvre, F. Clette, L. Wauters (POSTER)
Survey and Merging of Sunspot Catalogs: accessing the smallest sunspots details
ESWW8, Namur November 28th - December 2nd 2011

79. J. Magdalenić, C. Marqué
Electron Density and Alfvén speed Profiles in the Solar Corona (poster)
ESWW8, 28 November – 02 December 2011, Namur, Belgium

80. C. Marqué
CRAF activities
Radio Science Day (STCE), Brussels, Belgium, May 17th 2011

81. C. Marqué, S. Ranvier
Radio monitoring in Humain
Radio Science Day (STCE), Brussels, Belgium, May 17th 2011

82. C. Marqué, J. Magdalenić
The Humain Project: Solar Monitoring
SWWT Plenary, Brussels, Belgium, June 28th 2011

83. C. Marqué
Space Weather Tutorial: a concrete example
ESWW8, November 28th, 2011, Namur, Belgium

84. M.C. Martinez, P. Defraigne, Q. Baire, W. Aerts
Single-frequency time and frequency transfer with Galileo E5
EFTF-IFCS, San Francisco, 2011

85. M. Mierla, D.B. Seaton, D. Berghmans, I. Chifu, A. de Groof, Inhester, L. Rodriguez, G. Stenborg, A. Zhukov (poster)
Analysis of the 13 April 2010 prominence eruption using SWAP and EUVI data
Sun 360 workshop, Kiel, Germany, July 25 - 29, 2011

86. N. Murphy, D. Seaton, et al.
Asymmetric Magnetic Reconnection in Solar Flare and Corona Mass Ejection Current Sheets
American Geophysical Union Fall Meeting 2011, abstract #SH51A-1997 (Poster)

87. E. Nikitidou, V. De Bock, H. De Backer, A. Kazantzidis
Estimation of aerosol optical properties and their effect on UV radiance at Uccle, Belgium
Poster at 11th EMS Annual Meeting/ 10th European Conference on Application of meteorology, Berlin, Germany, 12-16 September 2011

88. S. Parenti
Observational properties of the hot active regions: a review
Invited talk to The Fifth Coronal Loop Workshop, Palma de Mallorca, 29 June – 2 July 2011

89. S. Parenti, S. Gunár, U. Anzer, P. Heinzel and J.-C. Vial
Prominence Differential Emission Measure: modeling vs. observations
ESPM 13, poster

90. G. Petit, P. Defraigne, A. Harmegnies, Z. Jiang
Progress in multi-GNSS time transfer: Some results with GPS and GLONASS
3rd colloquium Scientific and Fundamental Aspects of the Galileo Program, Copenhaegue, September 2011

91. V. Pierrard, F. Darrouzet, K. Borremans,
The dynamics of the plasmasphere
ESLAB2011/Cluster 21st workshop on 'Solar System Plasma Physics: Remote and in-situ Measurements', Bruges, Belgium, 19-23 September 2011 (oral, invited)

92. V. Pierrard, F. Darrouzet, J. Cabrera and K. Borremans
Space weather effects on the plasmasphere: links with the ionosphere and radiation belts
Space Weather Week, Namur, Belgique, 28 Nov-2 Dec 2011 (poster)

93. V. Pierrard
Dynamic model of the plasmasphere and links with space radiations
ISSI working team on "The Earth's Radiation Belts: Physical Processes and Dynamic Modelling", Bern (Switzerland), 8-11 February 2011 (oral, invited)

94. V. Pierrard
Kinetic models of space plasmas
Workshop on Modern Trends in Theoretical Plasma Physics, Ruhr University Bochum (Germany), 21-22 February 2011 (oral, invited)

95. V. Pierrard
The kinetic approach to model particle acceleration in space plasmas
10th anniversary of the International Astrophysics Conference, Physics of the Heliosphere: A 10-year Retrospective, Hawaii (USA), March 13-18, 2011 (oral, invited)

96. V. Pierrard
The dynamics of plasmasphere
EGU, Vienna (Austria), 3 to 8 April 2011 (oral, invited)

97. V. Pierrard, F. Darrouzet, M. Kruglanski, M. Voiculescu, S. Calders
A three-dimensional dynamic model of the plasmasphere coupled to the ionosphere
Space Weather Workshop, Boulder, Colorado (USA), April 26-29, 2011. (poster)

98. V. Pierrard, M. Lazar
Kappa velocity distribution functions to model space plasmas
BPS meeting, Namur, 25 May 2011. (poster)

99. V. Pierrard
Coupling the plasmasphere model with the ionosphere
Astronum2011, Valencia, Spain, 13-17 June 2011. (oral, invited)

100. E. Pottiaux, C. Bruyninx, N. Bergeot
GNSS research and service activities at ROB for nowcasting, SRNWP, NWP and climate applications
STCE Workshop 2011: Water Vapour, Meteorology and Climate, 19 May 2011, Brussels, Belgium

101. E. Pottiaux, C. Bruyninx
National Report of Belgium (ROB)
E-GVAP II Joint Expert Team Meeting 2011, 20-21 October 2011, Toulouse, France

102. E. Pottiaux, R. Van Malderen, H. Brenot, A. Deckmyn, M. Reyniers, I. Gorodetskaya
STCE Workshop on "Water Vapour, Meteorology and Climate" : Wrap Up
STCE Annual Meeting 2011, 07 June 2011, Brussels, Belgium

103. E. Robbrecht, E. D'Huys, R. Van der Linden, D. Berghmans (ROB, Belgium), M. Kruglanski, N. Crosby, E. De Donder (BISA, Belgium), Truls Lynne Hansen (TGO, Norway), E. Tanskanen (FMI, Finland), M. Danielides, N. Jakowski (DLR, Germany), J. Watermann, G. Lawrence, S. Reid, O. Valdes (Rhea System SA, Belgium)
European Space Weather assets and services review (SSA SN-I Task 1) (poster)
Space Weather Workshop, Boulder, CO, USA, April 2011

104. E. Robbrecht and the SIDC-team
The Regional Warning Centre Belgium (presentation)
ISES meeting, Boulder, CO, USA, April 2011

105. E. Robbrecht as ISES representative
ISES: The International Space Environment Service
World Meteorological Organisation (WMO) side event: Global Preparedness for Space Weather Hazards, May 2011

106. L. Rodriguez
Ionic charge state composition of Interplanetary Coronal Mass Ejections
IX COLAGE meeting of the Latin American Association of Space Geophysics, Punta Leona, Costa Rica, April 4 - 10, 2011 (invited, oral)

107. L. Rodriguez, M. Mierla, E. Kilpua, A.N. Zhukov, M. West
Linking remote with in situ observations of CMEs observed by STEREO
European Solar Physics Meeting, ESPM-13, Rhodes, Greece, 12-16 September 2011 (oral)

108. L. Rodriguez
Use of STEREO data to better forecast CME arrivals
Forecaster forum, European Space Weather Week 8 (ESWW8), Namur, Belgium, 28 November – 2 December 2011 (oral)

109. L. Rodriguez
Space weather forecast briefing, Sunday 13 – Wednesday 16 February 2011
SOTERIA Capacity Building Workshop, Brussels, Belgium, 15-16 February 2011 (oral)

110. D. Seaton, M. Mierla, D. Berghmans, A. Zhukov, L. Dolla
What Causes Solar Eruptions: Observations of a Mass-Loading Type CME
"The Sun 360", STEREO-4/SDO-2/SOHO-25 Workshop, Kiel, Germany, July 25–29 (invited, oral)

111. D. Seaton, E. D'Huys, K. Reeves, T. Forbes, S. Savage
Joint AIA-SWAP Observations of Reconnection-Related Processes During Coronal Eruptions
First LWS/SDO Workshop, May 1-5, Squaw Valley, CA

112. D. Seaton, K. Reeves, S. Savage, T. Forbes, & E. D'Huys
Studying Reconnection During Solar Eruptions Using AIA & SWAP: Observations and Modeling
Third SOTERIA General Meeting, Leuven, Belgium (Talk)

113. D. Seaton, K. Reeves, S. Savage, T. Forbes, & E. D'Huys
Joint AIA-SWAP Observations of Reconnection-Related Processes During Coronal Eruptions
LWS/SDO Workshop, Lake Tahoe, California (Talk)

114. V. Slemzin et al + PROBA2 SWAP team
EUV imaging of the solar corona and study of slow solar wind streams [link]
PROBA2 SWT at 8th European Space Weather Week, Nov 28 2011, Namur (Belgium)

115. J. Spits, R. Warnant
Enhancement of Total Electron Content Monitoring Using Triple Frequency GNSS Data
3rd International Colloquium - Scientific and Fundamental Aspects of the Galileo Program, Copenhagen, 31 August-2 September 2011, Copenhagen, Denmark

116. S. Stankov
RMI ionosphere/space weather research and developments
STCE Annual Meeting / Ionosphere Workshop, 26 May 2011, Royal Observatory, Brussels

117. K. Stegen
SWAP Reprocessing
PROBA2 SWT at 8th European Space Weather Week, November 28th , 2011, Namur (Belgium)

118. G. Thuillier, D. Bolsée, G. Schmidtke, K. Schmutz
The Solar Spectral Irradiance Measured on Board the International Space Station and the Picard Spacecraft
The AGU Fall Meeting 2011, 5-9 December, San Francisco (USA)

119. P. Vanlommel
Advances in WG3 : 'Exploitation, dissemination, education and outreach'
COST MCM, March 15, Alcala, Spain

120. P. Vanlommel
Future plans for WG3 : 'Exploitation, dissemination, education and outreach'
COST MCM, March 15, Alcala, Spain

121. P. Vanlommel
WG3 - Final Report: successes and work points
COST MCM, December 1, Namen, Belgium

122. P. Vanlommel and the RWC team
Solar wind forecast in practice
COST workshop on Assessment and Validation of Space Weather Models, Alcala, Spain, 16-17 March 2011

123. R. Van Malderen, H. Brenot, E. Pottiaux, M. De Mazière, C. Hermans, H. De Backer, C. Bruyninx
Integrated water vapor time series: instrumental inter-comparisons and trends
Atmospheric Water Vapour in the Climate System (WaVaCS) Final Workshop, 26-28 September 2011, Paris, France

124. R. Van Malderen, H. Brenot, E. Pottiaux, H. De Backer, K. Clémer, C. Hermans, M. De Mazière
Integrated water vapour observations at Space Pole: instrumental inter-comparisons
STCE Workshop 2011: Water Vapour, Meteorology and Climate, 19 May 2011, Brussels, Belgium

125. C. Verbeeck, B. Mampaey, V. Delouille, D. Berghmans, B. Callebaut
SPoCA results for SWAP, towards AFFECTS timelines
Proba2 Science Days, ROB, Belgium, February 17-18, 2011

126. C. Verbeeck, D. Berghmans, B. Callebaut
AFFECTS Work Package 3
AFFECTS kick-off meeting, Göttingen, Germany, March 22-23, 2011

127. C. Verbeeck, P.A. Higgins, T. Colak, F.T. Watson, V. Delouille, B. Mampaey, R. Qahwaji
A multi-wavelength analysis of active regions and sunspots by comparison of automatic detection algorithms
First SDO Workshop, Squaw Valley, CA, USA, May 1-5, 2011 (poster)

128. C. Verbeeck, B. Callebaut, D. Berghmans
The AFFECTS project
STCE workshop "Ionospheric research and services in the STCE: present status and future developments", ROB, Belgium, May 26, 2011

129. C. Verbeeck, P.A. Higgins, T. Colak, F.T. Watson, V. Delouille, B. Mampaey, R. Qahwaji
A multi-wavelength analysis of active regions and sunspots by comparison of automatic detection algorithms
ISSI meeting "Mining and Exploiting SDO data in Europe", Bern, Switzerland, May 30-June 1, 2011

130. C. Verbeeck, B. Mampaey, V. Delouille
Analysis of AR 11158 through SPoCA lenses
ISSI meeting "Mining and Exploiting SDO data in Europe", Bern, Switzerland, May 30-June 1, 2011

131. C. Verbeeck, B. Callebaut, D. Berghmans, V. Delouille, B. Mampaey and the AFFECTS team
The AFFECTS Solar Activity Viewer
Sun 360 Workshop, Kiel, Germany, July 25-29, 2011 (*poster*)

132. C. Verbeeck, B. Callebaut, D. Berghmans, V. Delouille, B. Mampaey and the AFFECTS team
The STAFF Viewer – Easy access to your favorite space weather time series
European Space Weather Week 8, Belgium, November 28-December 2, 2011 (poster)

133. A. Verdini, R. Grappin, M. Velli
The role of leakage in the turbulent heating of coronal loop
Poster contribution, ESPM 13 meeting, Rodos, Greece, 23 November 2011

134. A. Verdini, R. Grappin, M. Velli
Turbulent heating of coronal loop: effect of leakage in the chromosphere-corona coupling
Oral contribution, Workshop on Plasma Astrophysics, Univ. di Firenze, Firenze, Italy, 17 October 2011

135. N. Viereck, E. Araujo-Pradere, S. Solomon, J. Emmert, J. Lean, N. Bergeot
The Unusually Deep and Long Solar Minimum: How Unusual Was it?
Space Weather Workshop 2011, Boulder, USA, 26-29 April 2011

136. Y. Voitenko, J. De Keyser
Weakly dispersive sub-range of the solar wind turbulence
International Astrophysics Forum Alpbach (IAFA 2011) "Frontiers in Space Environment Research", Congress Center Alpbach, Tyrol – Austria, 20-24 June, 2011 (oral, invited)

137. Y. Voitenko, J. De Keyser, P. Shukla,
Nonlinear interaction and turbulence of inertial Alfvén waves
First Joint UK-Ukraine Meeting on Solar Physics and Space Science, Alushta, Crimea, Ukraine, 29 August - 2 September, 2011 (oral)

138. Y. Voitenko, J. De Keyser, and P. Shukla
Wave aspects and signatures in the magnetosphere-ionosphere coupling
8th European Space Weather Week ESWW-8, Namur, Belgium, 28 November - 3 December, 2011 (oral)

139. M.J. West, S. Parenti
Comparing the Radiative Signatures of Turbulent Heating in Coronal Loops Generated With Local and Non-local Conductive Cooling Models
The Fifth Coronal Loops Workshop, Palma (Mallorca) Spain, June 29 - July 2 2011

140. M.J. West, A.N. Zhukov, L. Dolla, L. Rodriguez
Coronal seismology using EIT Waves: Estimation of the coronal magnetic field in the quiet Sun
BUKS Workshop, Palma (Mallorca) Spain. June 27 - June 29 2011

141. M.J. West, A.N. Zhukov, L. Rodriguez, B.J. Thompson, L. Dolla
Coronal Observations in 2 parts: EIT Waves - Dimmings – CMEs
Seminar, Space & Atmospheric Physics Group, The Blackett Laboratory, Imperial College London, Prince Consort Road, London, SW7 2BW, UK. June 15 2011 (oral)

142. M.S. Yalim, I. Dammasch, D. Berghmans, M. Dominique, A. De Groof
Comparison between LYRA and SWAP Average Intensity during the July 11th , 2010 Solar Eclipse [link]
STCE Meeting on Occultations & Eclipses, May 5 2011, Brussels (Belgium)

143. J. Zender et al, including M. Dominique
LYRA Occultation Data Analysis in Search for Ablation Signals from the Geminid meteor shower 2010 [link]
PROBA2 SWT at 8th European Space Weather Week, November 28 2011, Namur (Belgium)

144. A.N. Zhukov, Dolla, L., Rodriguez, L., Verdini, A.
Establishing a connection between solar and interplanetary parameters in Fast solar wind streams
Workshop on fluctuating IMF and geomagnetic response, Alcalá de Henares, Spain, 24-28 October 2011 (invited presentation)

145. A.N. Zhukov
New Aspects of Space Weather Monitoring and Forecasting: SDO and PROBA-2 Data
Forecaster forum, 8th European Space Weather Week, Namur, Belgium, November 28 – December 2 (oral presentation)

146. A.N. Zhukov
Space weather monitoring and forecasting
The Sun: from quiet to active, International Moscow Workshop on Solar Physics, Moscow, Russia, August 29 – September 2, 2011 (invited presentation)

147. A.N. Zhukov
Thoughts on the EUI Science: What Have We Learned since the Proposal Submission?
Solar Orbiter/EUI consortium meeting, Royal Observatory of Belgium, October 19–21

List of abbreviations

2D	Two-dimensional
3D	Three dimensional
ACE	Advanced Composition Explorer
ACRIM	Active Cavity Radiometer Irradiance Monitor
AERONET	AErosol RObotic NETwork
AFFECTS	Advanced Forecast For Ensuring Communications Through Space
AGN	Active Geodetic Network
AIA	Atmospheric Imaging Assembly (SDO)
ALTIUS	Atmospheric Limb Tracker for Investigation of the Upcoming Stratosphere
AOD	Aerosol Optical Depth
APS	Active Pixel Sensor
ApJ	The Astrophysical Journal
APSOLUTE	APS Optimized for Low-noise and Ultraviolet Tests and Experiments
ATLAS	ATmospheric Laboratory for Applications and Science
AU	Astronomical Unit; about 150 million km
BELSPO	Belgian Science Policy Office
BESSY	Berliner Elektronenspeicherring-Gesellschaft für Synchrotronstrahlung
BIRA	Belgisch Instituut voor Ruimte-Aëronomie
BISA	Belgian Institute for Space Aeronomy
BKG	Bundesamt für Kartographie und Geodäsie
BOLD	Blind to Optical Light Detectors
BOS	Bolometric Oscillation Sensor
BRAMS	Belgian RAdio Meteor Stations
BSI	Back-Side Illuminated
BUSOC	Belgian User Support and Operation Center
CACTus	Computer Aided CME Tracking software
CALLISTO	Compound Astronomical Low frequency Low cost Instrument for Spectroscopy and Transportable Observatory
CB	Central Bureau
CCD	Charge-Coupled Device
CESRA	Community of European Solar Radio Astronomers
CH	Coronal Hole
CME	Coronal Mass Ejection
CMOS	Complementary Metal Oxide Semiconductor
CMOSIS	CMOS Image Sensor
CNES	Centre National d'Etudes Spatiales
CNSS	COMPASS Navigation Satellite System
Co60	Cobalt 60
CODE	Center for Orbit Determination in Europe
COMESEP	Coronal Mass Ejections and Solar Energetic Particles
COMPASS	Chinese navigation satellite system
COPUOS	COmmittee on the Peaceful Uses of Outer Space (UN)
COR1	inner CORonagraph (STEREO)
COR2	outer CORonagraph (STEREO)
COSPAR	COmmittee on SPAce Research
COST	(European) COoperation in Space & Technology
CPD	Coarse Pointing Device

CPG	Centre de Physique du Globe (Geophysical center Dourbes)
CSL	Centre Spatial de Liège
dBZ	decibels relative to Z (reflectivity)
DeMeLab	Detector Measurements Laboratory
DIARAD	DIfferential Absolute RADiometer
DIDBase	Digital Ionosonde network DataBase
DMVTEC	Daily Mean VTEC
DOY	Day Of Year
DPD	Debrecen Photographic Data
DPS-4D	Digital Portable Sounder-4D
DR	Dynamic Range
DSN	Deep Space Network
Dst	Disturbance Storm index
E-GVAP	EUMETNET EIG GNSS water VApour Program
ECV	Essential Climate Variable
EGU	European Geosciences Union
eHEROES	Environment for Human Exploration and RObotic Experimentation in Space
EIG	Economic Interest Grouping
EIS	Extreme-Ultraviolet Imaging Spectrometer (Hinode)
EIT	Extreme ultraviolet Imaging Telescope (SOHO)
ELIS	ELISabeth, Belgium station/receiver in Antarctica
ENVISAT	Environmental Satellite
EPN	EUREF Permanent Network
ERB(S)	Earth Radiation Budget (Satellite)
ESA	European Space Agency
ESWP	European Space Weather Portal
ESWW	European Space Weather Week
EU	European Union
EUI	Extreme-Ultraviolet Imager (Solar Orbiter)
EUMETNET	European Meteorological services Network
EUREF	EUropean Reference Frame
EUV	Extreme Ultraviolet
EUVI	Extreme Ultraviolet Imager (STEREO/SECCHI)
EVE	Extreme Ultraviolet Variability Experiment (SDO)
$F_{10.7\ cm}$	Solar radio flux at 10.7 cm wavelength
FAM	First Attendees Meeting
FFT	Feature Finding Team
FLEPOS	Flemish POsitioning Service
foE	maximum radio-frequency capable of reflecting from the ionospheric E-layer
foF2	maximum radio-frequency capable of reflecting from the ionospheric F2-layer
FP7	Framework Program 7
FPGA	Field Programmable Gate Array
FSI	Full Sun Imager
FWC	Full Well Capacity
GF	Geometric-Free
GIM	Global Ionospheric Map
GIOVE	Galileo In-Orbit Validation Element
GLONASS	GLObal NAvigation Satellite System (Russia)
GNSS	Global Navigation Satellite System
GOES	Geostationary Operational Environmental Satellite
GOME	Golbal Ozone Monitoring Experiment
GPS	Global Positioning System (USA)
GSTP	General Support Technology Programme (ESA)

HaSTeNet	H-alpha Solar flare patrol TElescopic NETwork
HEK	Heliophysics Event Knowledgebase
Hinode	Solar-B satellite ("sunrise")
hmF2	Ionospheric F2-layer Peak Density altitude
HRI	High-Resolution Imager
IAS(B)	Institut d'Aéronomie Spatiale de Belgique
IASI	Infrared Atmospheric Sounding Interferometer
IAW	Inertial Alfvén Waves
ICME	Interplanetary CME
IDL	Interactive Data Language
IEEE	Institute of Electrical and Electronics Engineers
IES	Ionospheric Effects Symposium
IGS	International GNSS Service
IR	Infrared
ISES	International Space Environment Service
ISS	International Space Station
IT	Information Technology
IWV	Integrated Water Vapor
JOREM	Jupiter Radiation Environment and Effects Models and Mitigation
JSWSC	Journal of Space Weather and Space Climate
KUL	Katholieke Universiteit Leuven
KAW	Kinetic Alfvén Waves
LASCO	Large Angle Spectrometric Coronagraph (SOHO)
LATMOS	Laboratoire Atmosphères, Milieux, Observations Spatiales
LET	Linear Energy Transfer
LIDAR	LIght Detection And Radar
LIEDR	Local Ionospheric Electron Density profile Reconstruction
LMSAL	Lockheed Martin Solar and Astrophysics Laboratory
LYRA	Lyman Alpha Radiometer (PROBA2)
M-flare	Medium x-ray flare
MASTER	Meteoroid and Space Debris Terrestrial Environment Reference
MESSENGER	Mercury, Surface, Space Environment, Geochemistry and Ranging mission
METEOSAT	Meteorological satellite
MHD	Magneto-Hydro-Dynamic
MLT	Magnetic Local Time
MSFC	Marshall Space Flight Center
MSSL	Mullard Space Science Laboratory
MSTID	Medium-Scale Traveling Ionospheric Disturbance
NASA	National Aeronautics and Space Administration
Ne	electron concentration
NEMO	Novel EIT wave Machine Observing
NIR	Near InfraRed
NmF2	Ionospheric F2-layer Peak Density
NOA	National Observatory of Athens
NOAA	National Oceanic and Atmospheric Administration (numbering of sunspots)
NOMAD	Nadir and Occultation for MArs Discovery (ExoMars)
NoRP	Nobeyama Radio Polarimeter
NRT	Near Real-Time
NSO	National Solar Observatory
NTRIP	Networked Transport of RTCM via Internet Protocol
NWP	Numerical Weather Prediction
PbS	Lead Sulfide
PCA	Principal Component Analysis
PCO	Phase Center Offset

PCV	Phase Center Variation
PI	Principal Investigator
PMOD	Physikalisch-Meteorologisches Observatorium Davos
PMT	Photo Multiplier Tube
ppm	parts per million
ppb	parts per billion
PREMOS	PREcision MOnitoring Sensor
PROBA	PRoject for OnBoard Autonomy
PRODEX	PROgram for the Development of scientific Experiments
PTB	Physikalisch-Technische Bundesanstalt
PTC	Photon Transfer Curve
QPP	Quasi-Periodic Pulsations
Radar	RAdio Detection And Ranging
RGP	Réseau GNSS Permanent
RHESSI	Reuven Ramaty High Energy Solar Spectroscopic Imager
Ri	International sunspot number
RINEX	Receiver Independent Exchange Format
RMI(B)	Royal Meteorological Institute (of Belgium)
RMI-DPS-4D	RMI-Digital Portable Sounder-4D
RMS	Root Mean Square
ROB	Royal Observatory of Belgium
ROTEC	Rate of TEC
Rs	Solar radius/radii
RTCM	Radio Technical Commission for Maritime Services
RTK	Real Time Kinematic
RWC	Regional Warning Centre
SAFIR	Système d'Alerte Foudre par Interférométrie Radioélectrique
SC24	Solar Cycle 24
SCIAMACHY	SCanning Imaging Absorption spectroMeter for Atmospheric CHartographY (ENVISAT)
SDO	Solar Dynamics Observatory
SECCHI	Sun Earth Connection Coronal and Heliospheric Investigation (STEREO)
SEP	Solar Energetic Particle
SEVIRI	Spinning Enhanced Visible and Infrared Imager
SIDC	Solar Influences Data analysis Center
Si	Silicon
SIM	Spectral Irradiance Monitor (SORCE)
SIMBA	Sun-earth IMBAlance radiometer
SODA	SOTERIA Data Archive
SoDIPE-RTK	Software for Determining the Ionospheric Positioning Error on RTK
SOHO	SOlar & Heliospheric Observatory
SOLSPEC	SOLar SPECtrum
SORCE	Solar Radiation and Climate Experiment
SOTERIA	SOlar-Terrestrial Investigations and Archives
SOVA	SOlar constant and VAriability
SOVAP	SOlar VAriability Picard
SPENVIS	Space Environment Information System
SPOCA	Spatial POssibilistic Clustering Algorithm
SSA	Single Scattering Albedo
SSA	Space Situational Awareness
SSN	SunSpot Number
STCE	Solar-Terrestrial Centre of Excellence
STEC	Slant Total Electron Content
STEREO	Solar-TErrestrial RElations Observatory

SUMER	Solar Ultraviolet Measurements of Emitted Radiation (SOHO)
SWANS	Space Weather and Navigation Systems
SWAP	Sun Watcher using APS detector and image Processing (PROBA2)
SWENET	(European) Space WEather NETwork
SWOC	Space Weather Operations Centre
SWSC	Space Weather and Space Climate journal
SWWT	(European) Space Weather Working Team
τ	ionospheric slab thickness
TEC	Total Electron Content
TECU	Total Electron Content Unit
THEMIS	Time History of Events and Macroscale Interactions during Substorms
TID	Travelling Ionospheric Disturbance
TIM	Total Irradiance Monitor
TOA	Top Of Atmosphere
TRL	Technology Readiness Level
TSI	Total Solar Irradiance
USAF	United States Air Force
USET	Uccle Solar Equatorial Table
UV	Ultraviolet
VIP	Very Important Partner
VIRGO	Variability of solar IRradiance and Gravity Oscillations
VIS	VISual
VITO	Flemish institute for technological research
VSC	Vliebergh-SencieCentrum
VTEC	Vertical Total Electron Content
VUV	Vacuum UV
WALCORS	WALlonia Continuous OpeRating System
WAVACS	WAter VApor in the Climate System
WDC	World Data Centre
WDS	World Data Services
WL	White Light
WMO	World Meteorological Organization
X-flare	Extreme flare
XUV	Extreme Ultraviolet
ZTD	Zenith Total Delay